

**Chemical Interferences on the Atomization
Yield of High Reduction Potential Elements
– Signal Suppression in the Plasma Source
Spectrometry**

Dem Fachbereich 6 (Chemie - Geographie)

Der

Gerhard-Mercator-Universität Duisburg

zur Erlangung des akademischen Grades eines

Doktor rer. nat.

genehmigte Dissertation

Von

Jian LIU

aus China

Duisburg, 2001

The whole work was completed from 03, 1999 to 01, 2001 in the Department of Instrumentally Analytical Chemistry, Fachbereiches 6 (Chemistry – Geography), Duisburg University. Parts of the experiments were carried out in the Research Lab of State Education Committee (SEDC) on Analytical Chemistry for Material and Life Science, Xiamen University, Xiamen, China (04, 1997 - 10, 1998) and in the Institute for Analytical Chemistry, Karl Franzens-University Graz, Graz, Austria (10, 1995 - 01, 1997 and 11, 1998 - 03, 1999).

Referent:	Prof. Dr. Alfred Golloch
Koreferent:	Prof. Dr. Karl Molt
Tag der Mündlichen Prüfung:	28, 02, 2001

Preface

This work was completed under the supervision of Dr. Ursula Telgheder in the Department of Instrumental Analytical Chemistry from March 1999 to January 2001.

Special thanks to Dr. Ursula Telgheder for encouraging me to work on this challenging topic and the full supervision. She had also provided me all the experimental conditions and financial support as she can. Without her helps, the study program could not be finished so smooth.

I sincerely thank o. Prof. Dr. Alfred Golloch for previewing and correcting this dissertation. During the Ph. D. study, I have got a lot of knowledge through the free discussions with him.

My special thanks also go to Prof. Huang Benli, Xiamen University, China. A part of the experiments was carried out when I worked as a visiting scholar in his group. His scientific suggestions are more important to the formation of this research topic.

I will never forget Prof. Dr. Kurt J. Irgolic. When I worked in his group, he directed me to the study field of mercury determination. That initiated the studies on the chemical interferences in the central channel of inductively coupled plasma.

I express my appreciation and many thanks to Prof. Dr. Karl Molt, Dr. Heinz Martin Kuss, Dr. Evelin Denkhau for the productive scientific discussions and all the kind helps.

My continued appreciation and many thanks to Dr. Walter Goessler, for his help and assistance in ICP-MS analysis and the constructive discussions on the dissertation.

Many thanks to Dr. Hai Ying, McGill University, Canada, for the calculations of the electron temperature and the electron number density in MIP.

I would like to thank all of the friends and colleagues who have contributed their time, thought and resources to the successful completion of this study at the Department of Instrumentally Analytical Chemistry, Duisburg University, Germany, the Institute for Analytical Chemistry, University Graz, Austria, and the SEDC Laboratory of Analytical Science, Xiamen University, China. Without your support and help, this work would never have been completed.

Finally, I would like to thank my parents for their boundless support and my wife and daughter for their continuous encouragement and everlasting love.

Contents

1 Introduction	1
2 Matrix effects on plasma source spectrometric signals	4
2.1 Liquid sample introduction into plasma	4
2.1.1 Aerosol generation and transport	5
2.1.2 Terms for aerosol droplet characterization and distributions	7
2.2 Acid matrix effects	11
2.2.1 Acid effects on the physical properties of solution	12
2.2.2 Influence on the liquid aspiration	13
2.2.3 Influences on the aerosol generation	14
2.2.4 Influence on the tertiary aerosol	15
2.2.5 Influence on the solution transport rate	17
2.2.6 Acid effect on the plasma conditions	19
2.2.7 Influence from desolvating droplets and vaporizing particles	24
2.2.8 Acid-caused transient effect	26
2.3 Other influences from acids	28
2.4 Easily ionizable element (EIE) effects	29
3 Experimental	33
3.1 Chemicals	33
3.2 Instrumentation	34
3.2.1 Inductively coupled plasma quadropole mass spectrometer (ICP-MS)	34
3.2.2 Inductively coupled plasma optical emission spectrometer (ICP-OES)	34
3.2.3 Simultaneous introduction for mercury cold vapor and acidified aerosol into inductively coupled plasma	35
3.2.4 High power microwave induced plasma optical emission spectrometer (MIP-OES)	35
3.2.5 Laser unit	36
3.2.6 Microwave digestion system	36

3.2.6.1	Sample digestion for mercury determination with ICP-MS 36
3.2.6.2	Sample digestion for mercury determination with MIP-OES	..37
4	Results and discussion 38
4.1	Nitric acid inhibition on mercury compounds dissociation in inductively coupled plasma source spectrometer 38
4.1.1	Procedures 40
4.1.1.1	Monitoring the time-resolved signals for ICP-MS 40
4.1.1.2	Acquisition for mercury optical emission signals 40
4.1.1.3	Simultaneous introduction of mercury cold vapor and acidic aerosol into plasma 41
4.1.2	Nitric acid influences on mercury mass spectrometric signals 41
4.1.3	Nitric acid influences on mercury transient signal of ICP-OES 45
4.1.4	Rf power influences on mercury optical emission 48
4.1.5	Rf frequency influences 50
4.1.6	Spray chamber structure and aerosol transport 53
4.1.7	Introduction of mercury cold vapor and nitric acid aerosol 54
4.1.8	Summary 56
4.2	The complex formation equilibria of mercury and ammonium nitrate in inductively coupled plasma 58
4.2.1	Mercury species distribution in ammonium nitrate solution 60
4.2.2	Monitoring the transient signals of mercury during the aspiration 63
4.2.3	Nitric acid influences on the equilibria of mercury and ammonium nitrate 67
4.2.4	Ammonium nitrate influences on the boiling point 68
4.2.5	Summary 71
4.3	Halogen complex formation equilibrium and the application in mercury determination with ICP-MS 72
4.3.1	Halogen complex formation equilibrium in inductively coupled plasma 72
4.3.2	Halogen ions interferences in dilute aqueous solution 73
4.3.3	Halogen complex formation equilibrium in concentrated aqueous solution 81
4.3.4	Halogen complex formation equilibrium	

in nitric acid solution in the ICP	83
4.3.5 Mercury determination with halide acid as modifier	87
4.4 Redox equilibria between nitric acid and precious metals	
in ICP and the influences on the mass spectrometric signals	89
4.4.1 Procedures	92
4.4.2 Gold memory and elimination	92
4.4.3 Time-resolved signal of platinum group elements and gold	96
4.4.4 Standard reduction potentials and the nitric acid effects	96
4.4.5 Summary	103
4.5 High power microwave induced plasma optical emission spectrometry	105
4.5.1 The make-up of the spectrometer and the system optimization	106
4.5.2 Nitric acid interference on the time-resolved signal of mercury	107
4.5.3 Nitric acid interference on the steady signal of mercury	110
4.5.4 The transient effect of nitric acid	
on the time-resolved signal of mercury	112
4.5.5 Transient effect on aerosol properties	
and the laser light scattering measurement	116
4.5.6 Sodium chloride interference on mercury signal intensity	120
4.5.7 Sodium chloride interference	
on the excitation temperature of MIP	123
4.5.8 Sodium chloride interference on the electron	
temperature and the electron number density of MIP	125
4.5.9 Sodium chloride interference	
on the rotational temperature of MIP	128
4.5.10 Cold vapor generation for mercury determination	132
5 Conclusion	134
References	137
Appendix	150

1. Introduction

Inductively coupled plasmas (ICPs) and microwave induced plasmas (MIPs) have long been recognized as extremely efficient excitation sources and ion sources. Practical considerations for the generation of ICPs were originally addressed by Reed [1-3] and further refined for spectrochemical analysis, which resulted in the first reports by the research groups of Greenfield [4] and Fassel [5]. In the past decades, ICP have been widely used in spectrometric analysis. It has the advantages of low detection limits, wide linear dynamic ranges, and relative freedom from chemical and physical interferences and from self-absorption. Recently, it has been noticed that mineral acids can strongly suppress the emission signal intensity in ICP. Although signal suppressions are sometimes dependent on the elements to be measured, the attentions were only drawn to the physical interferences on the plasma thermal conditions and aerosol properties. Little suspicion about the chemical matrix influences on the spectrometric signal intensity has been posed.

According to the publications, acid effects can be divided into two groups. The first group happens before aerosol exits the spray chamber. It exerts on the liquid aspiration, aerosol generation, and aerosol transport. That is mainly due to the changes in physical properties of the solution viscosity, surface tension, and viscosity. The second group happens after aerosol exits the spray chamber. It disturbs aerosol desolvation, vaporization, atomization, ionization, and excitation in plasma for the increased energy consumption for acid atomization.

Among all the publications available, there is no paper mentioned the chemical processes in the plasma or chemical interaction with inductively coupled plasma. However, in some instances, acid effects on the spectrometric signal intensities are obviously related to the chemical properties of the acids, especially related to the chemical properties of the analytes. A reasonable explanation is that the chemical interferences are related to the chemical reactions in the observation zone of plasma. The non-spectroscopic matrix effects often happen near the droplets and particles. Due to the lack in the knowledge about the real temperature of the droplets and about the thermal exchange efficiency in the central channel of plasma, Over-believe in the high temperature of plasma is unwise. It has been proven experimentally and theoretically that droplets and particles can survive and pass through the central channel of plasma.

Therefore, the chemical equilibrium is likely to exist in the droplet and to influence the spectrometric signal intensity.

Several facts strongly support this hypothesis. Liu et al. [6] reported that some mineral acids could severely suppress mercury signal. This has been proven to be a chemical inhibition on mercuric ion atomization in plasma [7]. Contrasted to pneumatic aerosol generation, cold vapor generation technique is free from the matrix influences for ICP source spectrometer [7-8]. It was also found that the mass spectrometric signal intensities of the platinum group elements (PGEs) and gold were drastically suppressed by nitric acid in the standard solutions [9]. The signal suppression is attributed to the high standard reduction potentials of the species of PGEs + Au. Therefore, nitric acid interferences on the atomization efficiency of mercury and PGEs + Au in the central channel of plasma should be responsible for the signal suppressions. The high standard reduction potentials and the varied chemical properties make it possible to uncover the chemical interferences in the central channel of plasma by means of mercury, gold and platinum group elements.

The main purpose of this work is to find out the possibly existed chemical interferences on the spectrometric signal intensity. Due to the signal suppression mainly relates to the pneumatic nebulization system, it may arise from the chemical reactions in liquid phase. Therefore, a systemic review about the acid interferences on the inductively coupled plasma spectrometric signal intensity was given in Chapter 2. Chemical interferences on the plasma source spectrometric signal intensity were discussed in many aspects in Chapter 4. At first, it was proven that nitric acid effect on mercury signal intensity of ICP-MS and ICP-OES relates to the redox equilibrium between mercury ions and nitric acid in the central channel of plasma. It depends on plasma thermal conditions and HNO_3 concentration in solution. The presence of nitric acid in the central channel of plasma has no significant effects on mercury ionization and excitation. The following discussion is about the complex formation equilibrium between mercury and ammonium nitrate in the central channel of plasma. The equilibrium state can be changed by the chemo-shift and the thermo-shift. The chemo-shift relates to the complex formation by ammonium nitrate and the complex dissociation by hydronium. The thermo-shift relates to the heat obtained from plasma. It shifts the equilibrium state to the complex dissociation direction. The complex formation equilibrium of mercury was further discussed for halogen ligands. Those equilibria are not sensitive to hydronium. Therefore, the formation of halogen

complexes is able to keep mercury free from nitric acid interferences and achieve a uniform mercury atomization in the central channel of plasma. This properties has been successfully applied to modify the sample solution and to measure mercury in Chinese Human Hair reference material GBW-09101. By means of mercury, the redox equilibrium, the complex formation equilibrium, and the acid-base neutralization equilibrium were observed in the central channel of plasma. Mercury signal intensity is influenced by those reactions. The existence of redox equilibrium and complex formation equilibrium in the central channel of plasma was confirmed by platinum group elements and gold (PGEs + Au). Nitric acid inhibition on the dissociation of PGEs + Au in the central channel of plasma reduces the atomization yields and suppress the mass spectrometric signals. It not only depends on nitric acid concentration, but also on the standard reduction potential (E°) of precious metal species in solution. In the last part of Chapter 4, chemical interferences on the signal intensity of MIP-OES were investigated. The excitation condition of MIP is independent to the acid matrix. Acids also have no significant chemical interferences on mercury signals. This is determined by the robustness of the plasma, which indicates the capabilities of plasma to ingest aerosol and to protect the foreign disturbance. Once the droplet enters the plasma, the liquid phase disappears immediately. As a result, chemical equilibrium does not exist. Sodium chloride influences on mercury signal intensity was also discussed in this part. The signal inhibition relates to the low atomization yield of mercury, which is likely related to the decrease in the gas-kinetic temperature of plasma. When applied cold vapor generation method, mercury determination with MIP-OES was free from sodium chloride interferences. Therefore, to realize the unified atomization is the best way to solve the chemical matrix interferences on the plasma source spectrometry.

2 Matrix effects on plasma source spectrometric signals

For its powerful excitation capability and as an excellent ion source, inductively coupled plasma (ICP) has been widely used in spectrometric analysis. Little suspicion about the chemical matrix influences on the ICP source spectrometric signal has been posed. However, mineral acids, the common chemical matrix, can strongly suppress the emission signal intensity in ICP. In many cases, the signal suppressions are related to the elements to be measured. Although a lot of work has been done to interpret the signal suppression, the attention was only paid for the physical interference on the plasma conditions and aerosol properties. The element-dependent interference indicates that, in some instances, signal suppression may relate to the chemical properties of element in the central channel of plasma. These chemical interferences are assumed to be related to the chemical equilibrium in the observation zone of plasma. Due to part of the aerosol can survive in the plasma, the chemical equilibrium in solution may take place. The high power microwave induced plasma (MIP) allows to introduce wet aerosol into the plasma. The signal intensity suppression may happen. Therefore, it is important to study on the chemical equilibrium in the droplets and the influences on the spectrometric signal intensity. To start this work, the basic knowledge about the aerosol properties and the behaviors in plasma are necessary. They are discussed below.

2.1 Liquid sample introduction into plasma

Sampling technique for inductively coupled plasma (ICP) source spectrometer is still the neck of the bottle. In some extents, it restricts the full use of the abilities of ICP for sample analysis. Since the development of inductively coupled plasma spectrometry, liquid sample introduction has been being the most commonly used sampling technique. The first reason is that almost every kind of samples can be changed into liquid solution by acid or mixture acid digestion. Hence, it is able to use aqueous standard solutions for various standard calibration methods. Secondly, aerosols provide easy means to introduce liquid samples into the plasma. With the development of ICP source spectrometry, people have accumulated a good deal of understanding about the aerosol sampling technique. On comparison with other sampling techniques, pneumatic nebulization system is rather simple, easy to operate, relatively stable signal response,

and low cost. It has become a standard apparatus in almost all of the commercial inductively coupled plasma spectrometer.

2.1.1 Aerosol generation and transport

The most commonly used aerosol generation method is pneumatic nebulization. This system consists of a nebulizer and a spray chamber. The nebulizer can be mainly divided into two types according to the geometric structures. That is the concentric type and the cross-flow type. With the nebulizer, certain amount of the kinetic energy of argon gas flow is consumed to transform the sample solution into an aerosol. Three main types of liquid breakup have been recognized. They are dropwise, stringwise, and filmwise. It depends on the relative velocity of the gas and the liquid. For the plasma source spectrometry, this relative velocity is higher than 50 m/s. Argon gas causes the drops to become flattened and subsequently blown out into the form of a bag or a casting net with a roughly circular rim. The bursting of this bag produces a large number of fine strings and filaments which, in turn, form droplets [10]. This primary aerosol then is introduced into a spray chamber. For the rapid desolvation, volatilization, and atomization of the aerosol droplets when they reach the plasma, a nebulizer must produce droplets less than 10 μ m in diameter. Unfortunately, nebulizers, particularly pneumatic nebulizers, produce aerosols that are highly polydisperse, with droplets up to 100 μ m. Those large droplets must be removed by means of a spray chamber. The spray chamber removes the large droplets by turbulent deposition on the inner walls of the chamber or by gravitational action. In the case of cyclone chamber, the centrifugal force acts on the droplet and throws them towards the wall. Once the selected aerosol (tertiary aerosol) enters the plasma, it undergoes the desolvation, volatilization, atomization, ionization, and excitation. A fraction of the analyte contained in it will produce the spectrometric signal.

A variety of pneumatic nebulizers are commercially available. The hydraulic high-pressure nebulizer (HHPN) was developed by Berndt and coworkers [11,12]. Sample solution is constantly forced through a nozzle with an orifice of 10 to 30 μ m using a high pressure pump. The liquid jet disintegrates into an aerosol and is converted into an aerosol cloud upon collision with an impact bead placed inside a spray chamber.

The ultrasonic nebulizer (USN) is another choice to produce an aerosol by means of the ultrasound to break the liquid into small droplets. In this method, an ultrasonic generator is used to drive a piezoelectric crystal at a frequency between 200 kHz and 10

kHz. The longitudinal wave, which is propagated perpendicularly from the surface of the crystal toward the liquid-air interface, produces a pressure that breaks the surface into an aerosol. The wavelength of the surface wave is given by:

$$\lambda = \left(\frac{8\pi\sigma}{\rho f^2} \right)^{1/3} \quad \text{eqn. 2-1}$$

where λ is wavelength, σ is surface tension, ρ is liquid density, and f is ultrasonic frequency [13]. The average droplet diameter is given as:

$$D = 0.34\lambda \quad \text{eqn. 2-2}$$

Since the aerosol production of USN is very large and independent on the gas flow rate, more analyte can be transported to the ICP at a slower flow rate of injection gas than can be achieved with a pneumatic nebulizer, thus give longer residence time for analytes in the plasma and subsequently more emitting species. Detection limits with ultrasonic nebulizers are an order of magnitude better than with pneumatic devices, if the matrix is not complicated [14].

The thermospray nebulizer (TN) realizes the nebulization by introducing the liquid into a heated capillary. The liquid starts to boil near the outlet of the capillary, and the vapor acts as nebulizing gas. The thermospray nebulizer provides an aerosol with finer droplets and higher solvent vapor loading compared to pneumatic nebulizers [15]. Meyer et al. [16] compared a thermospray and concentric nebulizer and attained better detection limits and calibration curve slopes for 18 elements using the thermospray.

All the nebulizers mentioned above must be equipped with a spray chamber, which is a crucial apparatus for collecting and transporting sample aerosol into the plasma. Most of the spray chambers are designed to select or to filter the qualified aerosol [17-18] and also to buffer the pressure impulse in the sampling system [19]. However, the phenomena happen in the simple chambers are more complicated. The primary aerosol produced by the nebulizer is modified as it passes through the spray chamber because of evaporation, impact and drop shattering, inertial deposition, and gravitational settling [20]. The drop collisions and coalescence to form larger droplets had been reported [21]. Canals et al. [22] also conclude that one of the main aerosol modification processes is coalescence of droplets. However, the opposite opinion is that the risk of droplet recombination is negligible within a few seconds after the formation of an aerosol [23]. More recently, Montaser [24] reported that the aerosol is often altered by passing it through a spray chamber or a desolvation device prior to introduction into the

plasma. This agrees well with our results that water and acid molecular transport through evaporation and adsorption could change the dimensions and the components of the droplets. As results, changing the chemical atmosphere in spray chamber can alter the chemical properties of aerosol and influence spectrometric signals [9].

The nebulizer-spray chamber arrangement suffers from shortcomings such as analyte loss, memory effects, interferences, and inferior precision, which are mainly attributed to the spray chamber. To overcome these drawbacks, several papers have been published to describe the new strategy of removing the spray chamber and directly inserting the high efficiency nebulizer (DIHEN) into the inductively coupled plasma [25-32]. With the novel nebulizer-torch arrangement, nearly 100% sample utilization is achieved without (sacrificing the separation efficiencies) adverse effects derived from the spray chamber (i.e., analyte-chamber interactions, band broadening, sample loss, etc.).

2.1.2 Terms for aerosol droplet characterization and distributions

The overall process of sample introduction consists of (1) nebulization, which produces the *primary* aerosol, (2) interaction with impact beads (if present) resulting in production of the *secondary* aerosol, and (3) loss of larger drops in the spray chamber, leading to the final *tertiary* aerosol. At each stage of the process, the aerosol possesses a different mean drop size and drop size distribution [33]. The interaction of the spray chamber with the primary aerosol determines the basic transport properties of the system. The kinetics of desolvation and vaporization which occur when the aerosol reaches the analytical measurement zone are partially determined by the properties of the tertiary aerosol, and hence are directly influenced by the interactions which lead to the formation of the tertiary aerosol.

Some terms are more important to describe the aerosol characteristic and distribution. It must be defined before the discussion of matrix interferences on the plasma-based spectrometric signal.

The Sauter mean diameter, or volume/surface mean diameter, which is used for transport efficiency studies [34], is defined as follows:

$$D_{3,2} = \frac{\sum_{i=1}^N n_i d_i^3}{\sum_{i=1}^N n_i d_i^2} \quad \text{eqn. 2-3}$$

where N is the total number of droplet classes, n_i is the number of droplets in each class i , and d_i is the diameter of size class i . It is probably the most commonly used term to describe the mean diameter of aerosols, and is the measure of the ratio of the total volume of droplets in an aerosol population to their total surface area.

Based on numerous experimental data of the pneumatic nebulization and the drop size distributions, Nukiyama and Tanasawa [35] established the empirical relationship between the Sauter mean diameter and the solution properties. That is the well-known Nukiyama and Tanasawa equation:

$$D_{3,2} = \frac{585}{V} \left(\frac{\sigma}{\rho} \right)^{0.5} + 597 \left[\frac{\eta}{(\sigma\rho)^{0.5}} \right]^{0.45} \left(\frac{10^3 Q_l}{Q_g} \right)^{1.5} \quad \text{eqn. 2-4}$$

where V is the difference between the gas and liquid velocities (m s^{-1}), σ the surface tension (dyn cm^{-1}), ρ the density of the liquid (g cm^{-3}), η the viscosity of the liquid (poise), Q_l and Q_g are the liquid and gas flows ($\text{cm}^3 \text{s}^{-1}$), respectively. This relationship was obtained for a given nebulizer design under special solution physical properties. The experimental range of the constants are $0.8 < \rho < 1.2$, $30 < \sigma < 73$, and $0.01 < \eta < 0.3$. Extrapolation is not advisable as it has been experimentally demonstrated [33]. With a forward scattering spectrometer probe, which employs Mie scattering of laser beam, Olsen and Strasheim [36] characterized the nebulizer sprays. They concluded that the emission signal was correlated to the total volume of droplets smaller than $8 \mu\text{m}$ which are produced by a nebulizer. Flicker noise decreased considerably when a narrow particle size distribution was supplied to the plasma. Irregular supply of droplets, particularly those larger than $8 \mu\text{m}$, results in a deterioration of the signal-noise ratios. The Nukiyama and Tanasawa equation was derived for $D_{3,2}$ values in the range of 15 to $90 \mu\text{m}$ in an empirical way. The geometrical structure of the nebulizers and the droplet size measuring techniques they employed are far away from those used in nowadays for atomic spectrometry. There is also no direct description about the physical process happens during the nebulization. Therefore, the practicability of Nukiyama and Tanasawa equation has been suspected. Canals et al. [37] found that the predictions of $D_{3,2}$ calculated from the Nukiyama and Tanasawa equation were dramatically different from the experimental data. In all instances, the Nukiyama and Tanasawa predictions were higher than the experimental values (1.7 to 25 times). The differences in the type of nebulizers, the differences in the drop size measuring techniques and the detectable

droplet ranges, and uncorrected solvent evaporation are believed to partially influence the accuracy of the absolute values. However, under certain conditions, this equation often goes wrong to give acceptable trend predictions. Overestimation in comparing water and acetic acid solution [38] and reversed trend prediction [37] were reported. In spite of these, this equation has been widely used in atomic spectrometry for many years because it has been considered as the first attempt to predict the characteristics, in terms of Sauter mean diameters, of the primary aerosol generated by pneumatic nebulizer [39]. An empirical equation with six parameters has been developed using two nebulizers to predict the Sauter mean diameters and the span [37]. The $D_{3,2}$ value used for calculation of the parameters were determined by laser diffraction. The equation has been checked by estimating Sauter mean diameters and spans for two additional concentric nebulizers. Good agreement has been obtained between experimental and estimated values. However, it is still lack of the physical meanings and more complicated to be used. The parameters of the equation change with nebulizer nozzle dimensions and solvent properties. Also the Sauter mean diameters were not corrected for solvent evaporation. It is unsuitable to compare this empirical equation to Nukiyama and Tanasawa equation. The preconditions to completely discard the Nukiyama and Tanasawa equation are that a new equation has been established, which can clearly express the physical processes of nebulization and accurately predict the aerosol characteristics for a variety of pneumatic nebulizers.

The mass mean diameter, or mass median equivalent diameters, is defined as follows:

$$D_{4,3} = \frac{\sum_{i=1}^N n_i d_i^4}{\sum_{i=1}^N n_i d_i^3} \quad \text{eqn. 2-5}$$

It can be used as $D_{3,2}$ for evaluating the acid interference on the aerosol drop size [39]. It has the advantage against Sauter mean diameters that it represents the mean of the distribution based on a property directly related to the emission signal.

The median of the volume drop size distribution D_{50} (μm) indicates that 50% of the liquid aerosol volume is contained below this diameter. It gives the central trend of the drop size distribution. The D_{50} is used to study the change in the aerosol drop diameters.

Span is defined as:

$$Span = \frac{D_{90} - D_{10}}{D_{50}} \quad \text{eqn. 2-6}$$

ninety, fifty and ten percent of the total volume of aerosol is contained in drops less than or equal to diameters of D_{90} , D_{50} and D_{10} , respectively. Because the span is dependent on D_{50} , it is a relative measure of the width of the distribution, analogous to relative standard deviation.

Volume percentage in droplets below 1.2 μm , $V_{1.2}$ (%), is defined as the aerosol liquid volume percentage that is present in form of droplets of diameter lower than 1.2 μm . The acid effects on the finest aerosol fraction are evaluated when considering this parameter.

Volume concentration, VC (%), is the percentage of the aerosol measurement volume that is occupied by liquid droplets. The measurement of this parameter at the exit of the spray chamber could be a relative indication of the influence of acids on the solution transport through it.

Volume flux of droplets ($\text{cm}^3 \text{s}^{-1} \text{cm}^{-2}$) is defined as the total volume of droplets passing a cross-sectional area in a given direction per unit time. It also indicates the mass transport rate and helps to detect the changes in the transport of the aerosol along the spray chamber induced by acids.

Total mass solvent transport rate, S_{tot} (mg min^{-1} or $\mu\text{g s}^{-1}$), directly indicates the amount of the solvent (liquid and vapor) that is introduced in the plasma bottom per unit of time. The acid phenomena occurring inside the spray chamber are mainly characterized by using this and the next parameter.

Total mass analyte transport rate, W_{tot} ($\mu\text{g min}^{-1}$ or $\mu\text{g s}^{-1}$), directly indicates the amount of analyte leaving the spray chamber per unit of time.

Drop size distributions for aerosols generated pneumatically can generally be well described by a log-normal model. This means that the density function of the drop volume has a normal distribution with respect to the logarithm of the particle size with mean, $\ln(X)$, and standard deviation, $\ln(N)$, given by:

$$W_D = \frac{1}{\ln(N)(2\pi)^{0.5}} \exp\left\{-0.5\left[\frac{\ln(D) - \ln(X)}{\ln(N)}\right]^2\right\} \quad \text{eqn. 2-7}$$

In this expression, W_D indicates a density function for drops of diameter D . From the definition of X and D_{50} described above it may be concluded that for a log-normal distribution $X = D_{50}$.

MgII/MgI net intensity ratio is used to evaluate the acid effect on the plasma excitation capability. A reduction in this parameter indicates that the plasma state is deviating from the local thermal equilibrium (LTE).

Excitation temperature T_{exc} (K) also indicates the deterioration or enhancement of the plasma thermal properties when dealing with acids.

2.2 Acid matrix effects

The inductively coupled plasma has been used for spectrometry analysis nearly 40 years. During the past decades, a variety of sampling techniques has been developed. However, liquid sample introduction is still the most commonly used sampling method for its homogeneity, direct concept of concentration, flexibility in choosing calibration methods, and the convenience to be automatically controlled for batch analysis. Acids are the most common matrixes that exist in the sample solutions. They are often introduced into sample solution during solid sample digestion, liquid sample pretreatment, analytes stabilization, and sample storage. Some special sample pretreatments are also the sources for introducing acids into sample solutions. These may involve acid leaching the interest species from ionic exchange resins or from the geological samples [40]. Therefore, a fundamental understanding about the acid effects on the ICP-based spectrometry is obviously important.

The liquid sample introduction system has been discussed in the sections 2.1.1. The function of such a system is to transform the liquid into an aerosol (primary) and to transport the filtered aerosol (tertiary) into the plasma. Once the tertiary aerosol enters the plasma, it undergoes a series of complicated physical processes and a fraction of the analyte is ionized and/or excited. These species finally contribute to the spectrometric signal. Therefore, acid effects can be divided into two groups. The first group happens before that the tertiary aerosol exits the spray chamber. It acts on the liquid aspiration, aerosol generation, and aerosol transport. The other group happens after the aerosol exits the spray chamber. It interferes aerosol desolvation, vaporization, atomization, ionization, and excitation in the plasma. The acid effect has also been attributed to the following causes:

1. Changes in the sample uptake rate due to changes in physical properties of the solution, mainly viscosity [41].
2. Changes in aerosol drop size distribution due to changes in physical properties of the solution, mainly surface tension and viscosity [42].
3. Changes in analyte transport rate due to the causes 1 and 2 [43-46].
4. Changes in the plasma excitation conditions due to the increased energy consumption for acid atomization [47-50].

The details are discussed in the following sections.

2.2.1 Acid effects on the physical properties of solution

Adding acids into water will inevitably lead to a series of physical property change. When introduce aqueous solutions into the inductively coupled plasma, the crucial step to get spectrometric signals, changes in viscosity and surface tension become more important. The obvious effects on aerosol drop size distribution have been shown in Nukiyama and Tanasawa equation [eqn.2-4]. Apart from this, the changes in viscosity and surface tension also interfere on aqueous solution aspiration whereas density and volatility affect the aerosol transport through the spray chamber. For convenience to discuss the acid effects on the pneumatic nebulization, some important physical properties of acid solutions are listed in the Table 2.1.

Table 2.1 Physical properties of different acid solutions at 25°C*

Acid	Concentration (%, w/w)	Surface tension (mN m ⁻¹)	Viscosity relative to water	Density (g cm ⁻³)
Nitric	4	72.15	1.014	1.022
Nitric	30	68.75	1.397	1.180
Hydrochloric	4	72.45	1.057	1.017
Hydrochloric	30	65.75	1.896	1.149
Perchloric	4	71.18	0.879	1.018
Perchloric	30	68.57	1.170	1.207
Sulfuric	4	72.21	1.083	1.029
Sulfuric	30	75.29	2.250	1.122
Phosphoric	4	–	1.121	1.025
Phosphoric	30	–	2.995	1.180
Acetic	4	60.10	1.082	–
Acetic	30	43.60	1.666	–

*From reference [39].

2.2.2 Influence on the liquid aspiration

In the early time, pneumatic nebulization is the most widely used technique for introducing liquid samples into the ICP-based spectrometry. The concentric nebulizer is one of the most typical apparatus to turn the aqueous solution into an aerosol. It can aspirate the liquid solutions by Venturi effect. The external pumping system is not necessary to force the liquid into the nebulizer. For this free aspiration system, a pressure differential created across the sample capillary draws the liquid solution through the capillary according to Poiseuille's equation [51]:

$$Q = \frac{\pi R^4 P}{8\eta L} \quad \text{eqn. 2-8}$$

where Q is the rate of flow of the liquid, R the capillary radius, P the pressure differential, η the viscosity of the liquid, and L the length of the capillary. Poiseuille's equation assumes that the velocity of the liquid at the capillary wall is zero, whereas the liquid slips over it. In this case, the R^4 term is replaced by $(R^4 + 4\eta R^3 / B)$, where B is the coefficient of sticking friction of the liquid on the wall.

Based on Poiseuille's equation, the increase in the liquid viscosity results in a decrease of the liquid uptake rate. This is usually encountered when aspirate the H_2SO_4 or H_3PO_4 aqueous solutions. With a concentric nebulizer, the values of Q obtained from 30% sulfuric acid and phosphoric acid were about a half comparing with the value obtained from water [41-42]. This has been believed as that the introduction of some mineral acids would lead to the emission intensity depression [41, 44]. The use of a peristaltic pump to ensure a constant uptake rate can only partially compensate for the signal reduction. Greenfield et al. [41] observed that under free aspiration, the emission intensity with a solution of 33% (w/w) phosphoric acid dropped by a factor of two with respect to the signal obtained for water. Such a phenomenon did not happen for some other mineral acids (HNO_3 , HCl , and HClO_4). They also found that the ratio of the solution uptake rate with and without acid was the same as the signal emission ratio with and without acid. Farino et al. [43] observed that the natural aspiration rates of 30% sulfuric acid and phosphoric acid solutions were reduced significantly comparing with water. Nevertheless, they observed that the normalization of the signal to the solution uptake rate provided good correction for phosphoric but not for sulfuric acid.

Obviously, in some instances, the emission signal depression can be attributed to the change in the viscosity of liquid solution [45, 52]. However, the viscosity does not

only affect on the liquid solution transport efficiency in a capillary, but also govern the nebulization process. There are also some other physical properties, which affect on the processes to get spectrometric signals. Therefore, the use of a peristaltic pump could not radically eliminate the acid effects on the emission intensity depression. No matter how, the forced aspiration can at least minimize the liquid transport resistance, hence to reduce the acid effects on the spectrometric signal depression.

2.2.3 Influences on the aerosol generation

The result of nebulization is to enlarge the surface area to volume ratio of a given liquid solution. Therefore, surface tension of sample solution becomes the most important physical properties that govern the primary aerosol generation and the characteristics [33, 53,]. When mineral acid is added into water, change in surface tension is expected. For pneumatic nebulization, this change can lead to a significant variation in the droplets size distribution. Farino et al. [43] speculated with an increase in the aerosol drop size when mineral acid, high viscosity solutions were introduced with a pneumatic nebulizer. This could account for the reduction observed in the transport of solution through the spray chamber. In contract, the experimental data indicate that liquid density and viscosity have relatively little influence on the mean drop size [37]. The change in viscosity will indirectly influences $D_{3,2}$ if solvent is allowed to aspirate naturally into the nebulizer, without external pumping. Clearly, to examine the physical properties interference on the drop size distribution, it is important to distinguish the liquid transport modes between free and forced aspiration.

With free aspiration, Canals et al. [52] found that for nitric, hydrochloric and perchloric acids the increase in the concentration led to the decreases in the aerosol mean diameters. Other acids like sulfuric and phosphoric acids exhibited a slight maximum in the aerosol mean diameters as the concentration was increased. This is because that the increase in the solution viscosity was partially counterbalanced by the decrease in the liquid uptake rate. Under the same gas flow rate, the gas kinetic energy exchange with liquid for surface generation increased.

With forced aspiration, for all the acids mentioned above, the higher the concentration of the solutions, the higher the mean diameters. This coheres with the increase of the viscosity of the solutions (Table 2-1). Obviously, these effects were less important for the less viscous solution (i.e. HNO_3 , HCl and HClO_4) than for H_2SO_4 and

H₃PO₄ [52, 54-56]. Under the same conditions the mass mean diameters $D_{4,3}$ of the aerosols generated by a glass concentric pneumatic nebulizer were 14.7 and 15.1 μm for water and 30% HNO₃ (w/w), respectively. These diameters were 13.9 and 18.2 μm for water and H₂SO₄ 30%, respectively. Other studies performed with perchloric acid [57] confirmed these observations.

The differences of surface tension among water and the organic acids are more significant. With a FAAS nebulizer under forced aspiration mode, More et al. [58] observed that, the D_{50} values were 16.9, 12.9 and 9.8 μm for water, formic and acetic acid, respectively. The decrease in the D_{50} values seems mainly related to the decrease in surface tension. It follows the order of the surface tension values of water, formic acid and acetic acid as 72.6, 37.6 and 27.8 mN m^{-1} .

2.2.4 Influence on the tertiary aerosol

The characterization of tertiary aerosols gives the information about acid influence on the aerosol transport and filtering in the spray chamber. It indicates the amount and the characteristics of the liquid fraction that enters the plasma central channel for producing the spectrometric signals.

It was observed that the differences between the tertiary drop size distributions of water and acetic acid were more pronounced than those for primary aerosols [38]. This has already been observed for inorganic acids and emphasizes the different aerosol transport mechanisms through the spray chamber [52]. At low acid concentration, the tertiary aerosol shows little variation, while at high concentrations it becomes finer ($D_{4,3}$, D_{50}) and more disperse (Span). The probability for a droplet to exit the spray chamber decreases on increasing the solution density for the increased inertia. This density-effect would be equivalent to a reduction in the cut-off diameter of the spray chamber. Therefore, the higher the solution density, the finer the tertiary aerosol. In addition, the amount of tertiary aerosol would also decrease on increasing the solution density. Marichy et al. [46] found that, comparing with water, a small increase in the proportion of droplets below 1.2 μm could be observed for a 1% HCl solution. In the larger drop diameter range, no significant variations in the aerosol liquid volume fraction were observed for the different solutions.

In the free uptake mode, Canals et al. [52] observed that the volume concentration (VC) of primary aerosol was decreased on increasing the acid concentration. The

viscosity of solutions became the main factor to affect the aerosol generation. Contrarily, the VC values of tertiary aerosol were almost constant. In the controlled uptake mode, for both the primary and tertiary aerosols, the VC values were not changed or shown little increases when acid solutions were nebulized with respect to water. Todoli et al. [54] observed that, with a microcentric nebulizer, the tertiary $D_{3,2}$ values were 2.1, 1.5, and 1.2 μm for water, 0.9 M nitric acid, and 3.6 M sulfuric acid, respectively. The percentages of aerosol liquid volume contained in droplets smaller than 1.2 μm are 13.6, 25.3, and 41.8%, respectively. The VC values followed the order: $VC_{\text{water}} \approx VC_{\text{nitric}} > VC_{\text{sulfuric}}$. It seems obvious that different aerosol transport processes for water and acid solution may exist. The variation of the VC with the acid concentration has proven to be dependent on the spray chamber design. Maestre et al. [56] observed the VC values of the tertiary aerosols increased with acid concentration. This growth was more pronounced for the Scott-type spray chamber than for the cyclonic spray chambers. For the Scott-type chamber, the VC value for water (0.011%) was improved by a factor of around two when 3 mol l^{-1} solutions of either nitric (0.022%) or sulfuric (0.023%) acid were employed. In contrast, for the glass cyclonic spray chamber the VC values varied only slightly (0.073, 0.078 and 0.074% for water, and 3 mol l^{-1} nitric and sulfuric acid, respectively).

As claimed by Olsen and Strasheim [36], the aerosol droplets with the diameter lower than 8 μm are suitable to be introduced into plasma for producing the stable spectrometric signals. Liu and Montaser [59] used a phase/Doppler sizer (PDPA) in order to study the tertiary drop size distribution of the aerosols generated with a high efficiency nebulizer [60-62]. They found that the higher the nitric and sulfuric acid concentration, the finer the tertiary aerosols. Accordingly, the aerosol liquid fraction percentage contained in droplets smaller than 8 μm was higher when the concentration of acid increased. Stewart and Olesik [55] observed the similar results. They found that the total aerosol volume of droplets less than 3 μm in diameter increased with increasing acid concentration while the total aerosol volume of droplets greater than 3 μm in diameter decreased with the increasing acid concentration.

Concerning about the amount of aerosol liquid fraction exiting the spray chamber, with a high-efficiency nebulizer (HEN), Liu and Montaser [59] found that the volume flux remained constant when the nitric and sulfuric acid concentration changed in the 5-10% range. However, with a cross flow nebulizer, the contrary experiment result was

observed by Stewart and Olesik [55]. They found a decrease in the volumetric flux on increasing the nitric acid concentration in the range of 0-25% (v/v). In addition, a reduction in the nebulizer gas flow rate will affect the severity of acid-dependent changes in the analyte transport as well as the robustness of the analysis to changes in acid concentration.

2.2.5 Influence on the solution transport rate

When the primary aerosol passes through the spray chamber, a series of complicated processes can affect the characteristics of the tertiary aerosol. A simple mechanical filter can not fully explain the practical processes. When acids were present, there might be a change in the magnitude of the solution mass transported into plasma. The total mass solvent transport rate S_{tot} (mg min^{-1} or $\mu\text{g s}^{-1}$) is one of the parameters to describe the behaviors when the solvent transports through the spray chamber. It can be measured by a direct method [63-64]. In this way, the aerosol exiting from the spray chamber was trapped in a U-shaped tube filled with dried silica gel. The weight difference before and after the exposition to the aerosol can be used to calculate the value of S_{tot} .

Todoli et al. [54] used direct method to investigate the acid effects on the value of S_{tot} . They found that the values of S_{tot} were 24.6 and 24.7 mg min^{-1} for water and 0.9 M nitric acid solution, respectively. Similar results were obtained for 3.6 M nitric acid and 0.9 M sulfuric acid solutions. For concentrated sulfuric acid a reduction in S_{tot} was produced with respect to water (24.6 and 22.4 mg min^{-1} for water and 3.6 M sulfuric acid, respectively). This fact was partially related to the coarser aerosols generated with this acid and the reduction in the evaporation processes inside the spray chamber as well as the intensification of the losses aroused from the increased solution density.

An indirect method can also be applied to determine the interferences of acid on the S_{tot} values [63, 65]. In this way, the weight difference between the liquid aspirated by the nebulizer and the drained solution from the spray chamber is continuously measured. This method could be considered as more suitable to examine the acid effect on the solvent transport because the use of silica did not result in an efficient trapping of the acid [57]. Maestre et al. [56] employed the indirect method to examine the acid effect on the solvent transport. They found the relative S_{tot} values, i.e.,

$(S_{tot})_{acid}/(S_{tot})_{water}$, were 0.97 and 1.09 for 3 M nitric and sulfuric acid solutions, respectively. The influence is not so significant.

The influence on the S_{tot} values is more pronounced for the organic acids than the inorganic acids. Dubuisson et al. [38] observed a slight increase in the total amount of solvent exiting the spray chamber when 5 and 10% acetic acid solution were introduced. Hettipathirana et al. [66] observed that, comparing with water, the S_{tot} values increased when 70% (v/v) acetic, formic and propionic acid solution were introduced. This should be related to the generation of finer aerosols and the enhanced solvent evaporation.

Another parameter to describe aerosol transport process is represented by W_{tot} , the total mass analyte transport rate ($\mu\text{g s}^{-1}$ or $\mu\text{g min}^{-1}$). It indicates the mass of analyte leaving the spray chamber per unit of time. The final spectrometric signal obtained from plasma should be proportional to the value of W_{tot} . It gives the criteria to distinguish the amount of analyte available to produce the signal changes by the presence of acids or not.

In general, adding mineral acid into water leads to a decrease in the W_{tot} value. Farino et al. [43] measured the W_{tot} values for concentrated acid solutions and observed that, when working with 30% of both sulfuric and phosphoric acids, the W_{tot} values were reduced by a factor of two with respect to water. It can be expected that the analyte transport should decrease on increasing acid concentration, under natural uptake mode, because of the decrease on Q_n , while under controlled uptake mode because of the larger size of the primary aerosol. Both effects are originated from the increased viscosity. Canals et al. [52] observed that, for the first group acids (HNO_3 , HCl and HClO_4), in controlled uptake mode, the W_{tot} values were almost constant. A small amount of analyte will be lost due to the increasing density of the solutions. Under naturally uptake mode, there are two opposite effects. On increasing acid concentration, primary aerosols are slightly finer, while the natural uptake rate decreases. The final result is that the W_{tot} values show a decrease. With the second group acids (H_2SO_4 and H_3PO_4), the physical properties of the solutions play a more significant role. Thus, in natural uptake mode they reduce noticeably the aspiration rate, while in controlled uptake mode they increase the drop size distribution of the primary aerosol. In fact, the decrease in analyte transport is more significant in the natural uptake mode. In

summary, the decreases in the W_{tot} value appear clearly just for the highest concentrations, 30% for the first group acids and 5% for the second group acids.

The change in gas flow rate can be a factor to influence the W_{tot} values. Stewart and Olesik [55] found that the lower the gas flow rate employed, the higher the W_{tot} drop for an acid solution with water. Hence, the $(W_{tot})_{25\%(v/v)\text{nitricacid}} / (W_{tot})_{\text{water}}$ increased from 0.8 to 0.9 when Q_g rose from 0.7 to 1.3 l min⁻¹.

It has been discussed above that the variation of the VC with the acid concentration depended on the spray chamber design. The cyclonic spray chamber has stronger ability than a Scott-type spray chamber to counterbalance the effect on the VC value with the increasing acid concentration. It is also true for the W_{tot} values. For 3 M sulfuric acid solution, the $(W_{tot})_{\text{acid}} / (W_{tot})_{\text{water}}$ ratios were 0.80 and 0.70 when using a cyclonic and double-pass spray chamber, respectively.

Marichy et al. [46] trapped the aerosol exiting a double-pass spray chamber by means of liquid nitrogen trap. Once the aerosol was back to the liquid form, the acid concentration was measured. Surprisingly, for an acid concentration near 0.001%, a drastic decrease (50%) in the acid concentration of the aerosol was observed, irrespective of the type of acid (HCl or HNO₃) and the use of a surfactant. A corresponding increase in the acid concentration was found in the drain, although less drastic because of the low efficiency of the nebulizer (2.7-3.3%).

Finally, increasing the concentration of volatile organic acids are expected to increase the W_{tot} values with respect to water for the enhanced vaporization.

2.2.6 Acid effect on the plasma conditions

The inductively coupled plasma has a donut structure that allows the efficient introduction of cold sample aerosol into the central channel of the plasma. This provides several unique analytical capabilities, such as low detection limits, wide linear dynamic ranges, and relative freedom from chemical and physical interferences and from self-absorption. In addition, the high temperatures and large electron number densities of the plasma provide higher emission intensities for ionic species than for neutral atom species. Therefore, it is also an excellent ion source for the atomic mass spectrometry.

Those advantages are more pronounced when comparing the inductively coupled plasma spectrometry with the classical atomic spectrometry. However, in the practical

applications, a variety of interferences may occur. The most frequently encountered interference relates to the sample matrix. In the beginning, the study of matrix interference on the inductively coupled plasma atomic emission spectrometry was confined to the easily ionizable elements that exist in sample solutions. Little attention has been paid to the acid effects, though acids may become the main component in the sample solutions during the sample pretreatment. Recently, mineral acid interference on the inductively coupled plasma spectrometry has been recognized as mentioned above. It exists not only in the aerosol generation and transport processes, but also inside the inductively coupled plasma. It has become one of the most attractive subjects in this field.

Acid effects on the plasma spectrometric signal can be roughly divided into two groups. The first group effects happen before sample aerosol enters the plasma. It includes the acid interferences on the liquid sample aspiration, aerosol generation and transport processes. These characteristics finally determine the total amount of analyte that is available to enter the inductively coupled plasma. Those have been discussed in the above sections. The second group effects happen after the aerosol enters the plasma, which influence the characteristics and thermodynamic processes in the inductively coupled plasma. These may include aerosol desolvation, particle or compounds cluster evaporation, atomization, ionization, and excitation. In general, the observed signal reduction when adding mineral acid into water solution is the combining results of both the two group effects [47, 48, 50]. What is the predominant factor of acid effect fairly depends on the acid concentration. The acid effects on the inductively coupled plasma spectrometric signals by changing plasma conditions are discussed in the following part.

On characterizing the inductively coupled plasma conditions, the excitation temperature T_{exe} , the electron temperature T_e , and the electron number density n_e are more important parameters. Because of the lack of local thermodynamic equilibrium in the ICP, various species and states can show a considerable difference in T_{exe} , and emission lines having different excitation potentials could be considered to have their own excitation temperature. Therefore, the MgII/MgI intensity ratio has been well accepted as the practicable parameter to indicate the plasma conditions.

Maessen et al. [48] observed that acid effects in low power plasmas could not be explained in terms of changing viscosity only. Changes in excitation conditions by acids notably contribute to acid effects in low power plasma. It seems that the ingestion

capacity for acids of ICP very critically depends on the power applied. In the acid concentration range of 0-2%, closely matched acid strength of digested sample and reference solutions could prevent a systematic error. A comparable results obtained at higher acid concentrations with and without use of a pump showed that the net line intensity depression is reduced by a factor of two if a pump-feed system is used instead of the conventional system with free uptake.

Chudinov et al. [49] systematically investigated the acid effects on the inductively coupled plasma optical emission signals with a variety of instruments and mineral acids. They observed that the change in the plasma temperature in the presence of acids is connected mainly with the difference in the dissociation energies of water and acid molecules. The acid-induced signal changes increase in the order: $\text{HCl} < \text{HNO}_3 < \text{HClO}_4 \ll \text{H}_3\text{PO}_4 < \text{H}_2\text{SO}_4$. They concluded that the signal depression not only correlates with the excitation energy, but also depends on the atomization energy of acid molecules. The same authors also found that the magnitude and character of acid effects depend strongly on the design features of RF-generators, the impedance matching network, and their tuning.

Yoshimura et al. [50] reported that the excitation temperature decreases with increasing concentration of mineral acids, and the extent of decreases in emission intensities of the atomic and ionic lines could be correlated with the excitation potentials. The decrease of excitation temperature may be related to the power applied to the plasma, which is consumed in decomposing the acid. Furthermore, they concluded that for low power plasmas and over low acid concentrations ($\leq 1 \text{ M}$), the acid effect is responsible for the decrease in excitation temperature rather than the reduction in rate of sample uptake. However, at higher concentrations of mineral acids ($\geq 1 \text{ M}$), the decrease in emission intensity by a reduced rate of sample uptake becomes predominant. The plots for Cu deviate from linearity with an increase in HNO_3 concentration. The similar behavior for Cu was observed with HCl , HClO_4 or H_2SO_4 .

Budic and Hudnik [67] also found that the behaviors of the Cu ionic line (224.70 nm, $E_{sum} = 15.96 \text{ eV}$) differed from other analytes in the phosphoric acid. This result was consisted with the observation of Yoshimura et al. [50]. It is possible, since the Cu II line lies near the ionization limit of Ar (16 eV), that this line is not excited by the same process as other lines. The similar phenomenon was also found when examined the acid effects on manganese lines [47]. This is because their sum of

energies is close to the ionization energy of argon. A charge transfer process is involved in the ionization and excitation of the manganese lines [68]. In addition, Maessen et al. [48] observed that the acid effect for copper atomic line Cu I (324.754 nm) in HCl appeared to be somewhat lower than that for the other elements and only a small effect in nitric acid.

It is worth to note that the T_{exe} value was found to be fairly constant regardless of the addition of KCl or H₃PO₄ [67]. These findings disagree with the observations of Chudinov et al. [49] and Yoshimura et al. [50]. Since no change in n_e and T_{exe} in the plasma was observed when KCl or H₃PO₄ were added, it seems more probable that in this case transportation and vaporization effects predominate on the signal decreases.

Apart from the excitation temperature T_{exe} , the ratio of MgII/MgI (MgII 280.270 nm, MgI 285.213 nm) is more practicable to describe the thermal excitation capability of plasma. Because of the well known characteristics of the two lines (i.e. the closeness of their excitation energies and acceptable accuracy on the statistical weight and transition probability values), this parameter has often been used to evaluate the robustness of the plasma [38, 47, 54, 57, 69-70]. The robustness of the plasma is referred to as the capability to resist the interference on the spectrometric signal when changing the sample matrix. The plasma robust conditions can be reached at high RF power and low carrier gas flow rate, which allows the analytes to have a long time stay in the plasma and enhances the thermal exchange. The ratio of MgII/MgI is normally used to evaluate how far the plasma thermal conditions deviate from the local thermodynamic equilibrium (LET). Fernandez et al. [47] demonstrated that it is possible to identify the origin of the acid interference from the value of the MgII/MgI intensity ratio. To discuss the relationship between the plasma thermal conditions and the MgII/MgI ratio, the instrumental working conditions in that work are listed in table 2.2.

Table 2.2 Operating instrumental conditions and plasma excitation conditions

Condition	Power/kW	Carrier gas	Intermediate	Excitation	Electronic density/cm ⁻³	MgII/MgI
		flow rate/ l min ⁻¹	gas flow rate/l min ⁻¹	temperature/ K		
1	1.08	0.75	0	5100	205 × 10 ⁻¹³	8.5
2	0.91	0.95	0.25	4765	95 × 10 ⁻¹³	4.9
3	0.91	1.00	0.38	4200	62 × 10 ⁻¹³	2.0

From reference [47].

In conditions 1, the MgII/MgI ratio was higher than 8. The plasma worked under the robust conditions. In conditions 3, the MgII/MgI ratio was lower than 4. The plasma worked under the non-robust conditions. Such criteria are valid when the emission is observed laterally.

Fernandez et al. [47] observed that the excitation temperature in ICP could not be changed by the increasing HCl, HNO₃, and H₂SO₄ concentration (< 2.0 M), although the plasma worked under conditions 1 or conditions 3 may lead to significantly different excitation temperatures. They also found that under the conditions 1, the slight decrease in the line intensity could be attributed to a change in the aerosol formation and transport. This result is in a good agreement with the conclusions drawn by Chudinov [49], Yoshimura [50], Budic and Hudnik [67]. However, a different conclusion was obtained for the electron number density. The density remained the same under conditions 1, whereas it was significantly decreased under conditions 3. The decrease was most significant over 0-1 mol l⁻¹ concentration range, which corresponded to the large decrease in ionic line intensities. Although no change in the excitation temperature was observed, there was a variation in the ion-to-atom equilibrium resulting from the change in the electron number density. This was confirmed by the measurement of the Mg II to Mg I line intensity ratio.

The sum of ionization and excitation energy can be written in the form of E_{sum} . During examining the acid effect on the ionic lines under conditions 3, it was found the higher the E_{sum} value, the stronger the effect of acid. The similar phenomena were observed by Maessen et al. [48] and Yoshimura et al. [50]. This confirms that there is a change in the excitation conditions under non-robust conditions.

To minimize the change in the ion-atom intensity ratio arising from the change in excitation temperature, the line pairs of atomic and ionic emissions with nearly equal excitation potentials were chosen [50]. The authors observed that the ion-atom intensity ratio for Ca increased with acid concentration, indicating a decrease in the electron density. Hence, the decrease in electron density increases the population of the ionic species and decrease the population of the atomic species. For Mg, Mn and Zn, the slight decrease in the intensity ratio suggests that the decrease in electron density is insignificant for elements with high ionization potentials. A major contribution to the decline in the intensity ratio may be responsible for the decline in ionization temperature.

Based upon the discussions above, it seems clear that acid effect can be partially contributed to the plasma thermal conditions. Under the robust conditions, there is no significant difference in n_e and T_{exc} between water and acid. Acid influence on the aerosol generation and transport mainly responds to the signal decrease. In this case, acid has the similar interferences on the atomic and ionic lines. Under the non-robust conditions, the reductions in T_{exc} and/or n_e and the dependence of the signal reduction on the E_{exc} and E_{sum} of the ionic line happened. It can also be found that acid effect on atomic and ionic lines are significantly different. Therefore, by means of the ratio of MgII/MgI, it is possible to predict the signal reduction is related to the process before aerosol exiting from spray chamber under the robust conditions. Truly robust conditions imply that the plasma is capable of accepting a change in the concentration of acid matrix without changing plasma conditions such as temperature, electron number density or the spatial distribution of analyte within the plasma. However, for non-robust conditions, it is difficult to distinguish whether changes in the analytical signal originate in the plasma, in the sample introduction system, or both [71]. Higher nebulizer gas flow rates are thought to contribute significantly to local cooling in the plasma central channel due to the passage of larger numbers of incompletely desolvated droplets [72-73].

2.2.7 Influence from desolvating droplets and vaporizing particles

Olesik [20] claimed that atoms and ions produced from small drops, together with vaporizing particles and desolvating drops, can all be in the observation volume. This makes it difficult to gain an accurate understanding of the fundamental processes of the signals production.

For the first group of acid (HNO_3 , HCl , HClO_4), analyte transport is almost constant up to 30% acid concentration under controlled uptake mode, and up to 5% in natural uptake mode [52]. The reduction in the signal to transport ratio indicates a loss of efficiency in the production of analytical signal. Like reported by Fernandez et al. [47], at low concentration, T_{exc} does not change with acid concentration. Also the variations in W_{tot} and T_{exc} values, at low acid concentration (< 5%), are so small that they can hardly explain the extent of the interference. Apparently, this deduction is due to that the energy consumption to atomize the increasing amount of acid is getting higher, thus causing the plasma cooling.

Aerosol desolvation likely occurs during the time when droplet travels from the tip of the center tube to the top of the load coil, although, this time is not the time in the plasma [74]. The gas temperature (which describes the kinetic energy of the argon atoms) likely controls the desolvation of the sample [20]. After desolvation, the larger drops will in turn give rise to larger analyte particles, which will then vaporize more slowly in the atomizer, owing to their reduced surface area-to-mass ratio [22]. Some aerosol drops survive even in the normal analytical zone of the ICP [75-76]. Each drop and vaporizing particle acts as a heat sink that affects a surprisingly larger volume of the plasma [77], and average temperatures in this locally cold region can be more than 1500 K cooler than the surrounding plasma [73].

Fister and Olesik [72] found that there is a direct link between the number of incompletely vaporized droplets and time-integrated vertical atom emission profiles. In particular, the number of droplets is similar at the location of peak time-integrated atom emission intensity, regardless of the robustness of the plasma. It is also true for the ion emission. Radial emission profiles are also affected by the presence of vaporizing aerosol droplets. Normalized atom emission radial profiles high in the plasma are narrower when a vaporizing droplet is present because atom emission is highest near droplets. Normalized ion emission radial profiles low in the plasma are wider and peak off axis when a vaporizing droplet is present, in contrast to narrower, on-axis peaks when no droplet is present. Ion to atom emission intensity ratios appear to be controlled by the fraction of time an incompletely desolvated droplet or cloud of droplet vaporization products is near the observation zone. Time-resolved Ca ion to atom emission intensity ratios vary from 2 to 70 in the normal analytical zone of the plasma. Time-integrated ion to atom emission intensity ratios may be biased by the widely varying time-dependent fluctuations. Other diagnostic measurements, such as excitation temperature, could also be biased.

The energy required to desolvate/vaporize droplets depends on the size of the droplet and the liquid matrix, especially in terms of bond breaking for various matrix species. Also the energy transfer to the central channel is important and can affect the rates of these processes [71]. The same authors claimed that the role of the nitric acid matrix on the analytical signal in the plasma is difficult to predict. There are several important events which contribute to the overall energy consumption. First, the nature of the vaporization/evaporation of HNO_3 from a droplet's surface must be promoted photothermally or by collisions with energetic species in the plasma. Second is the

relative contribution of bond breaking to the overall energy consumption of which the N=O bond (6.1 eV) is the most energetic. Finally, the contribution of the decomposition products to the efficient transfer of energy to the central channel through the production of species with thermal conductivities greater than that of Ar must be considered.

Vaporizing aerosol droplets have a large, local effect on atom and ion emission intensities in the Ar ICP [77]. The vaporization products from individual droplets or heat conduction to the droplet itself affects analyte atom and ion emission intensities from small, previously vaporized and atomized droplets. Ionization and excitation conditions in the region within about one or two millimeters of a vaporizing droplet are different from the regions of the plasma far from a vaporizing droplet. Droplets with original diameters of about 10 μm or larger when exiting the spray chamber produce the observed laser light scattering and emission intensity fluctuations. Droplets with diameters of about 20 μm or larger are incompletely desolvated in the normal analytical zone of a 1.0 kW Ar ICP when the nebulizer gas flow rate of 0.8 l min^{-1} is used.

2.2.8 Acid-caused transient effect

A total different effect connected with the use of acid in plasma is due to the influence exerted by acid on the duration of the pre-nebulizing period required for ensuring steady state conditions. It was called as “adaptation effects” [48]. The duration of the adaptation takes about 5 min to get the steady state conditions. The adaptation effects found for the seven elements and the three acids (HCl, H₂SO₄, and HNO₃) proved to be of the same order of magnitude. The magnitude of the overshoot (or undershoot) and the time dependent drift are dependent on the change in acid concentration. There are a number of possible explanations for the overshoot and consequent drift. There could be a torch equilibration period dictated by new plasma conditions that are imposed by the changing levels of acid matrix. Alternatively, a time dependent change in the transport rate could be responsible. The sample uptake, aerosol generation and transport must be all considered.

In general, the magnitude of the transient effect was similar for most lines under robust conditions [78]. The actual time to reach a steady state may appear to decrease at different rates initially for the given lines; however, the duration of the drift seems to be similar for most lines. This suggests that in general the transient effect is not linked specifically to a given element or line energy; rather it is similar in nature for all analytes. However, the Ar I line shows a more pronounced change than Sr II line in acid

transient effect. Although the changes in the local conditions can be minimized through the judicious choice of operating conditions, the effect cannot be completely eliminated. It also indicates that the difference must be due to changes in the sample introduction system such as the tertiary aerosol size distribution and transport rate.

There are two important results for ICP-MS [78]. First, the magnitude of the transient effect is proportional to the change in acid concentration, consistent with the emission measurements. Second, the magnitude of the transient effect seems to be most severe at the lowest nebulizer gas flow rate. This may be related to a longer aerosol residence time in the spray chamber at a lower nebulizer gas flow rate or dependence on the aerosol drop size. Transport rate measurements confirm an increase in the amount of analyte delivered to the plasma when the acid matrix is switched from high to low acid concentration whereas tertiary aerosol volumetric flux measurements seem to indicate a decrease in the total liquid aerosol volume transported to the plasma. This strongly suggested that the analyte is more concentrated in the aerosol, consistent with more extensive aerosol desolvation in the spray chamber.

Stewart and Olesik [78] proposed a physics model to elucidate the transient effect. It is related to the aerosol evaporation process in the spray chamber. There are two sources of water vapor: (1) evaporation from the solution layer on the walls of the spray chamber and (2) evaporation from aerosol droplets. The extent of droplet evaporation will be linked to the relative extent of solution evaporation from the spray chamber walls. Further, the relative contributions of water vapor from aerosol droplet evaporation versus the liquid on the spray chamber walls will be controlled by the relative acid concentrations. In theory, when the droplets enter a drier environment, smaller droplets have a greater relative evaporation. The transport efficiency of these smaller, more concentrated droplets probably increases, resulting in more analyte reaching the plasma per unit time and a net increase in the analytical signals. It is most likely that the larger droplets are not significantly affected by the evaporation and that their main influence is to change the composition of the liquid on the walls which controls the relative water evaporation equilibrium. The opposite effect can be rationalized for a spray chamber conditioned with a low acid matrix where larger more diluted aerosol particles are delivered to the plasma due to a decrease in the droplet evaporation rate and perhaps further hydration of droplets. The authors have proven this model by a series of carefully designed experiments. Furthermore, the transient effects are not necessarily linked to acids. A change in solution matrix that affects the water

vapor pressure will produce the effect. That is the transient effect is due to the evaporation equilibrium between the solution layer and the aerosol in the spray chamber.

2.3 Other influences from acids

In the study of some effects of low acid concentrations on the ICP-OES signals, Marichy et.al., [46] found that the enhancement effect of dilute HCl (below 1%) cannot be explained by any physical change in the aerosol characteristics (droplets size distribution, nebulizer and transport efficiency) but rather by a variation of the chemical properties of the aerosol as a strong decrease in the acid concentration was observed and consequently, a change in the anion concentration.

Mineral acid suppressions on mercury spectrometric signal have been examined for HCl, HNO₃, HClO₄, H₂SO₄ and H₃PO₄ at the concentrations lower than 1 mol l⁻¹ [6]. The acid effects could also be divided into two groups. The first group includes HCl, HNO₃, HClO₄. The second group includes H₂SO₄ and H₃PO₄. The mercury signal suppression by H₂SO₄ and H₃PO₄ were more severe than by the first group acids in the forced aspiration mode and robust plasma. Under such conditions, acid effect on aerosol generation and transport seems not so important. However, nitric acid suppressed mercury signal significantly. The plasma thermal conditions could not be significantly changed by nitric acid in such low concentration. This phenomenon could not be explained by the higher first ionization potential of mercury, because As and Zn (also with higher first ionization potentials) did not show the same suppressions. Therefore, this element-dependent acid effect should be related to the chemical properties of the element itself. The authors suggested that an accurate mercury result can be obtained by acid matrix matching method, standard addition method, or mathematically corrected external calibration method.

The rare earth elements (REEs) exhibit similar physical and chemical properties. It could be expected that a change in acid concentration would lead to an identical behavior of the REEs. However, in the study of nitric and hydrochloric acids influences on the ICP-AES relative signal intensities for (REEs), Brenner et al. [79-80] observed that, with a single REE property such as the ionization energy, the excitation energy, the oxide bond strength, the melting and boiling points could not explain the depressive effect. This suggests that the total energy to bring a REE from the molecule to the excited state of an ion (including the oxide bond strength, ionization energy, and

excitation energy) should be taken into account. With the application of a principal component analysis (PCA), they [80] succeeded to group the different elements by taking into consideration parameters such as oxide bond strength and ionization energy. In addition, this grouping is in good agreement with the so-called small periodic system of the REE group. Their results showed that the slight difference in their ionization energy and oxide bond strength is sufficient to differentiate their behaviors to a change in nitric acid concentration. It should be noted that, although the excitation energy has to be taken into account, this parameter did not play a role in the acid effect as lines of Ce with different excitation energies provided similar results [79]. As both the oxide bond strength and the ionization energy are involved in the acid effect, it suggests that the presence of a high nitric acid concentration results in a change in the dissociation and atomization efficiency. These conclusions indicated that the acid effect is more complicated than what we have known.

2.4 Easily ionizable element (EIE) effects

Kalnicky and coworkers [81] measured the radial profile of T_{exe} for Fe I at three observation heights, with and without the presence of an easily ionizable element (6900 $\mu\text{g}/\text{ml}$ Na). Their observations showed that the large amount of sodium did not change T_{exe} under the commonly used operating conditions. Cesium, which severely affects on combustion flames and the dc arc, has minor influences on T_{exe} [82].

The total dissolved solids, normally relates to the easily ionizable elements, lead to severe matrix interference on the inductively coupled plasma mass spectrometric signals. Vandecasteele et al. [83] observed that the signal suppression by NaCl is mass dependent. For human serum sample, the dissolved salts mainly are the easily ionizable elements such as Na, Mg, K and Ca. Those ions (approximately 10 g l^{-1}) are most likely contribute to the suppression. The authors found that, for 4 g l^{-1} of NaCl, the suppression increased with increasing mass number, from 33% for Li to 56% for U. It is obvious that not every element can be used as an internal standard, and several such internal standards over the mass range must be used.

The suppression on the mass spectrometric signal is more pronounced for the elements with higher ionization potentials. Mercury has received a lot of attentions on such a study. On determining organomercury in biological reference materials, Beauchemin et al. [84] observed more noisy mercury signals due to the high

concentration of the total dissolved solids. Also the mercury signal was suppressed by a factor of about 8 by concomitant elements in the samples. In a relevant work [85], the absolute minimum detectable amount (MDA) of ICP-MS for mercury extracts was estimated to be 10 times worse than that for aqueous solutions run under flow injection. This was resulting from mercury signal suppression due to the presence of excessive concentrations of concomitant substances (e.g. about 4% sodium).

Shum et al. [86] observed that the dilution for urine samples minimized the matrix effect of Na on Hg signals. The chromatography results showed that the sensitivity for Hg^{2+} was similar to that obtained for the Hg species in the simple aqueous solution. However, the sensitivities for MeHg^+ and EtHg^+ were reduced by a factor of 2 in the urine matrix. In that chromatographic condition, Hg^{2+} eluted without Na^+ , but MeHg^+ and EtHg^+ eluted with Na^+ . Therefore, the diminished signal was due to matrix suppression from Na (≈ 1000 ppm Na).

Many easily ionizable elements, such as Li, from salts that are more volatile than those of calcium and many other analytes [87]. The spatial emission patterns of Ca I and Ca II in an ICP are altered when an easily ionizable element is added to a sample solution. The EIE effect was investigated by two-dimensional lateral mapping of Ca atomic and ionic emissions by means of a monochromatic imaging spectrometer. Lithium served as the EIE at added concentrations from 0 to 1000 $\mu\text{g/ml}$. The resulting Ca radial emission image displayed in most regions a linear change in intensity with Li concentration. Because the added EIE often constitutes the bulk of the solute mass, it will affect markedly the rate or even mechanism of solute-particle vaporization. In turn, the more rapid vaporization of Li salt, or the consequent break-up of solute particles would yield an overall vaporization process that begins lower in the plasma. As the resulting analyte-containing vapor cloud travels upward through the plasma, its volume increases by diffusion; the temporally integrated emission will therefore appear to have a “V”-shape. Consequently, a vapor cloud that is larger and more dilute, and the “V” will have moved downward.

Hobbs and Olesik [88] stated that the extent of the EIE matrix effects on ionization and ion excitation was more severe near an incompletely desolvated droplet or vaporizing particle than away from a droplet or particle. This is consistent with lower temperatures and electron number densities as well as higher analyte and matrix species concentration near an incompletely desolvated drop or a vaporizing particle. Depressions in analyte ion number densities due to the presence of the EIE were, by a

factor of two to three, more severe near an incompletely desolvated drop or a vaporizing particle than when no droplet or particle was in the observation volume. Near a droplet or particle there was a shift in the relative number of ions and atoms towards atoms due to the EIE. However, the numbers of analyte ions and atoms were depressed by the EIE near and away from a droplet or particle. Away from a droplet or particle, ionization was either not affected by the EIE or appeared to shift slightly towards ions. Ion excitation was enhanced by a factor of two to three near a droplet or particle due to the EIE, but changed little away from a droplet or particle. Atom excitation was similarly enhanced by the presence of the EIE, whether or not a droplet or particle was nearby. This kind of effect may be more severe in ICP-MS than in ICP-OES, because the analyte ion concentrations were depressed more severely near droplets and particles than emission intensities, due to the presence of EIE.

The effect of sodium on the intensity of ionic lines in ICP-AES has been studied under extreme operating conditions, especially under robust conditions [89]. The effect was assigned both to a change in the excitation and ionization processes in the plasma and to a change in the aerosol formation and transport. Some ionic lines were very sensitive to the Na effect, particularly lines with an energy sum E_{sum} near 11.5 eV. It was considered that argon-metastable atoms ionized the analytes through Penning ionization reaction. Use of robust conditions, including a large injector bore, makes it possible to minimize the Na effect due to the plasma and to assess the contribution of the aerosol formation and transport. This is similar to the conclusion reached for the acid effect.

To end the discussions in this chapter, it must be stressed that all the subjects mentioned above are the physical processes and physical properties about the acid effect and easily ionizable element influence on the signal intensity of plasma-based spectrometry. A lot of attentions have been paid to the acid influences on (1) the liquid aspiration; (2) aerosol generation, transport, and characterization; (3) interactions between aerosol and plasma. Among all the publications available, there is no paper clearly described the chemical processes in the plasma or chemical interaction with the plasma. However, in some instances, acid effects on the spectrometric signal intensities are obviously related to the chemical properties of the acids, especially related to the chemical properties of the elements involved. It has been proven experimentally and theoretically that droplets and particles can survive and pass through the central channel

of plasma. The non-spectroscopic matrix effects often happen around those droplets and particles. Unfortunately, we are lack in the knowledge about the real temperature of the droplets and particles, about their thermal exchange efficiency in the plasma. Overbelieve in the high temperature of plasma is unwise. It is the time to turn our views on the chemical interference on the signal intensity of plasma-based spectrometry.

To uncover the chemical interference on spectrometric signal intensity, some high reduction potential elements of mercury, gold, and platinum group elements were employed. They are useful to examine the redox equilibrium and complex formation equilibrium in the central channel of plasma. In addition, the acid effect on the stable constant of complex formation equilibrium may indicate the neutralization equilibrium. Comparing with inductively coupled plasma, the use of high power microwave induced plasma may give more information about the aerosol behavior in the central channel of plasma.

3 Experimental

3.1 Chemicals

Nitric acid, (65%, p.a.), Merck, No. 456. (distilled in a sub-boiling all-quartz distillation unit produced a purified, 14.5 mol dm^{-3} nitric acid).

Nitric acid, (65%, GR), Shanghai Chemicals Corporation, Shanghai, China.

Hydrochloric acid, (30%, Suprapur[®]), Merck, No. 1.00319.

Hydrochloric acid, (36%, GR), Shanghai Chemicals Corporation, Shanghai, China.

Hydrobromic acid, (47%, suprapur[®]), Merck, No. 306.

Hydriodic acid, (67%, p.a.), Merck, No. 100341.

Mercury dinitrate Titrisol[®] solution, (in dilute nitric acid), Merck, No. 9916. (for preparing 1000 mg cm^{-3} mercury standard solution), used at Graz University, Austria.

Mercury dichloride, (purity: HgCl_2 , 99.5%), used at Xiamen University, China.

Mercury dichloride, (purity: sublimed), used at Duisburg University, Germany.

Gold standard, (spectrum-pure, $1.00 \text{ mg Au cm}^{-3}$ in 10% HCl).

ICP-MS multielement standard C, (ICP/MS Standard III, contains $10 \text{ } \mu\text{g cm}^{-3}$ Au, Pt, Ir, Pd, Rh, Ru in 10% HCl), Innovative Laboratory, Lot # 704315.

Potassium chloride, (p.a.), Merck, No. 4936.

Potassium bromide, (Uvasol[®], for spectroscopy), Merck, No. 4907.

Potassium iodide, (Suprapur[®]), Merck, No. 105044.

Sodium chloride, (p.a.), Merck, No. 1.06404.

$\text{In}_2(\text{SO}_4)_3 \cdot 5 \text{ H}_2\text{O}$, (cryst, >98%), Fluka, No. 57161.

Ammonium nitrate, (AR), Shanghai Chemicals Corporation, Shanghai, China.

Tin(II) chloride dihydrate, (AR) Shanghai Chemicals Corporation, Shanghai, China.

Sodium borohydride, (p.a., for CVAAS), Fluka, No. 71321.

Indium internal standard solution (1.0 mg dm^{-3}), prepared by dissolving 0.0529 g $\text{In}_2(\text{SO}_4)_3 \cdot 5 \text{ H}_2\text{O}$ into 20 cm^3 $0.0145 \text{ mol dm}^{-3}$ nitric acid solution.

Reductant solutions for mercury cold vapor generation:

- (1) A 3% SnCl_2 in 15% HCl (v/v) solution, for mercury cold vapor generation ICP-OES, was prepared daily from tin(II) chloride dihydrate.
- (2) A 0.1% NaBH_4 in 0.1% NaOH (w/v) solution, for mercury cold vapor generation MIP-OES, was prepared daily from sodium borohydride

Leaching solution, prepared by dissolving 1.0 cm³ HNO₃ and 3.0 cm³ HCl into pure water and made the final volume to 100 cm³.

High-purity water, (18.2 MΩ cm), obtained with a Milli-Q water purification system (Millipore, Bedford, MA, USA) or a NANOpure water purification system (Barnstead, Boston, USA).

Chinese human hair certified reference material GBW-09101, produced by Shanghai Institute of Nuclear Research, Academia Sinica, Shanghai, China.

Dogfish muscle certified reference material DORM-2, produced by National Research Council of Canada, Ottawa, Canada.

3.2 Instrumentation

3.2.1 Inductively coupled plasma quadrupole mass spectrometer (ICP-MS)

A Plasma Quad 2 Turbo Plus inductively coupled plasma mass spectrometer (VG Elemental Ltd., Winsford, Cheshire, UK) was equipped with a Gilson-Minipuls-3 peristaltic pump, a Meinhard concentric glass nebulizer (type TR-30-A3), a water-jacketed, Scott double pass spray chamber, and a Fassel-type torch. The spray chamber was kept at 2 C°.

For mercury measurement, the operating conditions were: rf frequency 27.12 MHz; rf power 1350 W; reflected power < 5 W; plasma gas 13.5 dm³ min⁻¹; auxiliary gas 0.9 dm³ min⁻¹; nebulizer gas ~ 1.0 dm³ min⁻¹, sampling depth 14 mm, solution uptake rate 1.40 cm³ min⁻¹, instrument response optimized daily on the signal for ¹¹⁵In. The transient signals of isotope ²⁰²Hg were monitored.

For precious metals measurement, the operating conditions were: rf power 1350W; reflected power < 1 W; plasma gas 13.5 dm³ min⁻¹; auxiliary gas 0.9 dm³ min⁻¹; nebulizer gas 0.7 dm³ min⁻¹ (with a mass flow controller); The isotopes of 197, 195, 193, 106, 103, 102, were monitored for Au, Pt, Ir, Pd, Rh, and Ru, respectively. The standard solution uptake rate was 1.0 cm³ min⁻¹.

3.2.2 Inductively coupled plasma optical emission spectrometer (ICP-OES)

A sequential spectrometer ICP 2070 (Baird Corp. MA, USA) was equipped with a peristaltic pump, a Meinhard concentric glass nebulizer, a donut-shaped spray chamber [19], or a Scott double pass spray chamber, and a low flow torch. The operating conditions were: rf frequency 40.68 MHz; rf power 1350 W; reflected power < 1 W;

plasma gas $11.5 \text{ dm}^3 \text{ min}^{-1}$; auxiliary gas $0.75 \text{ dm}^3 \text{ min}^{-1}$; nebulizer gas $\sim 1.0 \text{ dm}^3 \text{ min}^{-1}$; solution uptake rate $1.40 \text{ cm}^3 \text{ min}^{-1}$; observation height 14 mm above the load coil. The wavelength calibration of the sequential spectrometer ICP 2070 was routinely performed with the argon atomic line at 415.859 nm after the plasma was initiated and warmed up for about 20 min. The data were collected in transient mode (two points per second) for monitoring the aspirating procedures at Hg II 194.164 nm, and in sequential read-out mode (integration time: $10 \text{ s.} \times 4$) for recording the steady signal at both Hg II 194.164 nm and Hg I 253.652 nm.

3.2.3 Simultaneous introduction for mercury cold vapor and acidified aerosol into inductively coupled plasma

The nitric acid solutions in certain concentrations were nebulized with a Meinhard nebulizer and introduced into the donut-shaped spray chamber. Meanwhile, mercury solution ($0.100 \text{ mg Hg dm}^{-3}$) and the reductant were inputted separately with a peristaltic pump at the rate of $1.4 \text{ cm}^3 \text{ min}^{-1}$. After merged in a mini T-piece, the mixture was swept into donut-shaped spray chamber by an argon flow ($0.15 \text{ dm}^3 \text{ min}^{-1}$). The gas-liquid separation was accomplished in the spray chamber. The waste was quickly drained out. Mercury cold vapor together with the acidified aerosol was brought into the plasma.

3.2.4 High power microwave induced plasma optical emission spectrometer (MIP-OES)

A laboratory-constructed high power induced plasma optical emission spectrometer was equipped with a peristaltic pump, a Meinhard concentric glass nebulizer, a donut-shaped spray chamber, and a hand-made quartz torch with an injector of aluminum oxide. The operating conditions were: rf frequency 2.46 GHz; rf power 408 W; reflected power $< 25 \text{ W}$; plasma gas $2.75 \text{ dm}^3 \text{ min}^{-1}$ (with a mass flow controller); nebulizer gas $0.9 \text{ dm}^3 \text{ min}^{-1}$ (with a mass flow controller); solution uptake rate $0.20 \text{ cm}^3 \text{ min}^{-1}$. The emission was axially focused onto the end of a light fiber, by which the emission signal was transferred into the spectrometer. The wavelength calibration was routinely performed with mercury lamp inside the spectrometer. The data were collected in the transient mode (two points per second) for monitoring the aspirating procedures at Hg I

253.652 nm. The steady signal intensity of mercury was acquired at Hg I 253.652 nm (integration time: 6 s. \times 20).

3.2.5 Laser unit

The transient acid effect on the aerosol properties and mercury emission signal intensity was examined with the laser light scattering method. The laser unit HeNe-Laser 25-1.2 (Spindler & Hoyer, Göttingen, Germany) was used for this purpose. The typical power output is 1.2 mW. The maximum power output is 5 mW. The wavelength is 632.8 nm. The beam diameter is 0.6 mm. The beam divergence is 3 mrad. The angle between the injecting laser beam and the horizontal line was in 60 degree. The torch was mounted horizontally and connected with the donut-shaped spray chamber with a glass-made elbow adapter. The laser beam crossed the biggest diameter of the glass tube adapter which part is concentric to the torch inject. The scattering light that went through the injector tube was focused onto the end of the light fiber. The scattering light intensity was monitored at 632.8 nm.

3.2.6 Microwave digestion system

3.2.6.1 Sample digestion for mercury determination with ICP-MS

To verify the method for mercury determination with ICP-MS, the reference material of Chinese human hair GBW-09101 was digested with MLS-1200 MEGA microwave digestion system (Milestone, Germany). An aliquot (~200 mg) of the Chinese human hair weighed to 0.1 mg was transferred into a pre-cleaned, 120 cm³ Teflon digestion vessel. After addition of 14.5 mol dm⁻³ distilled HNO₃ (2.50 cm³) and 30% H₂O₂ (0.50 cm³), the vessel was closed and kept at room temperature for 15 min. Six similarly loaded vessels were placed into the microwave oven, and the 9-step digestion program started (time in min, power in W): 2, 250; 0.5, 0; 10, 250; 0.5, 0; 5, 450; 0.5, 0; 3, 600; 7, 500; 2, 0 for cooling within the microwave oven. The vessels were further cooled with flowing tap water for 30 min in the cooling unit and then opened carefully. The digests were transferred into 50 cm³ volumetric flasks. The flask was filled to the mark with NANOpure water. Each of these diluted digests was divided into four parts. They were added with 0.2 cm³ HCl, 0.5 cm³ HCl, 0.2 cm³ HBr, and 0.5 cm³ HBr, respectively. Then they were directly measured with external standard calibration method.

3.2.6.2 Sample digestion for mercury determination with MIP-OES

To verify the cold vapor generation method for mercury determination with high power microwave induced optical emission spectrometry, Dogfish muscle tissue DORM-2 was taken as the certified reference material. It was digested with Mars-5 microwave digestion system (CEM Corporation, Lintfort, Germany). An aliquot (~300 mg) of the Dogfish muscle tissue weighed to 0.1 mg was transferred into a pre-cleaned, 100 cm³ Teflon digestion vessel. After addition of concentrated HNO₃ (3.0 cm³) and 30% H₂O₂ (1.0 cm³), the vessel was closed and kept at room temperature for 15 min. Then six similarly loaded vessels were placed into the microwave oven, and the 3-step digestion program started (see Table 3.1). After then, the system was naturally cooled down within the microwave oven. The digests were transferred into 50 cm³ volumetric flasks. The flask was filled to the mark with Milli-Q water. Each of these diluted digests was divided into four aliquots of the exactly 10 cm³ sample solution, respectively. The standard addition calibration method was employed to measure mercury in the digests of certified reference material DORM-2. In this way, 50, 100, and 150 mm⁻³ mercury standard solution, which contained 5.0 mg dm⁻³ Hg, were added into each of 10 cm³ sample solutions, respectively. The reductant solution was prepared by dissolving 0.1 g sodium borohydride into 0.1% NaOH solution. The sample solution and the reductant solution were aspirated by the peristaltic pump. After these two solutions merged and reacted in a Teflon-made mini T-piece, the mixture was nebulized with a concentric nebulizer and the released mercury vapor was forced into the microwave induced plasma.

Table 3.1 Microwave digestion program for DORM-2

Step	Power (W)	Input (%)	Ramp (min)	Temperature (C°)	Hold time (min)
1	600	60	4	80	3
2	600	80	3	120	3
3	600	100	2	170	10

4 Results and discussion

4.1 Nitric acid inhibition on mercury compounds dissociation in inductively coupled plasma source spectrometer

Generally, the toxic element mercury is present at very low concentrations in the atmosphere, hydrosphere, lithosphere, and biosphere. Mercury emissions from natural sources exceed anthropogenic emissions, for instance, by coal or oil fired electric power plants, by alkali chloride and polyvinyl chloride plants, and through agricultural use of organic mercury compounds [90]. To monitor mercury in the environment, several reliable analytical methods such as cold-vapor atomic absorption spectrometry (CVAAS) [91], cold-vapor atomic fluorescence spectrometry (CVAFS) [92], and gas chromatography with electron capture detection (GC-ECD) [93] are available. These methods have low detection limits for mercury, but lack the capability for the simultaneous determination of other trace elements.

Inductively coupled argon plasma mass spectrometry (ICP-MS) valued for its multielement capability and its excellent detection limits (< 0.01 mg/L for many elements including mercury) could be the method of choice for the determination of mercury and many other elements. Whereas many other elements were and are routinely quantified by ICP-MS in biological and non-biological samples, mercury was determined only occasionally. The study of the relevant literature raises the suspicion that mercury is difficult to determine accurately by ICP-MS under routine operating conditions.

Reports claim that the thermal ionization of mercury, an element with the high first ionization potential of 10.44 eV, is suppressed by easily ionizable elements (EIEs) when they present at high concentrations [83-86]. Mercury determinations are influenced by high concentrations of dissolved solids and very likely by the ratio of inorganic to organic mercury compounds in the sample solutions. Mineralization, a necessary pretreatment for the determination of mercury by liquid sample introduction, is often carried out in closed vessels with microwave-assisted heating to prevent losses of mercury or its compounds. However, when cod muscle was digested with $\text{HNO}_3/\text{H}_2\text{O}_2$ in a closed microwave system and mercury was then determined in the sample solution by ICP-MS and CVAFS, the ICP-MS concentrations based on an external calibration

curve established with mercury dinitrate were only half of the CVAFS concentrations. The quantification of mercury by standard addition (solutions of mercury dinitrate) with ICP-MS gave results in agreement with CVAFS, only when the sample had been spiked approximately 12 h before the digestion in a closed microwave system [92]. When cod muscle was mineralized with a microwave system in open vessels and mercury determined by ICP-MS (external calibration with mercury dinitrate) [94], only 86% of the certified concentration was found in the digest obtained with $\text{H}_2\text{SO}_4 / \text{HNO}_3 / \text{H}_2\text{O}_2$ and 78% with $\text{HNO}_3 / \text{H}_2\text{O}_2$. Recently, accurate determinations of mercury were reported by slurry sampling electrothermal vaporization ICP-MS [95], flow injection ICP-MS [96], and isotope dilution ICP-MS [97]. Most of these procedures are rather complicated compared to pneumatic nebulization into an inductively coupled plasma and are not well suited for routine application. In the laboratory of the Institute for Analytical Chemistry (University Graz, Austria), mercury determinations with ICP-MS in standard reference materials after microwave digestion in closed vessels always gave concentrations at most 75% of the certified values [98]. After examining the effect of the possible matrix in digest, such as mineral acids, they proved that the unmatched nitric acid concentrations between the sample digest and the external standard calibration solutions are responsible for the failure to reproduce the certified concentrations. Then they developed a procedure yielding results in agreement with the certified value [6].

Acid effect on the inductively coupled plasma emission and mass spectrometric signal intensity has been discussed in many aspects (see Chapter 1). In general, acid effects can be attributed to the interference on (1) liquid aspiration; (2) aerosol generation and transport; (3) plasma thermal conditions. The first two cases are mainly related to the physical properties of acid solutions. The third one is often rely on the plasma working parameters. Under the robust conditions, the plasma is capable to resist acid disturbances on its thermal conditions. Acid influence on the aerosol formation and transport are mainly responds to the signal decrease. Under the non-robust conditions, the reductions in T_{exc} and/or n_e and the dependence of the signal reduction on the E_{exc} and E_{sum} of the ionic line happened. It can also be found that acid effect on atomic and ionic lines are significantly different. In this case, it is difficult to distinguish whether changes in the spectrometric signal originate in the plasma, in the sample introduction system, or both.

When examining mineral acid effect on mercury signal intensities, the ICP-MS system was running under the so-called robust conditions [6]. The acid concentration ranged over 0-0.8 mol dm⁻³. The physical properties of standard solutions, such as the viscosity, surface tension and the density, were not changed too much. Therefore, the suspicion on the acid effect on mercury signal intensity should have been ruled out. However, mercury signal intensities were suppressed more significantly than other elements over low nitric acid concentrations. Under the same experimental conditions, the signal intensities of high ionization potential elements, Zn and As, were not changed so much with the changing HNO₃ concentration and there was also no significant amount of easily ionizable elements (< 0.01% w/w) in those Hg²⁺ standard solutions. Obviously, mercury signal suppression is not directly related to the ionization for the high first ionization potential. Instead, the chemical properties of mercury and its compounds were considered to be in charge of the mercury signal depression in plasma. So far there is not a satisfactory explanation on the low mercury recoveries when ICP-MS and pneumatic nebulization technique is used. In this chapter, nitric acid effect on mercury signal intensity will be discussed as chemical matrix influence in inductively coupled plasma.

4.1.1 Procedures

4.1.1.1 Monitoring the time-resolved signals for ICP-MS

Mercury working solutions (20 µg dm⁻³ Hg) were prepared in water, 0.00075, 0.15, 0.30, 0.45, 0.60, and 0.75 mol dm⁻³ HNO₃ matrixes. The transient signal of isotope ²⁰²Hg was monitored to examine nitric acid influence. The solution aspiration schedule was: 0-120 sec., blank nitric acid solution; 121-420 sec., mercury working solution in the same nitric acid matrix; and 421-600 sec., the leaching solution, which has been proved can efficiently wash out the memorized mercury that accumulated in sampling system.

4.1.1.2 Acquisition for mercury optical emission signals

Both Scott-type spray chamber and donut-shaped spray chamber were used. Mercury working solutions (1.00 mg Hg dm⁻³) were prepared in water, 0.00004, 0.001, 0.002, 0.004, 0.006, 0.008, 0.010, 0.015, and 0.020 mol dm⁻³ HNO₃ matrix. To eliminate the uncertain signals arose from the wavelength drift, data were acquired with monochromator wavelength scan mode. A mean of emission intensity came out of five

individual peak heights (at 194.2 nm or 253.7 nm). Those data were used to examine the possible influences of rf power and the spray chamber structure. Time-resolved signal was monitored at Hg II 194.2 nm. The aspiration schedule was: two-minute equilibrium with blank HNO₃ solution; 0-240 sec., mercury working solution in the same nitric acid matrix; and 241-420 sec., leaching solution for washing out the memorized mercury.

4.1.1.3 Simultaneous introduction of mercury cold vapor and acidic aerosol into plasma

The nitric acid solutions in certain concentrations were nebulized with a Meinhard nebulizer and introduced into a donut-shaped spray chamber. Meanwhile, mercury solution (0.100 mg Hg dm⁻³) and the reductant were aspirated separately with a peristaltic pump at the rate of 1.4 cm³ min⁻¹. After merged in a mini T-piece, the mixture was swept into donut-shaped spray chamber by an argon flow (0.15 dm³ min⁻¹). The gas-liquid separation was accomplished in the spray chamber. The waste was quickly drained out. Mercury cold vapor together with the aerosol was brought into plasma.

4.1.2 Nitric acid influences on mercury mass spectrometric signals

To get a fundamental understanding of nitric acid influences on mercury ICP-MS signal, the time-resolved signal of isotope ²⁰²Hg was monitored in the whole aspiration process. At the beginning, blank solution in certain HNO₃ concentration was aspirated to get the background signal. Then, mercury working solution in the same HNO₃ matrix was immediately switched on. The monitoring plots clearly show that the steady state signal intensities decreased gradually with the increasing HNO₃ concentrations (see Fig. 4.1.1). There is an exception that the lowest signal response came out of the non-acidified mercury standard solution. The monitoring plot shows that it is difficult to reach the invariable mercury signal intensity in the limited monitoring period. When HNO₃ changed from 0 to 0.00075 mol dm⁻³, mercury signal intensity increased vigorously. However, similar to the monitoring plot of non-acidified mercury standard solution, it was still difficult to obtain the invariable signal intensity in the limited monitoring period.

When the leaching solution was nebulized, a sharp peak appeared immediately after the invariable mercury signals. The peak height decreased with the increasing HNO₃ concentration in mercury standard solutions. That indicates that mercury accumulation

in the sampling system depends on the nitric acid concentration of mercury standard solution. It seemed that mercury dinitrate in aerosol was partially reduced as mercury (b.p. 356.73 C°) and adsorbed onto the tip wall of injector before it went into plasma. It led to the inconstant amount of mercury and/or compounds was fed into plasma in the unit time. However, to ignore the possibility of mercury dinitrate adsorption onto the inner surface of the pumping tube, nebulizer, and the spray chamber is completely wrong. When mercury adsorption and evaporation reached the equilibrium, signal became stable. The thermal dissociation of mercury dinitrate is governed by HNO₃ in the standard solution. The higher the HNO₃ concentration, the more serious the inhibition. In the case of non-acidified mercury solution, mercury adsorption was far from the equilibrium. Large amount of mercury was adsorbed onto the tip wall of the injector. As a result, mercury population in the plasma central channel was greatly reduced. After introducing the leaching solution, the adsorbed mercury was quickly released and produced the largest peak.

At the beginning, the leaching solution is nothing but a dilute acid mixture. However, when this aerosol passes by the injector, it is concentrated through desolvation and acts as *aqua regia*. The adsorbed mercury was then oxidized and released as mercury dichloride (b.p. 304 C°) into the plasma. Nitric acid (1%, v/v) could not quickly wash out the memorized mercury [6].

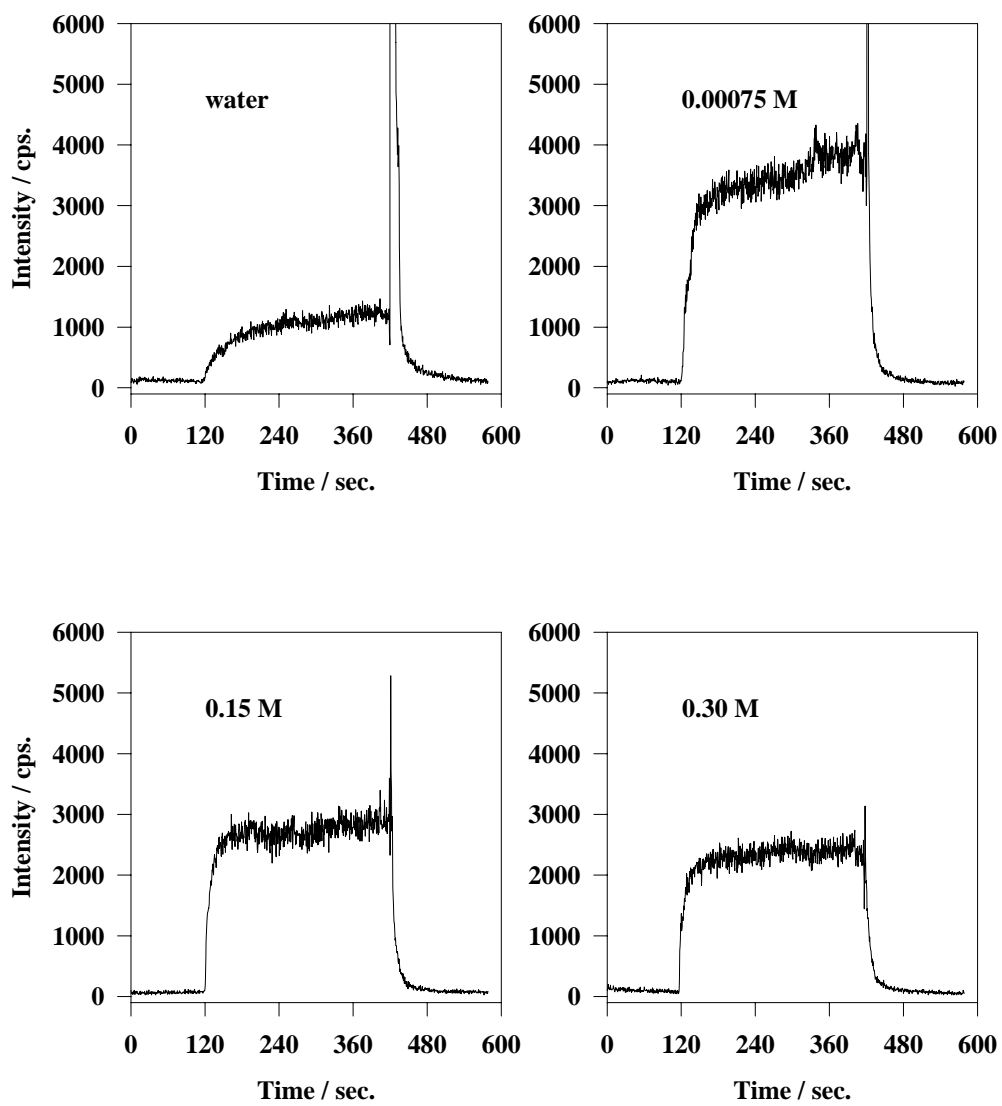


Fig. 4.1.1a. The transient mass spectrometry signals of mercury at m/z 202 in different nitric acid solutions. The concentration of $\text{Hg}(\text{NO}_3)_2$ is $20 \mu\text{g dm}^{-3}$ Hg.

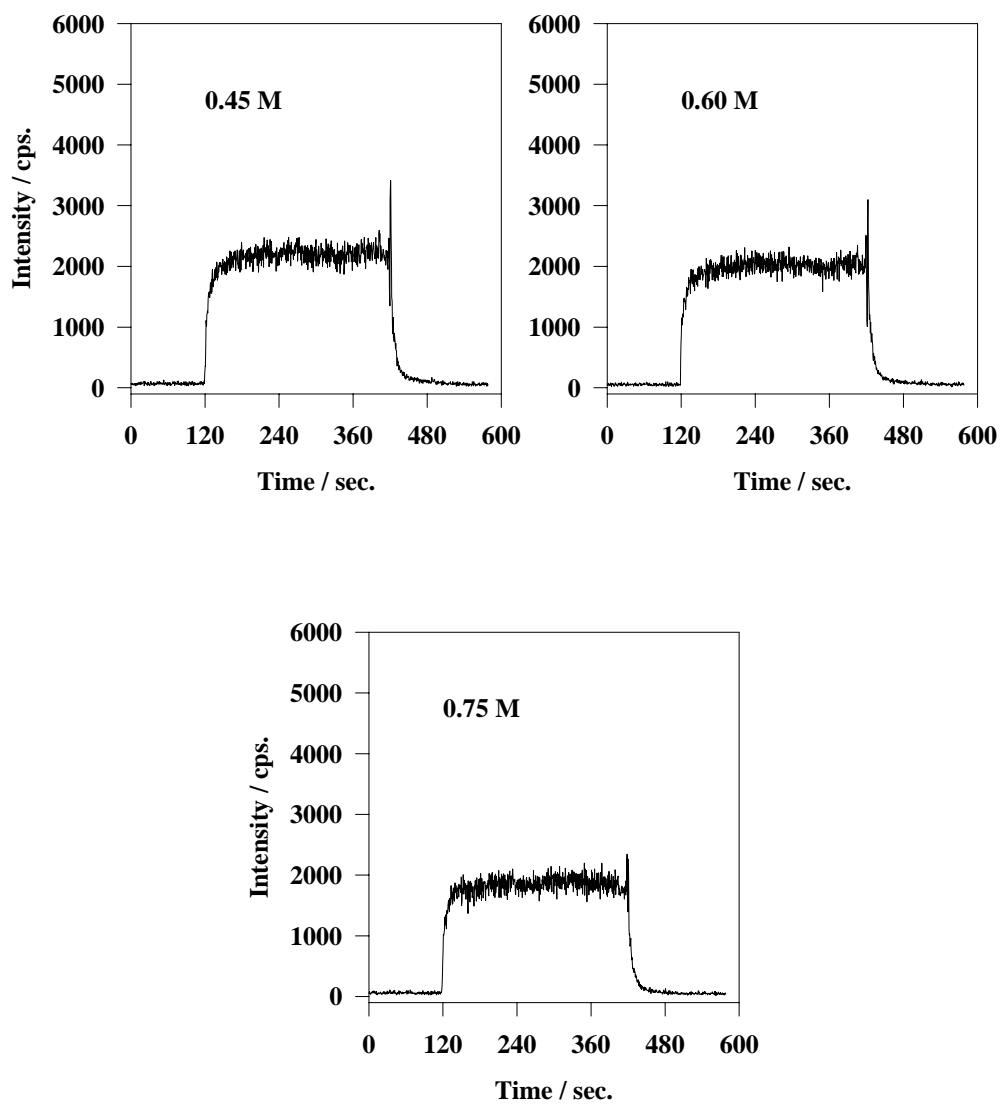


Fig. 4.1.1b. The transient mass spectrometry signals for mercury at m/z 202 in different nitric acid solutions. The concentration of $\text{Hg}(\text{NO}_3)_2$ is $20 \mu\text{g dm}^{-3} \text{Hg}$.

4.1.3 Nitric acid influences on mercury transient signal of ICP-OES

Mercury emission signals at 194.2 nm were monitored with Monochromator ICP 2070 (see Fig. 4.1.2). To start a sampling-rinsing circle, a blank nitric acid aqueous solution was aspirated for two minutes. After switching on the monitor, mercury working solution in the same HNO₃ matrix was aspirated immediately. As found in ICP-MS, except the non-acidified solution, the invariable mercury signal intensity decreased drastically with the increasing HNO₃ concentration and no longer changed when HNO₃ concentration was higher than 0.004 mol dm⁻³. The highest mercury signal intensity was observed in 0.00004 mol dm⁻³ HNO₃ matrix, which was slightly higher than observed in water. The aspiration of mercury working solution was held for 3 minutes. Then, the leaching solution was aspirated. When washout started, a broad peak with a sharp leading edge emerged instantly. It took long time to wash out the memorized mercury which constructed in the sampling system. Similar signal response was also observed with a Scott-type spray chamber. Mercury adsorption is related to the HNO₃ concentration in solution. As expected, the non-acidified mercury solution suffered from the most serious memory effect and brought about the highest washout peak. However, when mercury standard solution contained only 0.00004 mol dm⁻³ HNO₃, the peak height and area were reduced significantly. When nitric acid concentration in mercury solution was higher than 0.004 mol dm⁻³, mercury signal could not be distinguished from the washout plot. It indicated that there was no mercury memory in the sampling system.

It is easy to confirm that mercury memory is related to the mercury adsorption onto the inner surface of torch injector. After aspirating a neutral mercury standard solution, no matter how long the washout performed, the memorized mercury bled continually and it seemed impossible to reach the original background (see Fig. 4.1.2). Provided that the memory is only related to mercury compounds adsorption onto the inner surface of the pumping tube, the washout should be more quick and efficient for the direct contact between the leaching solution and the tube inner surface. On contrary, if mercury memory occurs on the inner surface of the injector, the probability and efficiency of the interaction between acidic aerosol and mercury is significantly reduced. As a result, the washout is not so efficient. After taken off the torch and soaked it in *aqua regia* for one hour, the torch was mounted again. Although the pumping tube was not changed or washed, the emission intensity always reproduced the original

background. It indicates that mercury memory occurs on the inner surface of the torch injector.

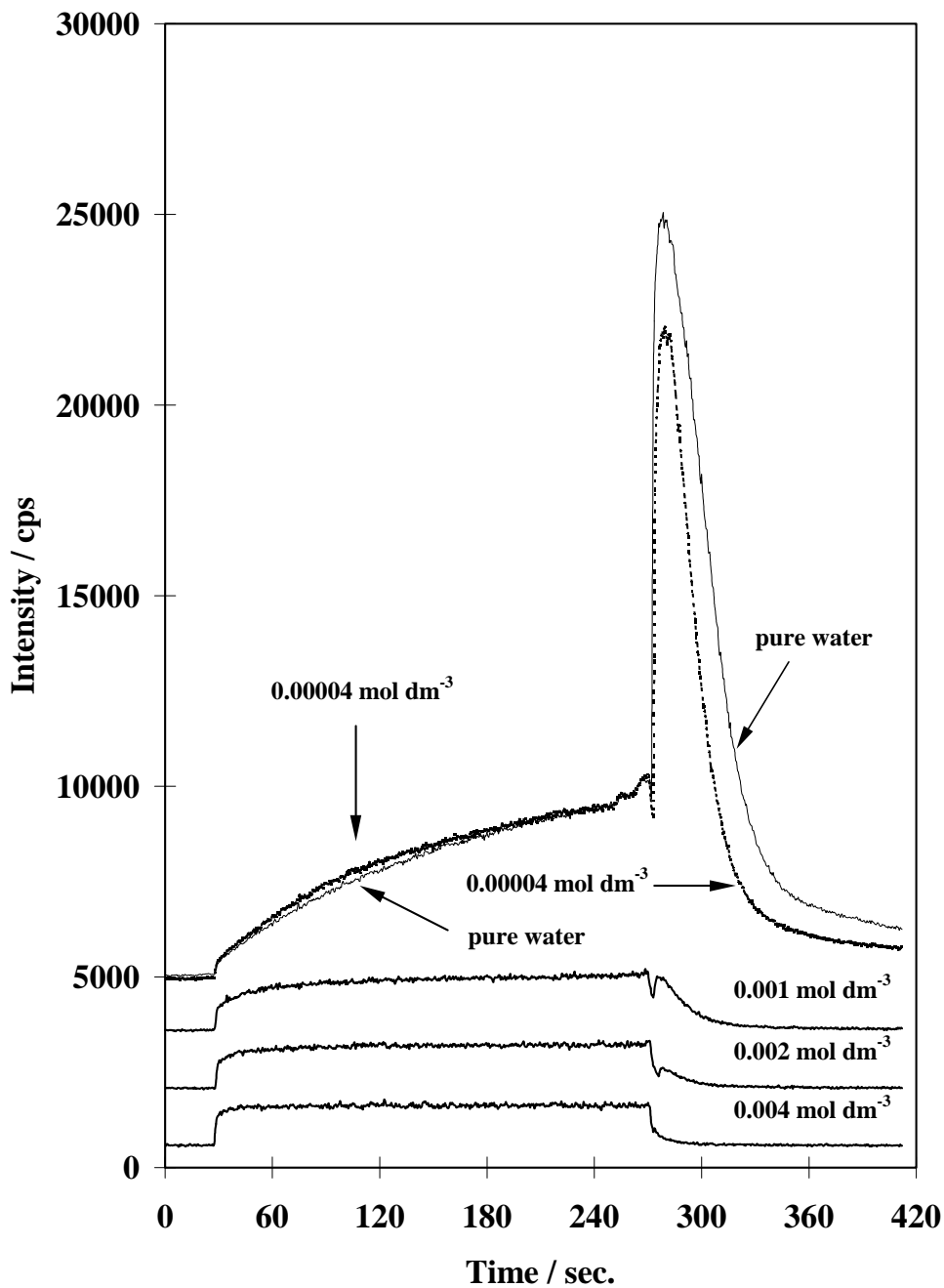


Fig. 4.1.2. Transient optical emission signals for mercury at 194.2 nm in different nitric acid solutions. The concentration of HgCl_2 is $1.00 \text{ mg dm}^{-3} \text{ Hg}$.

The temperature spatial distribution and the thermal exchange efficiency of 40.68 MHz plasma are significantly different from 27.12 MHz one. The geometric structure

differences between two torch injectors and some other differences between two plasma thermal conditions also exist. Therefore, mercury sorption and desorption equilibrium states are different. The time needed to reach a new equilibrium is also determined by these factors. With the same RF input power and argon flow rates, the axial temperatures of 40.68 MHz plasma are lower than a 27.12 MHz one. Hence, it was observed that mercury released from the injector of a 40.68 MHz plasma more slowly than from a 27.12 MHz one.

For both ICP-MS and ICP-OES, the signal intensity and the time needed to reach an invariable signal are governed by HNO_3 concentration in mercury solution. At the washout stage, the amount of mercury released from sampling system, that proportions to the amount of memorized mercury, is determined by HNO_3 concentration in mercury standard solution. When nitric acid concentration increased from 0.00004 to 0.001 mol dm^{-3} , the invariable emission signal intensity of mercury and the area of washout peak concurrently and drastically decreased. It indicates that mercury memory in sampling system was not the direct reason for the signal depression observed in this experiment. Neither the physical properties of mercury standard solution nor the thermal conditions of plasma can be changed significantly by the presence of HNO_3 in such a low concentration. Nevertheless, mercury signal suppression may arise from the chemical inhibition on mercury compounds atomization. Some results showed that the signal suppression was governed by the chemical properties of sample solution other than mercury ionization or excitation in plasma (see below). When droplets passed by the central tube, mercury compounds could be partially decomposed and adsorbed onto the injector before they entered the plasma. The thermal dissociation near the tip of injector was inhibited by HNO_3 in droplets. The concentration-related inhibition depends on the competition of the heat energy from plasma and the chemical energy (oxidizing power) of HNO_3 . After reaching the adsorption equilibrium, mercury signal became stable. In the case of non-acidified mercury solution, it was far from mercury sorption and desorption equilibrium. Therefore, large amount of mercury was adsorbed onto the injector and then produced the biggest washout peak. The hypothesis of chemical inhibition is able to interpret nitric acid caused mercury signal depression in inductively coupled plasma spectrometry, because mercury compounds exist in the similar thermal and chemical circumstances as it near the tip of injector, except the differences in temperature and HNO_3 concentration. Although the total amount of mercury in plasma central channel increased with the increasing HNO_3 concentration, the observed

mercury signal was the combined results of HNO₃ inhibition on mercury atomization in plasma and mercury memory in sampling system.

4.1.4 Rf power influences on mercury optical emission

Rf power is an important plasma parameter that, to a great extent, determines the thermal conditions and robustness of plasma. It strongly affects the interactions between aerosol and plasma in the desolvation, vaporization, dissociation, ionization, and excitation. Increasing nitric acid concentration, the emission intensities of mercury ionic line and atomic line (see Fig. 4.1.3) were reduced drastically and became steady when HNO₃ concentrations were higher than 0.004 mol dm⁻³. Increasing rf power, the plasma became more robust. Mercury emission intensities of ionic line and atomic line were increased for the enhanced excitation abilities. The intensity ratios of mercury ionic line (194.2 nm) to atomic line (253.7 nm) were calculated from the corresponding data pair and then took average in the same rf power series. The intensity ratios are 1150 W: 0.51 ± 0.01; 1250 W: 0.53 ± 0.01; 1350 W: 0.57 ± 0.01. The high precision (RSD: 1.6~2.4%) strongly suggested that the intensity ratio of ionic to atomic line of mercury do not change with the increasing nitric acid concentration. That is the emission intensity of mercury ionic line and atomic line suffered from the same suppression by nitric acid. There is no doubt, mercury signal depression happens before mercury compound atomization. Therefore, the signal suppression is not related to mercury ionization and excitation under the current working conditions. At least, nitric acid has not detectable influence on the quickly established mercury ionization equilibrium and excitation equilibrium in plasma.

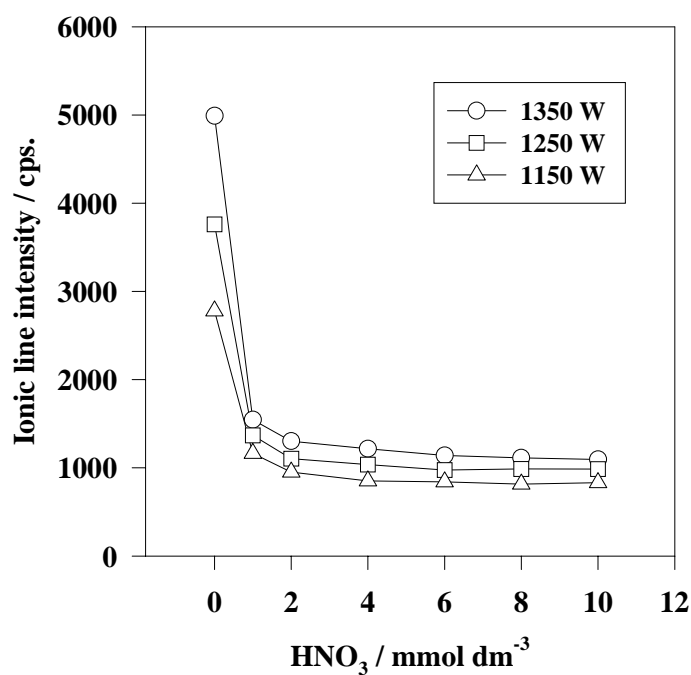
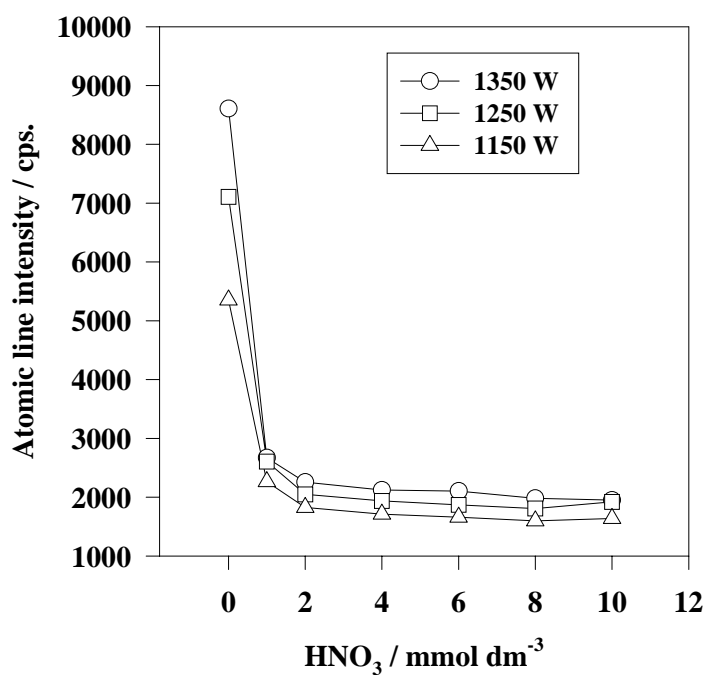


Fig. 4.1.3. Dependence of mercury emission signal intensities at 253.7 nm and 194.2 nm ($1.00 \text{ mg dm}^{-3} \text{ Hg}$) on nitric acid concentration with different rf powers. The sampling system is a donut-shaped spray chamber with a concentric nebulizer.

4.1.5 Rf frequency influences

Capelle et al. [99] examined rf frequency influences on the plasma thermal conditions. Three parameters were compared among 5, 27, 40, 56 MHz inductively coupled plasma with different commercially available instruments. They found that when the frequency increases, the excitation temperature and the electron number density decrease. The intensity ratio of Mg II (280.27 nm) to Mg I (285.21 nm), which indicates the robustness of the plasma, also decreased with the increasing rf frequency. Huang et al. [100] made a more complete and unambiguous comparison of the fundamental characteristics of 27 and 40 MHz ICPs. The Leco 2000 ICP system, with a solid-state generator, can be operated at 27 or 40 MHz using the same impedance-matching network. Both ICPs were sustained with the same load coil, torch and torch box and under the same operating conditions. Under the same conditions, the 40 MHz ICP shows a larger and clearer central channel than the 27 MHz ICP. This spatial characteristic cannot be created in the 27 MHz ICP simply by lowering the rf forward power. The measured Fe excitation temperature also declines with increasing rf frequency. Changes in the ICP fundamental parameters with rf frequency seem to be caused by the *skin effect* that occurs primarily in the load coil region, but which apparently also influences the behaviors of the discharge above the load coil as the plasma travels upward and decays. The enhanced “skin effect” cools down the central channel of plasma. As results, the electron number density, the plasma temperatures, and the line emission intensity in that zone are decreased. Therefore, under the same working conditions and in the plasma central channel, a 27.12 MHz ICP is more robust than a 40.68 MHz one. With a 27.12 MHz ICP, the variety of mercury mass spectrometric signals ranged over 0-0.75 mol dm⁻³ HNO₃. The ratio of the highest signal intensity to the invariable one was 1.9. However, for a 40.68 MHz ICP, the variety of mercury emission signals merely ranged over 0-0.004 mol dm⁻³ HNO₃ with the intensity ratio of 3.4. It means that the signal suppression by nitric acid in a 40.68 MHz ICP is more serious than in a 27.12 MHz ICP. This conclusion is in a good agreement with the results of Chudinov *et al.* [49].

Huang et al. [100] observed that electron temperature T_e , electron number density n_e and gas-kinetic temperature T_g decreased when rf frequency raised from 27 to 40 MHz. The dropping degree depends mainly on spatial position in the plasma. the maximum effect generally located in the central channel. The effect of operating

frequency on T_g is greatest low in the plasma and near the central channel. The radial profiles showed that the gas temperature T_g decreased vigorously in a 2.5 mm radius central channel with increasing rf frequency. At the bottom of plasma, T_g decreased more serious with the increase of carrier gas flow rate. However, at the outer periphery of the discharge, the value of T_g is almost constant with increasing rf frequency.

Aerosol desolvation likely occurs during the time when droplet travels from the tip of the center tube to the top of the load coil [74]. The gas temperature (which describes the kinetic energy of the argon atoms) likely controls sample desolvation [20]. Under the same working conditions, the T_g value of a 27 MHz ICP is higher than a 40 MHz ICP, especially at the bottom of plasma [100]. Therefore, the central channel of a 27 MHz ICP is more robust than a 40 MHz ICP. Based on these arguments, the desolvation in the central channel of a 27 MHz ICP is higher than a 40 MHz ICP.

Mercury signal intensity relies on nitric acid concentration and the operating frequency of rf generator. The rf frequency governs the axial temperatures of plasma. Due to a certain amount of desolvating droplets exist in the central channel of plasma, it is reasonable to hypothesize that the chemical inhibition by HNO_3 occurs in or nearby the droplet. Mercury compounds are easily atomized at low temperature [101]. The processes of desolvation and dissociation may overlap in plasma. It implies that the redox reaction between mercury and HNO_3 could affect mercury atomization efficiency. Therefore, the difference in T_g becomes more important. It controls the thermal exchange between droplet and plasma atmosphere and the desolvation progress. The redox equilibrium between mercury and HNO_3 can be shifted by changing nitric acid concentration and by the heat exchange with plasma. The equilibrium position relies on the plasma thermal conditions, especially on the gas temperature. At low HNO_3 concentration ($< 1.0\text{M}$), the heat obtained from “robust” 27.12 MHz plasma is enough to minimize the oxidizing power of HNO_3 and favors mercury atomization. As results, the dependence of mercury signals on HNO_3 concentration was observed in a wide range. As to the 40.68 MHz plasma, the gas temperature in the central channel is lower than a 27.12 MHz ICP. It favors to keep the oxidizing power of HNO_3 against mercury compounds dissociation. This leads to a serious chemical inhibition on mercury atomization and narrows the range of HNO_3 influence on mercury signals.

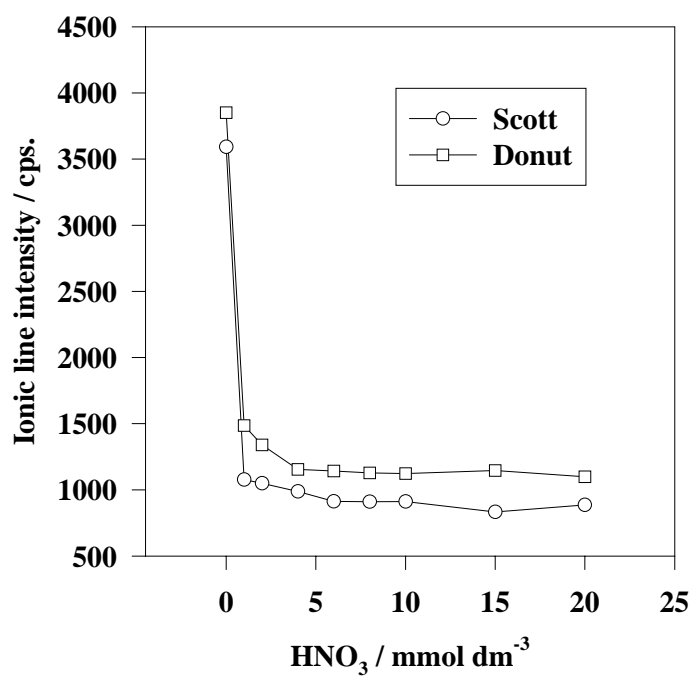
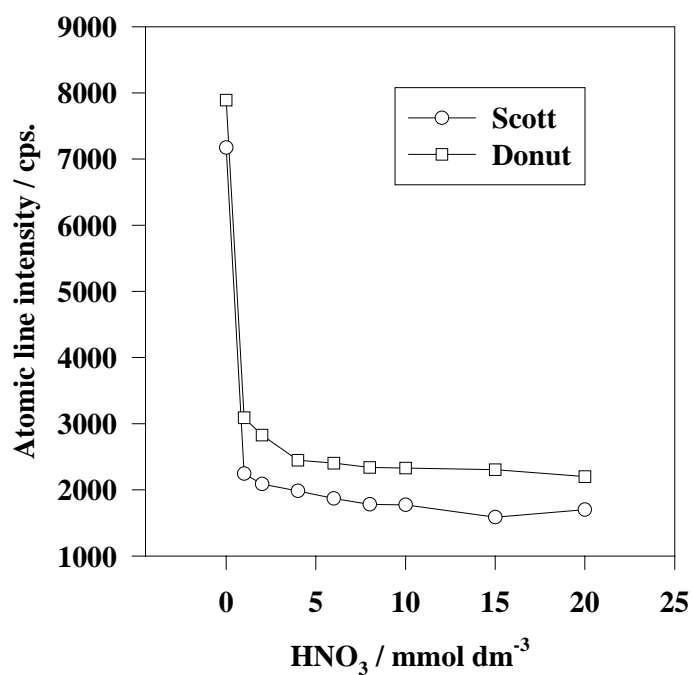


Fig. 4.1.4. Dependence of mercury emission signal intensities at 194.2 nm and 253.7 nm ($1.00 \text{ mg dm}^{-3} \text{ Hg}$) on nitric acid concentration with different spray chambers.

4.1.6 Spray chamber structure and aerosol transport

In this experiment, the Monochromator ICP-2070 was equipped with two different spray chambers (Scott-type and donut-shaped). They are significantly different in structure and aerosol transport mode. It is expected that the volume concentration of droplets, the volume flux of droplets, the total mass solvent transport rate, the total mass analyte transport rate, and the tertiary aerosols droplet distribution are significantly different between these two spray chambers. It has been reported that for all the examined elements, donut-shaped spray chamber has the higher signal intensities than Scott-type spray chamber [19].

With a concentric nebulizer and under the same working conditions, although the emission intensities obtained with donut-shaped spray chamber were slightly higher than the Scott-type one, the similar signal depression trends were observed (see Fig. 4.1.4). As the plasma was running under the robust conditions, nitric acid effects on the plasma thermal conditions were negligible. The presence of nitric acid showed no significant difference in the depression trends between mercury atomic and ionic lines. Another possible interpretation for the depression trend should be related to the sample transport processes before the analyte entering the plasma. It is reasonable to ignore the acid effects on the liquid aspiration, aerosol formation and transport efficiencies. This is because nitric acid caused mercury signal variation ranged from 0 to $0.004 \text{ mol dm}^{-3}$. The physical properties of solutions have not detectable changes in such low acid concentrations. In addition, mercury accumulation in the sampling system, in fact, will reduce the amount of mercury entering into the plasma. If though, increasing nitric acid concentration will lead to a mercury signal enhancement. It could not explain the observed suppression effect by nitric acid in the opposite direction. Therefore, mercury signal suppression by nitric acid is most likely due to the chemical inhibition on mercury compound dissociation.

The ICP-MS was equipped with a similar Scott-type spray chamber as it was used in the ICP-OES. The plasma run under the robust conditions. Nitric acid effect was examined at low concentrations (from 0 to 0.75 mol dm^{-3}). The changes in the physical properties of solution and in the plasma thermal conditions are negligible. However, the range of nitric acid concentration, which hampered to get an invariable mercury signal, was completely different from the results obtained with ICP-OES sustained by a 40.68 MHz generator. This suggests that mercury signal suppression be not related to aerosol generation and transport. It must happen behind the spray chambers. That means

mercury signal depression is due to the chemical reaction in or near by the desolvating droplets in the observation zone or sampling volume. It inhibits mercury compounds thermal dissociation through the red-ox equilibrium in the central channel of plasma.

4.1.7 Introduction of mercury cold vapor and nitric acid aerosol

As discussed above, nitric acid caused mercury signal depression was not related to the ionization and excitation. Liu et al. [6] reported that mercury signal could be selectively inhibited by nitric acid. By no means, elemental discrimination on mercury should happen during aerosol generation, transport, and desolvation. It is also unreasonable that slight increase in HNO_3 concentration ($0\text{-}0.001 \text{ mol dm}^{-3}$) can significantly change the temperature around drops and restrain mercury compounds vaporization. Therefore, chemical inhibition on mercury compounds dissociation in plasma should be the reason for mercury signal suppression.

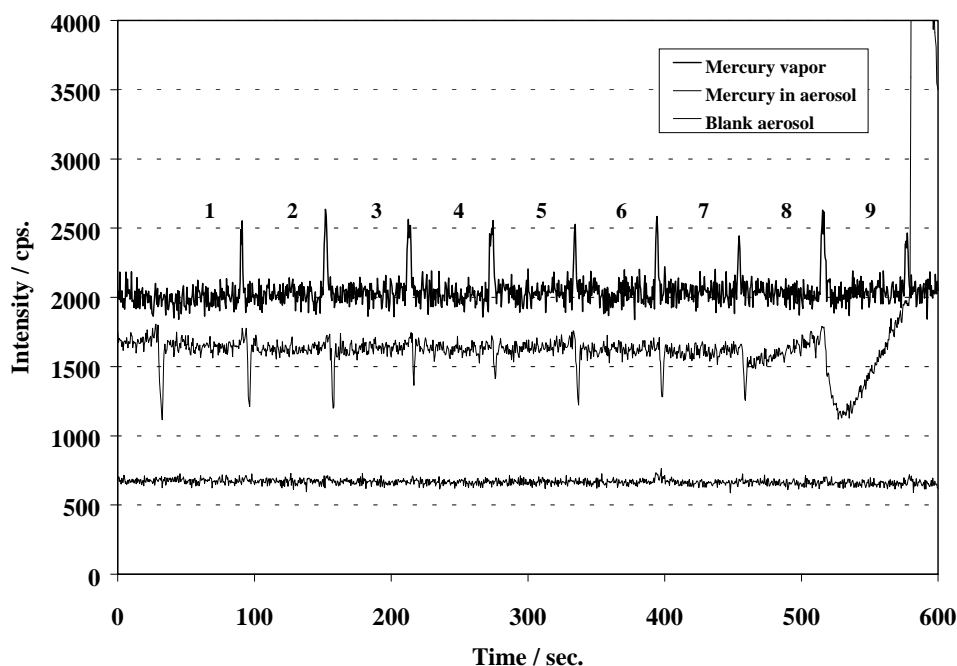


Fig. 4.1.5. Comparison of nitric acid influences on mercury emission intensities at 194.2 nm. A) mercury cold vapor with the aerosol of blank nitric acid; B) aerosol of mercury working solutions; C) aerosol of blank nitric acid. The concentrations of nitric acid (in mol dm^{-3}) are: 1, 0.020; 2, 0.015; 3, 0.010; 4, 0.008; 5, 0.006; 6, 0.004; 7, 0.002; 8, 0.001; 9, pure water.

Mercury chloride can be atomized by a chemical reaction at room temperature. In this way, mercury dissociation could be accomplished by chemical process other than by a thermal process in plasma. It offers the possibility to identify that mercury signal was suppressed by HNO₃ during mercury compounds dissociation. To testify this hypothesis, mercury cold vapor was introduced into the donut-shaped spray chamber by a small inlet on the side wall. Meanwhile, HNO₃ solutions were nebulized with a concentric nebulizer and introduced into the same chamber as usual. The monitor was started when mercury emission signal at 194.2 nm became stable. Nitric acid solutions were aspirated and changed each minute in the decreasing concentration in order to eliminate the suspicion on mercury memory that might occur when introduces mercury solution at low HNO₃ concentration. The results are shown in Fig. 4.1.5. It is obvious that mercury signal intensities are not changed. The narrow periodic peaks formed when nitric acid solutions were changed. The temporary shortage of aerosol heated the central channel of plasma and increased the population of excited ions. A comparable experiment was performed without mercury cold vapor generation. The acidic mercury working solutions were aspirated instead of the blank HNO₃ solutions. When nitric acid matrix changed from 0.002 to 0.020 mol dm⁻³, mercury signal intensities were almost constant. However, if the matrix was water or 0.001 mol dm⁻³ HNO₃ solution, mercury signal intensities went down firstly and then raised up. This phenomenon occurred as mercury compound was thermally dissociated and adsorbed onto the tip wall of the injector. At the beginning, owing to the adsorption, mercury went into plasma was less than in a high HNO₃ concentration solution. The signal intensities were lower than the general level. When the adsorption gradually reduced, mercury went into plasma was increased appropriately. The signal intensity increased too. Obviously, one minute is too short to reach mercury adsorption equilibrium (see Fig.4.1.2). The narrow periodic hills show the temporary shortage of aerosol during changing mercury working solutions. When the aspiration was stopped, no energy was consumed for the heat exchange with aerosol. The injector was quickly heated. As a result, the adsorbed mercury was instantly released into plasma and produced an extremely high peak (see Fig. 4.1.5).

The results from Fig. 4.1.5 illustrate that: 1) the aerosol of dilute HNO₃ did not change the physical state of plasma; 2) nitric acid molecular released from aerosol may be quickly decomposed in plasma or it cannot rapidly and efficiently oxidize mercury cold vapor; 3) only the HNO₃ molecule which exists in the vaporizing droplets or nearby the vaporized mercury compounds can inhibit mercury signals. Once mercury

compounds are dissociated, mercury ionization equilibrium and excitation equilibrium will be soon established. Therefore, it is very likely that HNO_3 inhibits mercury compounds dissociation in plasma and depresses their atomic and ionic line emission intensities.

4.1.8 Summary

Mercury signal suppression by nitric acid in inductively coupled plasma depends on plasma characteristics and HNO_3 concentration in solution. Among all the plasma parameters, rf frequency is one of the most important factors which affects mercury signal intensity in a great extent. Signal suppression in a 40.68 MHz ICP is more serious than it in a 27.12 MHz one. Despite of this, accurate results could be obtained with a 40.68 MHz plasma at normal acid matrix. However, with a 27.12 MHz plasma, nitric acid effect range over a wide acidity and lead to variable results. Increasing rf power would enhance mercury emission signal intensities. The correspondingly increased intensity ratios of ionic to atomic lines were almost stable to the change in nitric acid concentration. The aerosol of nitric acid could not affect the ionic line intensity of mercury cold vapor. Those suggested that the presence of HNO_3 in solution do not obviously disturb mercury ionization equilibrium in the central channel of plasma. However, with a 27.12 MHz “robust” plasma, mercury mass spectrometric signals were dependent on HNO_3 concentration. A reasonable interpretation is that mercury signal suppression occurs at the stage of mercury compounds dissociation. The monitor plot of mercury solutions aspiration showed that, when the aerosol passed by the injector, a part of mercury compounds would be thermally decomposed. The released Hg atoms would be partially adsorbed onto the tip wall of the torch injector. The dissociation extent was determined by the concentration of HNO_3 , as the competition result between the oxidizing power of HNO_3 and the heat obtained from plasma. The chemical and thermal surroundings in the central channel are quite similar to that near the tip of the injector. When aerosol goes into plasma, mercury compound dissociation will also be inhibited by HNO_3 in the desolvating drops or nearby the vaporizing mercury compounds like it happens near the tip of injector. Once dissociated, mercury atoms will instantly reach its ionization equilibrium. As results, mercury emission intensities of atomic and ionic lines are suppressed in the same extent. The dependence of mercury spectrometric signal on nitric acid concentration and heat exchange efficiency with plasma shows a

great possibility that a red-ox equilibrium between mercury and nitric acid really exists in plasma central channel, the extremely hot space as it is believed.

4.2 The complex formation equilibria of mercury and ammonium nitrate in inductively coupled plasma

For the irreplaceably physical and chemical properties, mercury has been for a long time and widely used in varied purposes. Mercury consumption and leakage, followed by biological methylation, will inevitably lead to serious pollution. Owing to mercury compounds accumulate exceptionally intensively in sediments and aqueous flora and fauna [102], the assessment on mercury environmental pollution becomes more important.

Mercury exists in real samples at extremely low levels. The ordinary inductively coupled plasma optical emission spectrometry (ICP-OES) is difficult to fit the requirement on mercury determination for the poor detection limits. Although inductively coupled plasma mass spectrometry (ICP-MS) has been well developed as a high sensitive analytical technique with multielement detectability, the accuracy and precision of mercury determination is still troublesome for the serious matrix influences, memory effect, and species discrimination. To find out where they come from is the prerequisite to eliminate them and validate a proposed determination method. Matrix influences were generally attributed to the low ionization potential elements, which often exist abundantly in sample solutions. They are believed can inhibit the thermal ionization of mercury for its high first ionization potential. Some mineral acids can severely suppress mercury signal [6]. This has been proven to be a chemical inhibition on mercuric ion atomization in plasma [7]. Contrasted to pneumatic aerosol generation, cold vapor generation technique is free from the matrix influences for ICP source spectrometer [7-8]. Memory effect has been considered as a slow build-up of mercury vapor within the spray chamber [92]. It is probably due to an increase in the volatility of mercury species in the standard caused by the large pressure drop during high-pressure pneumatic nebulization as the aerosol expends into the spray chamber. It caused the calibration deviated from linearity at higher concentration level with an apparent increase in sensitivity. This problem was overcome by adding ammonia solution to make the solution alkaline and followed by complexing mercury with EDTA. It was assumed that complexation transformed mercury into a more uniform and inert form, so no losses from volatilization and no sensitivity changes due to vapor build-up in the nebulization spray chamber occurred [96]. Yoshinaga and

Morita [97] found that a pure standard solution produced a greater memory effect than a sample solution of the same mercury concentration. Unfortunately, the same authors did not pay more attention on the interesting phenomenon. This fact shows that some chemicals in the matrix can uniform mercury species and minimize mercury memory in the sampling system. Moreton and Delves [103] reported a simply direct method for total mercury determination in blood, urine, and fish digest. The digests were neutralized with ammonia then diluted with further ammonia and $(\text{NH}_4)_2\text{H}_2\text{EDTA}$. They believed, during the pneumatic aerosol generation, Hg remained in the sample solution since it was complexed with $(\text{NH}_4)_2\text{H}_2\text{EDTA}$ and also owing to the vapor pressure of the ammonia in the sample solution, which shortened the washout time. In the last chapter, mercury signal depression was concluded as the chemical inhibition on mercury compounds thermal dissociation. Therefore, any attempt to optimize the atomization efficiency is possible to minimize mercury signal suppression. Modifiers are commonly used in ETV-ICP-MS. Although most effects of the modifier are believed to be physical, it is likely that chemical effects could also be involved in specific instances. A more symmetrical sharp peak was obtained when 1% EDTA was used as the modifier for ETV-ICP-MS [104]. The authors believed that was due to the high volatility of the EDTA complex, which can promote mercury vaporization before the vaporization of the bulk matrix. In fact, it is the uniformed mercury species, EDTA complex, that made the uniformed mercury compound atomization. Therefore, it is the time to introduce modifier into sample solutions to eliminate the matrix effect on inductively coupled plasma spectrometry. Species discrimination exists in ICP. It is possible that the extra energy required to dissociate the mercury from the organic component causes a specific suppression of the extent of ionization in the plasma [92]. In fact, all the three phenomena exist in the ICP-OES. In other words, the influences are from the ICP system other than from the detector [7].

In this section, chemical influences on mercury compounds atomization in ICP will be discussed and proved in another aspect. Ammonium nitrate, the commonly used mild complexing reagent for mercuric ions, was applied to uncover the complex formation equilibrium that exists in the plasma. It enables to explain the matrix influences, memory effects, and species discrimination.

Thinking about the memory effect, the sequence for mercury aspiration is more crucial. For collecting the time-resolved signal, the wavelength of Hg II at 194.164 nm

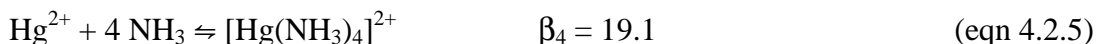
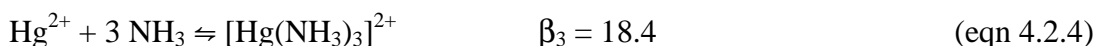
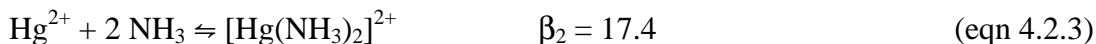
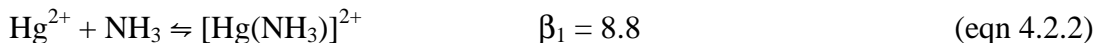
was adjusted with mercury standard solution. After the sampling system was rinsed by aspirating dilute aqua regia (*AR*) for 5 min and pure water for 2 min to repel all the acidic aerosol out, switched on the mercury-ammonium testing solution and the transient signal recorder simultaneously. The aspiration was continued for 3 min. Then, dilute *AR* was turned on immediately and aspired in the next 5 min. The signal collection was stopped after it started 6.0 min. The next collection also started with a 2-min pure water precondition. Mercury solutions were changed in the order of 0.10, 0.05, 0.02, 0.01, 0 mol dm⁻³ NH₄NO₃. For the steady state signal collection, the signal integration started exactly 2.0 min after the mercury testing solution aspiration. The integration time was 10 s. × 4 at each wavelength. The testing solutions were aspired in the order of: the series of 0.05, 0.02, 0.01, 0 mol dm⁻³ NH₄NO₃. In the same series, blank solution was ahead of mercury testing solutions and the HNO₃ concentration changed in the descending order: 20, 15, 10, 8.0, 6.0, 4.0, 2.0, 1.0, and 0.0 mmol dm⁻³. Each aspiration was followed by a 2-min washout with dilute *AR* and a 1-min clean-up with pure water. Before going on the next series, a 5-min washout with dilute *AR* was necessary to get rid of the memory in this system.

During the investigation of nitric acid suppression on mercury emission signal [7], the ICP-2070 monochromator system has been found to be sensitive to the presence of nitric acid at low concentrations. The signal suppression has been attributed to the chemical matrix inhibition on mercury compound atomization that relates to the oxidation-reduction equilibrium in the central channel of plasma. The equilibrium in plasma can be shifted by HNO₃ oxidizing ability and the heat exchanged with plasma. Ammonium nitrate is another kind of chemical matrix in mercury standard solution. Owing to its stepwise formation of successive complexes and moderate complex formation constants with mercuric ions, NH₄NO₃ is helpful to reveal whether the complex-formation equilibrium exists in the central channel of plasma and it can also be shifted by the complexing ability of ammonia and the heat exchanged with plasma.

4.2.1 Mercury species distribution in ammonium nitrate solution

In a given Hg²⁺-NH₄NO₃-HNO₃ aqueous system, following chemical equilibria exist and are shifted normally by changing the pH and the concentration of ammonium nitrate. However, the equilibrium positions are determined by the temperature of

mercury solution because the values of the equilibrium constants are dependent on the temperature.



β_n means the overall formation constant.

On the equilibrium status, the distribution of the successive complexes is predictable from the overall formation constants β_n of $[\text{Hg}(\text{NH}_3)_n]^{2+}$ ($n = 1\sim 4$), the dissociation constant K_a of NH_4^+ , and the concentrations of NH_4NO_3 and H_3O^+ in mercury standard solution. The mercury(II) ion-ammonia system is unusual in that the last two of the successive complexes are of much less stability than the first two. In this work, the concentrations of ammonium nitrate were changed from 0 to 0.1 mol dm⁻³, the concentrations of hydronium ions were changed by addition of 0 to 20.0 mmol dm⁻³ nitric acid in solutions. According to these parameters, the species distributions in different $\text{NH}_4\text{NO}_3\text{--HNO}_3$ solutions were calculated and shown in Fig. 4.2.1. Due to the pH of all the NH_4NO_3 solutions are lower than 7.0, the majority of ammonium ions are in the protonated form. As a result, the last two higher complex species are less than 0.5% and not shown in Fig. 4.2.1.

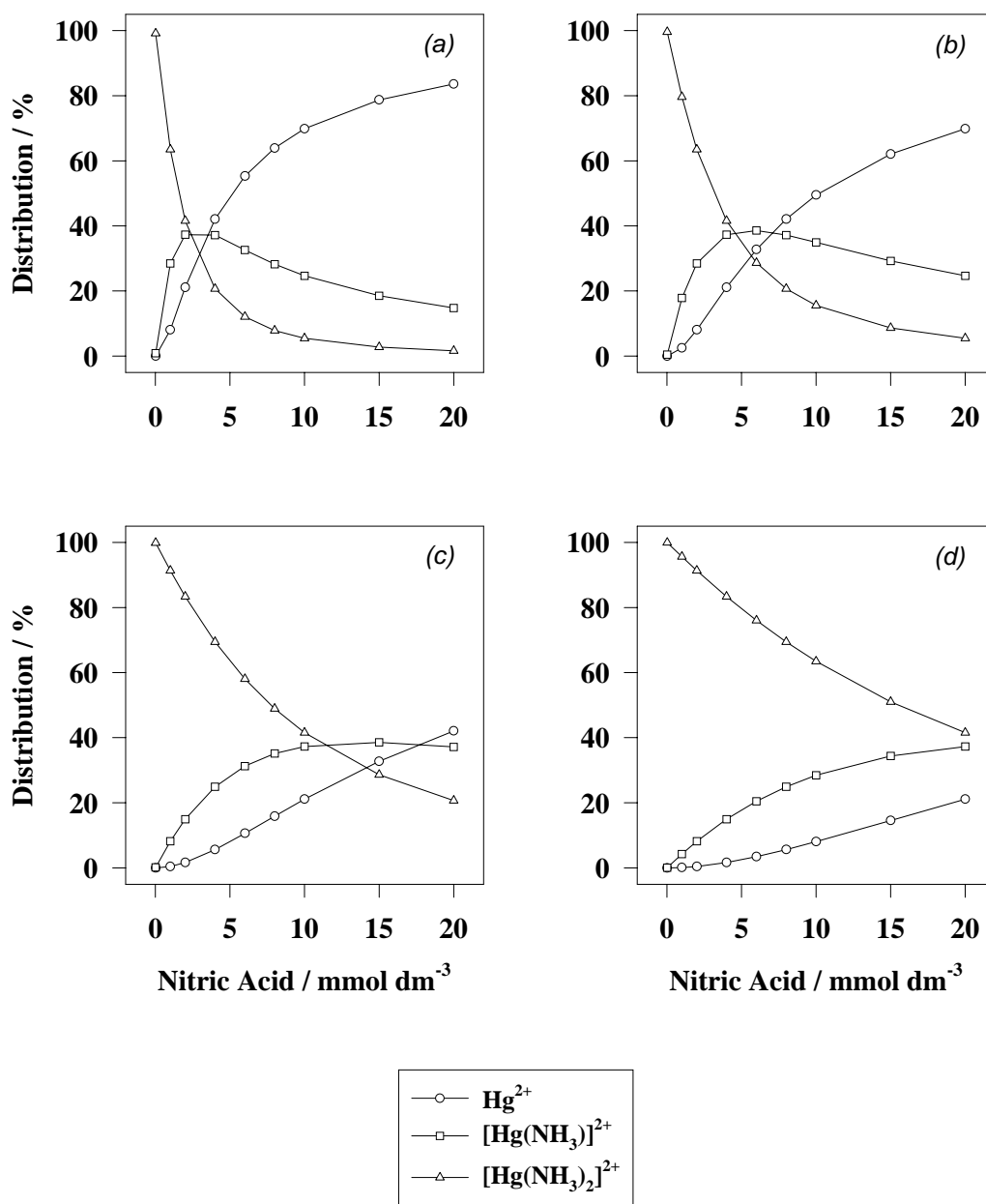


Fig. 4.2.1: Mercury species distribution in varying NH₄NO₃-HNO₃ solutions. The NH₄NO₃ concentrations are: *a*, 0.01; *b*, 0.02; *c*, 0.05; and *d*, 0.10 mol dm⁻³.

The concentration of endogenous H_3O^+ , released by Hg^{2+} from NH_4^+ , is $2.0 \times 10^{-2} \text{ mmol dm}^{-3}$ (Hg^{2+} is $1.0 \times 10^{-2} \text{ mmol dm}^{-3}$). It has been taken into account in calculating the mercury complexes distribution. Obviously, in those solutions without adding nitric acid as exogenous H_3O^+ , the major complex species is $[\text{Hg}(\text{NH}_3)_2]^{2+}$. Increasing acid concentration can shift the equilibria to the left side and lead to mercury complexes dissociation. Increasing the concentration of ammonium nitrate can shift the equilibria to the right side. It reduces free Hg^{2+} concentration and increases the stability of mercury complexes. As results, it enhances the capability of mercury complexes to minimize the acid effect on mercury complexes dissociation. However, in 0.1 mol dm^{-3} ammonium nitrate solution, even though the nitric acid concentration is as high as 20 mmol dm^{-3} , the complexes are still in appreciable levels.

4.2.2 Monitoring the transient signals of mercury during the aspiration

The process of sampling and washout of mercury solutions was monitored at the ionic line Hg II 194.164 nm. The plots clearly show that mercury signals are suppressed by the concomitant NH_4NO_3 (see Fig. 4.2.2). The suppression extent is fairly dependent on the concentration of NH_4NO_3 . Plot A was obtained with HgCl_2 water solution. On starting the nebulization of HgCl_2 water solution, as described in the last chapter, the intensity of mercury signal was increasing continually. After starting the aspiration for 180 seconds, the increase of mercury signal was gradually slowing down and closing to an invariable level. No signal inhibition can be attributed to the matrix effects from this pure water solution. Contrarily, more considerable effects on mercury time-resolved signals are due to the mercury compounds deposition on the inner wall of the sampling system. After aspirating a dilute AR solution, the memorized mercury in the sampling system was immediately washed out. Then, it gradually went down and took a long time to reach the background. Mercury compounds deposition could be inhibited by the concomitant NH_4NO_3 in solution. It clearly shows, from plot B to plot E (see Fig. 4.2.2), that the time needed to reach a invariable mercury signal is successively shortened with the increasing NH_4NO_3 concentrations. Meanwhile, during the washout, the peak height, the time needed to reach the background, and the area under the washout peak (see Fig. 4.2.3) is correspondingly reduced. Obviously, mercury signals are significantly inhibited by the concomitant NH_4NO_3 in solutions.

An interesting phenomenon is that the time-resolved signal obtained with $0.1 \text{ mol dm}^{-3} \text{ NH}_4\text{NO}_3$ solution is quite similar to the plot obtained with $0.001 \text{ mol dm}^{-3} \text{ HNO}_3$ solution. The similarities can be found in the signal suppression extents and in the shape and the scale of washout peaks. It means that the inhibiting capability of nitric acid is at least a hundred times higher than ammonium nitrate. In other words, the signal inhibition by a redox reaction is more severe than by a complex formation reaction. This finding may be thought of another evidence to prove that the redox inhibition on mercury compound atomization in the plasma can lead to mercury signal suppression.

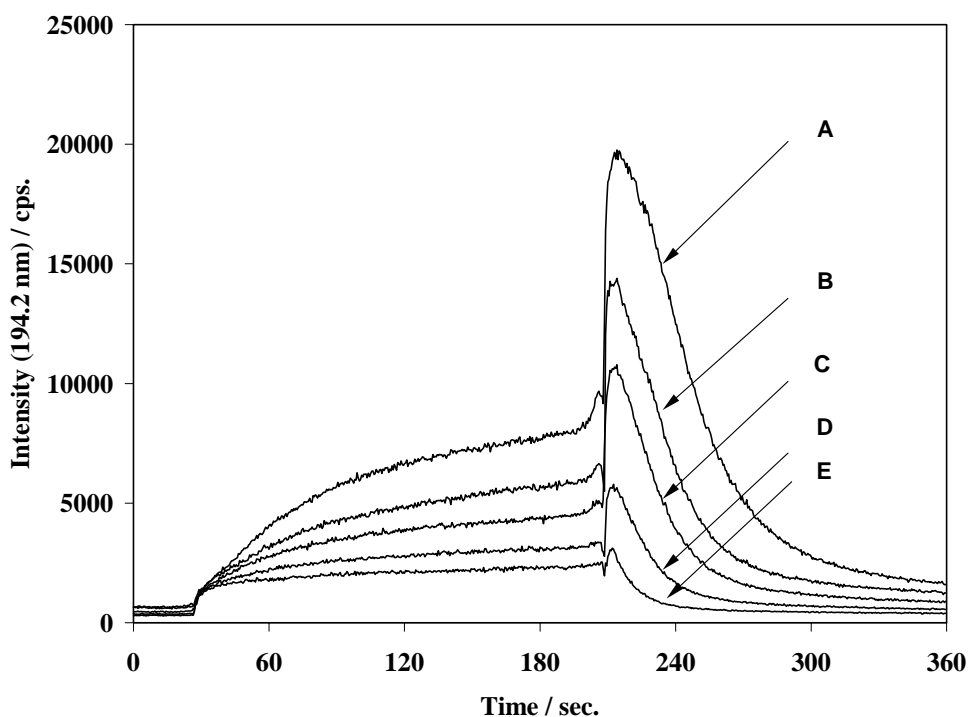
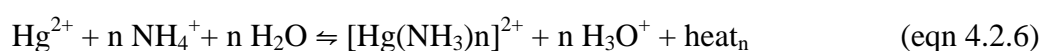


Fig. 4.2.2: Time-resolved signal of mercury at Hg II 194.164 nm ($2.0 \text{ mg dm}^{-3} \text{ Hg}$) during aspirating standard solutions and the *d-AR*. The NH_4NO_3 concentration of each plot is: A, 0; B, 0.01; C, 0.02; D, 0.05; and E, 0.10 mol dm^{-3} .

Matrix effect on mercury signal depression may be attributed to two aspects. That is the changes in the physical properties and in the chemical properties. Increasing the concentration of ammonium nitrate in mercury standard solution will reduce the partial pressure of water vapor and lead to the increase in the boiling point (physical properties). Ignoring the influences from the tertiary aerosol characteristics, the increase

in boiling point will reduce the desolvation efficiency of aerosol and lead to the low emission intensities. Mercury complex is less susceptible to reduction than mercury compounds. As a result, the formation of mercury complexes will enhance the capability of mercury compounds to resist the thermal dissociation (atomization or reduction) in the central channel of plasma (chemical properties). Therefore, the presence of ammonium nitrate in solution will inhibit the atomization efficiency of mercury compound. The formation of mercury complexes contributes the major part for the signal suppression because the energy consumption for breaking down the chemical bonds in molecule is much more than for weakening the *Van der Waals'force* among the molecules.

In a non-acidified NH_4NO_3 solution, $[\text{Hg}(\text{NH}_3)_2]^{2+}$ is the predominant mercury specie (more than 99 %). Provided that the signal only depends on mercury species, the time-resolved signals from different NH_4NO_3 solutions should be similar. In fact, the experimental results were failure to support such an assumption. With the increase in ammonium nitrate concentration, the boiling point of mercury standard solution increases too. However, the boiling point increase is expected to change the emission intensity other than the shape of the monitoring plot. Therefore, the change in boiling point is unable to give a satisfactory explanation (see below in more detail). A reasonable interpretation is that the mercury signals are mainly governed by the complexing capabilities of NH_4NO_3 . The following expression is more helpful to describe the chemical inhibition on mercury signals:



The chemical potentiality to keep mercury in a stable complex is negatively related to the Hg^{2+} concentration in solution. In the mercury-ammonium aqua system, the temperature of solution determines the equilibrium position. Meanwhile, the equilibrium state can be shifted by changing the concentration of NH_4NO_3 and the pH value in solution. Increasing NH_4NO_3 concentration leads to non-complexed Hg^{2+} reduce gradually (see Fig. 4.2.1). That means the chemical potentiality to keep Hg^{2+} in more stable complex species is increased. Lowering the pH value leads to mercury complexes dissociation. The temperature influences on the equilibrium through the heat exchange between droplet and plasma. Due to the varying droplet temperature, it is

more meaningful to take heat as a component in the expression (eqn 4.2.6) other than think the overall formation constants β_n as a function of temperature. It is also convenient for discussing the real function of the heat exchange between the droplet and the plasma. For mercury complexes, the complexing capability of ammonia to resist the *thermal atomization* in plasma is quite similar to ammonia to resist the *chemical dissociation* by hydronium. Therefore, heat and hydronium are in the same position to reduce the complexing capability of NH_4NO_3 . Vice versa, increasing the concentration of NH_4NO_3 will enhance the capability of mercury complexes to resist the thermal dissociation, thus lead to low atomization efficiency in plasma. As a result, low mercury emission signal in plasma is expected. In general, the heat exchange and the droplet temperature rely on the salty of solution and the plasma thermal conditions. Therefore, in the ammonium nitrate system, mercury signals are radically affected by the concentrations of NH_4^+ and H_3O^+ , through which they can shift the complex formation equilibrium state and alter the droplet temperature for the change in the amount of total soluble solid in solution. Furthermore, the heat_n corresponding to each complex species is different. The higher the ligand number, the higher the heat of formation, and the more the energy consumption for mercury atomization. This may responds for the species discrimination in plasma.

Comparing with Hg^{2+} , mercury complexes are more inert to the inner surface of tubing and spray chamber. The mercury memory in liquid and aerosol transport systems could be significantly reduced. As a result, the amount of mercury entering into the plasma is increased. Even though, mercury emission in plasma is still suppressed by the chemical inhibition on mercury complexes atomization.

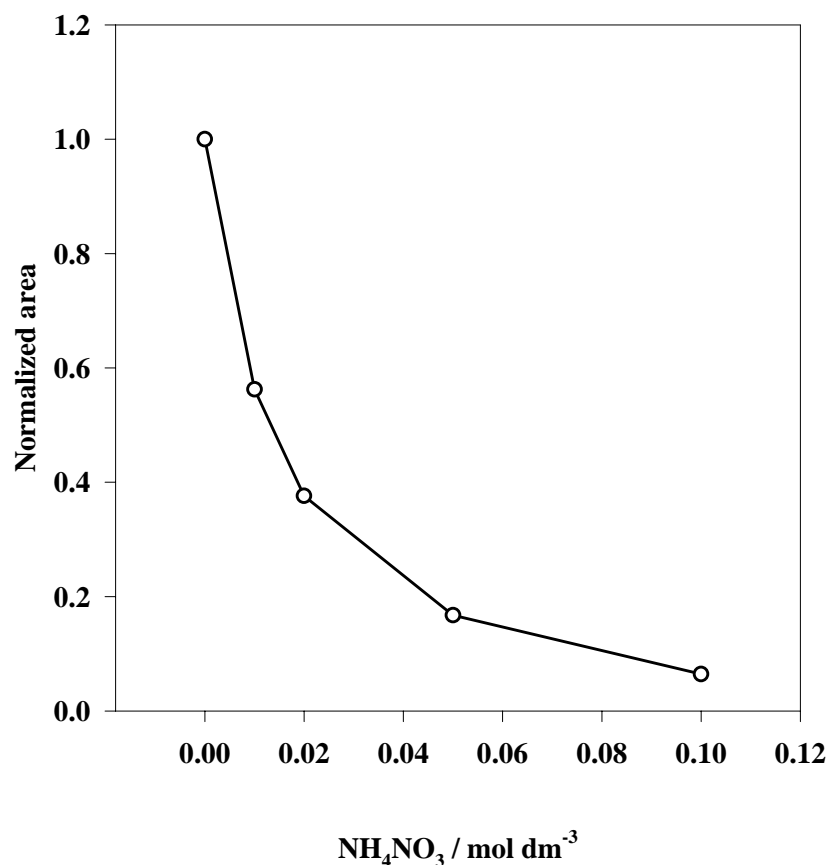


Fig. 4.2.3: Dependence of the relative area under the washout peaks on the concentration of ammonium nitrate.

4.2.3 Nitric acid influences on the equilibria of mercury and ammonium nitrate

In non-acidified $\text{HgCl}_2\text{-NH}_4\text{NO}_3$ aqueous system, increasing the concentration of NH_4NO_3 may lead to a more serious chemical inhibition on mercury complexes atomization. As a result, the emission from mercury is suppressed (see Fig. 4.2.4).

When nitric acid is introduced, this exogenous acid will dominate the pH value of mercury aqueous solutions. It leads to the redistribution of mercury species in the new $\text{HgCl}_2\text{-NH}_4\text{NO}_3\text{-HNO}_3$ aqueous system. In this experiment range, the main species of mercury are $[\text{Hg}(\text{NH}_3)_2]^{2+}$, $[\text{Hg}(\text{NH}_3)]^{2+}$, and Hg^{2+} . It is clear that the higher the ligand

number, the more the energy consumption for atomization, the lower the ground state population of mercury atoms and ions in the plasma, and the less sensitive the mercury signal response. The sharp change in the species distribution, especially in the portion of $[\text{Hg}(\text{NH}_3)_2]^{2+}$, drastically decreases the capability of ammonium nitrate to resist mercury thermal dissociation in plasma. Agreed to the prediction, mercury signal increase was observed at low nitric acid concentrations (see Fig. 4.2.4).

Apart from shifting the complex formation equilibrium, the introduction of HNO_3 also leads to a low emission signal for the red-ox inhibition on the atomization efficiency of mercuric ions (see fig. 4.2.4, the plots of 0.01 and 0.02 mol dm^{-3} in NH_4NO_3). Obviously, nitric acid inhibition plays more important roles in mercury signal suppression. No matter what mechanism may be involved into the signal suppression, in fact, the atomization is nothing but a reduction process. A notable fact is that those chemical matrix influences on the ionic line and atomic line in the same manner. It proves that mercury ionization is little influenced by those chemicals. In other words, chemical inhibition on mercury emission intensities happens before or at the atomization stage.

The steady signal increases at 10 mmol dm^{-3} nitric acid (in 0.01 mol dm^{-3} NH_4NO_3) and at 15 mmol dm^{-3} nitric acid (in 0.05 mol dm^{-3} NH_4NO_3) can be observed reproducibly. It is still unclear whether this phenomenon relates to the change in the successive complexes components or it is the combination results with the oxidizing influences from nitric acid.

4.2.4 Ammonium nitrate influences on the boiling point

The influence on boiling point of a droplet is more complicate than a solution. It depends on the salt concentration, the radius or curvature of droplet, the surface tension, etc. Under the same nebulizing conditions, the tertiary aerosol distribution would not be changed significantly. Therefore, ammonium nitrate is the main source for the boiling point increase. When the aerosol passing by the tip of torch injector, the retention time and the heat obtained from that zone is not enough to completely eliminate the complexing capabilities of NH_4NO_3 . In this case, increase in boiling point is helpful to delay the desolvation and inhibit mercury complex thermolysis and adsorption. In the central channel of plasma, almost all the droplets are desolvated and vaporized. Due to the heating time (depends on the life-time of a droplet) is prolonged for the higher boiling point, the average temperature of a droplet is increased. The heat obtained from

plasma is enough to become a major factor to shift all the equilibria mentioned above toward the mercuric ion direction (left direction) and favors the thermal dissociation of mercury complexes. A quantitative description about the equilibrium state of each dissolving droplet in a varying temperature system is nearly impossible. However, in the low HNO_3 concentration range ($\leq 4.0 \text{ mmol dm}^{-3}$), it was really observed that the equilibria were shifted by the presence of nitric acid (see fig. 4.2.4). The complexing capability of ammonia was reduced by HNO_3 , which led to a mercury signal increase. When HNO_3 concentration are higher than 4.0 mmol dm^{-3} , the signals mainly reflect the influences from the oxidizing inhibition of HNO_3 and the heat exchange for the boiling point increase. In this case, the oxidizing power of HNO_3 is partially counteracted by the thermo-shift for the boiling point increase. It may be one of the reasons that the signal level rises up with the increase of NH_4NO_3 concentration at high acidity.

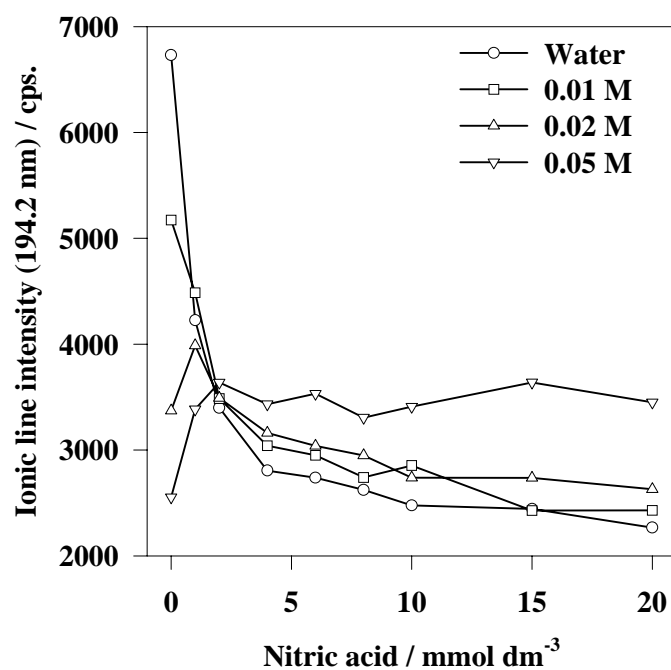
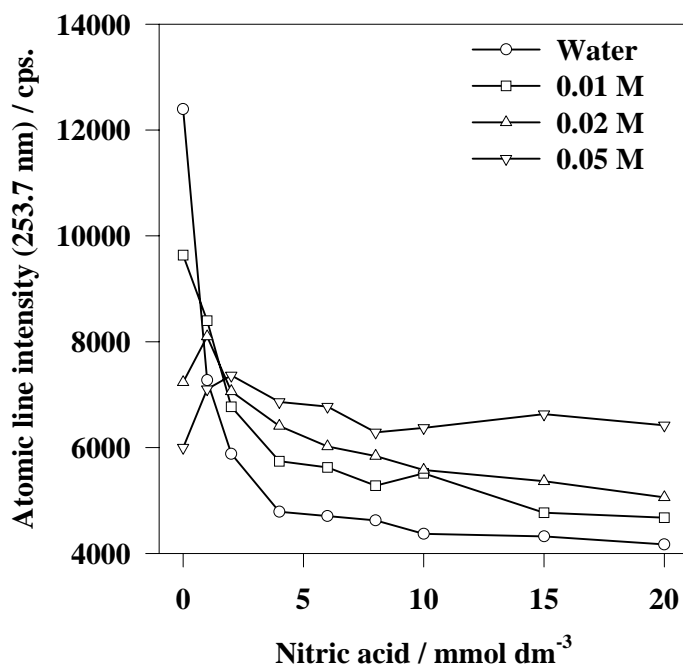


Fig. 4.2.4: Mercury emission signals intensity in varying $\text{NH}_4\text{NO}_3\text{-HNO}_3$ solutions.

The temperature of a droplet is unforeseen. As a result, it is extremely hard to exactly separate the influences from chemo-shift and the thermo-shift on the equilibria.

However, the change of mercury emission intensity by shifting the complex formation equilibria at low acidity are more vigorous than it is by increasing the NH_4NO_3 concentration at high acidity. In the same ammonium nitrate concentration, a slight increase in nitric acid concentration (at the low acidity) can significantly change the mercury signals. Conversely, at the high acidity, the signals are mainly effected by the oxidizing power of HNO_3 and the thermo-shift by boiling point increase. The complexing capabilities of NH_4NO_3 are reduced considerably.

4.2.5 Summary

The concept of mercury complex formation equilibrium at ambient temperature has been proven to be valid for the heated aerosol in plasma. It was found that the concomitant NH_4NO_3 could inhibit mercury atomization and lead to a low emission signal. The equilibrium state is changed by the chemo-shift and the thermo-shift. The chemo-shift relates to the complex formation by ammonium nitrate and the complex dissociation by nitric acid. At low nitric acid concentration ($<4 \text{ mmol dm}^{-3}$), the equilibrium state is easily shifted by changing the concentration of NH_4NO_3 and HNO_3 . Therefore, uncertain mercury atomization and emission occurred. At high nitric acid concentration, the oxidizing power of HNO_3 becomes the main factor to inhibit mercury atomization. The thermo-shift relates to the heat obtained from plasma. With the increase of boiling point, the heat exchange between droplet and plasma is enhanced. It shifts the equilibrium state to the complex dissociation direction and reduces the red-ox inhibition of HNO_3 . As a result, it is observed that all the mercury signals increase with the increasing NH_4NO_3 concentration at high nitric acid concentration. The increase in boiling point also leads to a little influence on the desolvation efficiency of droplets. The concept of chemical equilibrium in plasma is useful to elucidate the matrix influences, the mercury memory, and the species discrimination in practical samples. It also offers the possibility to eliminate the matrix influences and memory effects by the chemical modification on sample solution to get a precise and accurate method for mercury determination.

4.3 Halogen complex formation equilibrium and the application in mercury determination with ICP-MS

4.3.1 Halogen complex formation equilibrium in inductively coupled plasma

The presence of nitric acid in sample solution leads to a selective suppression on ICP-based spectrometric signal intensity of mercury. It happens when nitric acid concentrations in external calibration standard solutions and in sample solution are not exactly matched. In Section 4.1, it has been proven that the signal suppression arose from the redox equilibrium between mercury and nitric acid in the central channel of plasma. The increase in nitric acid concentration leads to the redox equilibrium shift toward to the mercury dinitrate formation direction. As a result, mercury dinitrate reduction, that is the dissociation in the central channel of plasma, is inhibited. Then the suppressed mercury signal intensity is observed.

Mercury signal suppression also happens when ammonium nitrate exists in sample solution (see Section 4.2). The inhibition extent depends on the concentrations of ammonium nitrate and concomitant nitric acid. This has been proven as the complex formation equilibrium between ammonium nitrate and mercuric ion. Changing the concentration of NH_4NO_3 and HNO_3 can shift this equilibrium and alter mercury signal response. In some senses, by changing the boiling point, the presence of ammonium nitrate in sample solution may change the interaction between the droplet and the plasma.

It has been reported that the increase in hydrochloric acid has little influence on mercury signal intensity, except the change from pure water to the HCl solution [6]. Although, at low concentration, nitric acid has the similar physical properties to the hydrochloric acid, the interference on mercury spectrometric signals are significantly different. Based on the discussions about redox and/or complex formation equilibria in the central channel of plasma among mercury, nitric acid and ammonium nitrate, it is reasonable to hypothesize that the effect of chemical reaction equilibrium on mercury spectrometric signal intensity has its general meanings. According to the basic principle of redox equilibrium, the formation of metal complexes affects reduction potentials because the ability of the complex to accept or release an electron is different from that of the corresponding aqua ion with H_2O ligands. Similar to ammonia, the halogen ions, such as chloric and bromic ions, are able to form more stable complexes. The overall stable constants are in the same scale (see Table 4.3.1). Therefore, the formation of

halogen complexes and their influences on the equilibrium of mercury and nitric acid are expected.

Table 4.3.1. β values for HgL_x

Hg L_x	Cl^-	Br^-	I^-	NH_3
HgL	7.2	9.6	12.87	8.8
HgL ₂	14.0	18.0	23.82	17.4
HgL ₃	15.1	20.3	27.60	18.4
HgL ₄	15.4	21.6	29.83	19.1

In this section, some chemical interferences on mercury mass spectrometric signals will be discussed in detail. These chemical properties of halogen complexes have been applied to the determination of total mercury in Chinese Human Hair reference material GBW-09101. When hydrochloric or hydrobromic acid were taken as a modifier, the measured results met the certified value very well by using the external calibration method.

4.3.2 Halogen ions interferences in dilute aqueous solution

Provided that the formation of halogen complexes can suppress mercury compound dissociation in the central channel of plasma, the effects on mercury signal intensities are easy to be observed at low halogen concentrations. To prove this assumption, the processes of mercury standard aspiration and washout were monitored for hydrochloric acid at low concentrations. The aspiration program was the same as employed in the Section 4.2. Mercury standard solution ($20 \mu\text{g dm}^{-3}$, with $20 \mu\text{g dm}^{-3}$ indium as internal standard) was introduced into the plasma with a pneumatic nebulizer. The washout was performed with the dilute *aqua regia* solution. After starting the nebulization of mercury solution, a gradually increased mercury signal was observed. It was slowly closing to the invariable signal (see Fig. 4.3.1). As expected, the time-resolved signals show that the formation of halogen complexes leads to the mercury signal depression like it happens in ammonium nitrate solutions. The suppression trend on mercury signal intensity becomes more severe with the increase in hydrochloride acid concentration. Mercury memory in the sampling system is also gradually reduced with the increase in the concentration of hydrochloride acid. Although the memory still existed in the

sampling system and could be washed out by the leaching solution, there was not a washout peak appeared in the plot when the concentration of HCl was higher than 1.0 mmol dm^{-3} . It shows that mercury memory can be reduced by the presence of hydrochloric acid. A notable phenomenon is that, in this experiment, the time-resolved signal of water solution is higher than in the pure water solution showed in Section 4.1. That is because the addition of indium internal standard brought about 0.3 mmol dm^{-3} nitric acid into mercury standard solution. As a result, the monitored plot of mercury in water solution (exactly in $0.3 \text{ mmol dm}^{-3} \text{ HNO}_3$) produced the highest signal intensity and the most severe memory.

At the beginning, indium, the internal standard element, was just used as the indicator for the instrumental working conditions. Therefore, the time-resolved signals of mercury and indium were monitored simultaneously. In fact, indium also suffers from hydrochloric acid effect at extremely low concentration (see Fig. 4.3.1). For indium, the shape of the time-resolved signal is fairly dependent on the hydrochloric acid concentration in solution. This is due to the solubility of indium ion in aqueous standard solutions. At low acid concentration, there is certain amount of indium hydrolyzes and adsorbs in the sampling system. With the increase in HCl concentration, the adsorption is gradually inhibited. It could be found that the time needed to reach an invariable signal was shortened with the increase in hydrochloric acid concentration. Meanwhile, the washout peak became narrower and the area under the washout peak was significantly decreased. However, the total area under the time-resolved signal was almost kept in constant. It seems that chloric ion has no influence on indium mass spectrometric signals in the central channel of plasma.

The influences of hydrochloric acid on mercury and indium ions are quite different. Hydrochloric acid minimizes the memory of both mercury and indium in the same way. For the mass spectrometric signal intensity, with the increase in HCl concentration, mercury signal intensity decreases gradually. Meanwhile, the shapes of the time-resolved signal of indium change and gradually reach an invariable rectangle (see Fig. 4.3.1). These facts indicate that hydrochloric acid influence on mercury mass spectrometric signals is due to the chemical interference more than a physical effect.

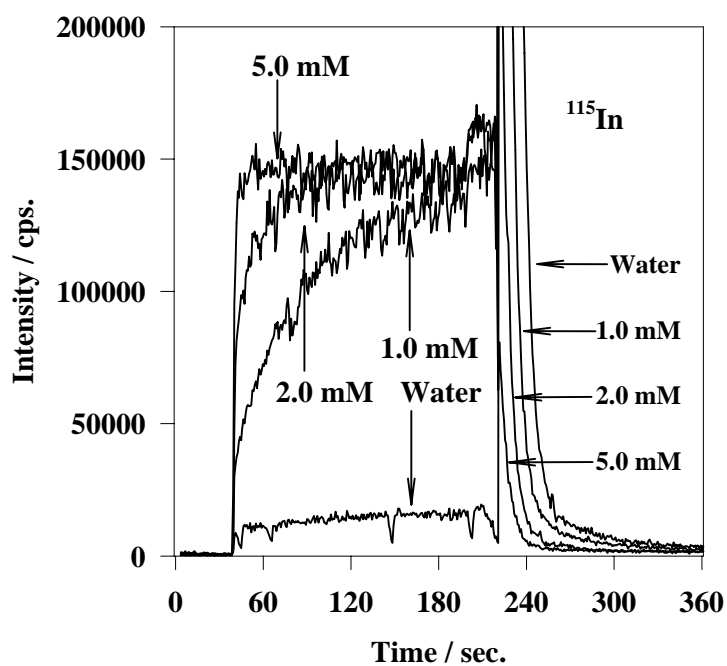
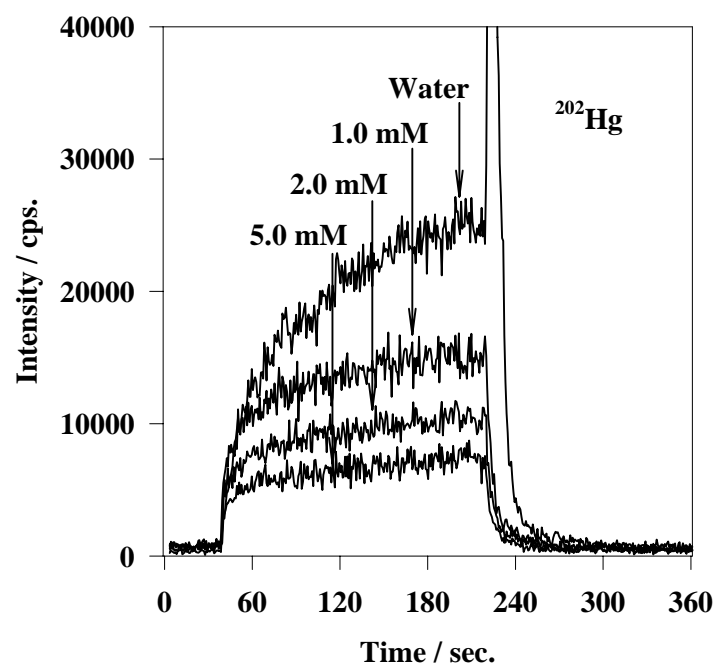


Fig. 4.3.1: Hydrochloric acid influences on the time-resolved signals of mercury and indium at very low concentrations. Mercury concentration: $20 \mu\text{g dm}^{-3}$; Indium concentration: $20 \mu\text{g dm}^{-3}$.

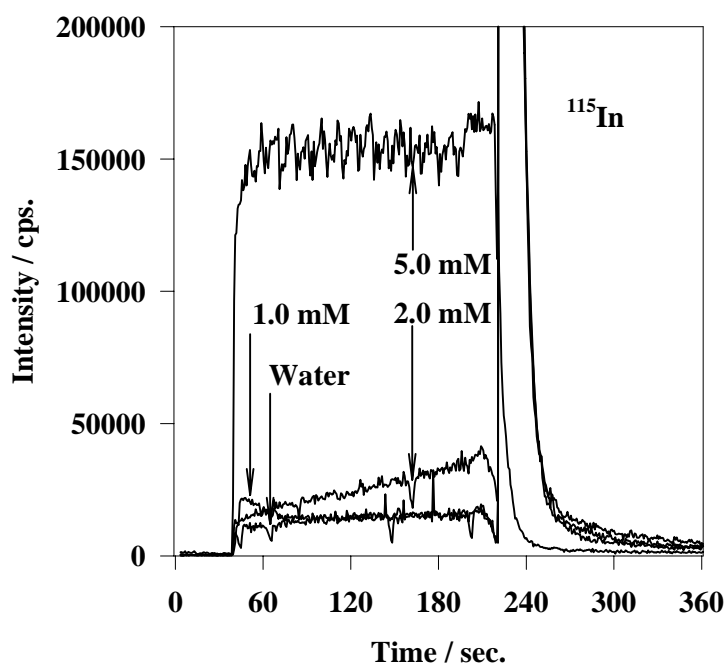
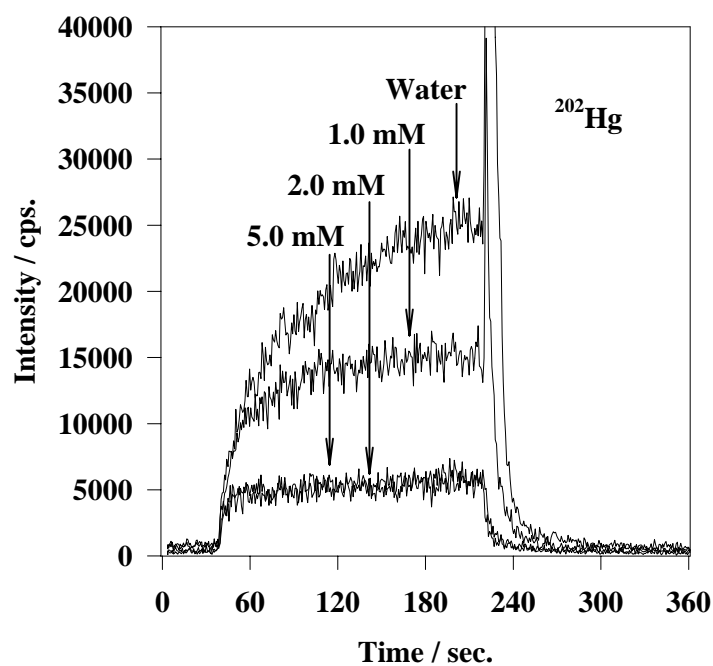


Fig. 4.3.2: Sodium chloride influences on the time-resolved signals of mercury and indium at very low concentrations. Mercury concentration: $20 \mu\text{g dm}^{-3}$; Indium concentration: $20 \mu\text{g dm}^{-3}$.

It has been shown that the presence of hydrochloric acid results in the suppression on mercury mass spectrometric signals. In theory, chloric ion is able to form stable mercury complexes. As has been discussed in Section 4.2, the formation of mercury ammonia complexes leads to the chemical suppression on mercury dissociation in the central channel of plasma. The property of ligands governs the stability of mercury complexes. However, other chemical properties of mercury, such as the tendency to be reduced as metal, are still remained. Therefore, it is reasonable to hypothesize that hydrochloric acid effects on the mercury signal intensity arise from chloric ion that leads to the formation of mercury complex. As a result, mercury compounds dissociation in the central channel of plasma is suppressed by the concomitant chloric ions in mercury standard solution. It is followed by the suppression on mercury mass spectrometric signal as discussed in Section 4.2.

To confirm this hypothesis, a comparing experiment with sodium chloride solutions was carried out under the same conditions. The plots show that the time-resolved signals of indium suffered a severe suppression from the hydrolyzation. This effect can be reduced by increasing sodium chloride concentration in mercury standard solution (see Fig. 4.3.2). The possible interpretation is that the presence of sodium chloride is able to enhance the solubility of indium ion in aqueous solution. When sodium chloride concentration is higher than 5.0 mmol dm^{-3} , the time-resolved signal of indium is very similar to the plot obtained with the standard solution of 5.0 mmol dm^{-3} hydrochloric acid. It means that the hydrolyzation has been inhibited. Due to indium hydrolyzation happens at low sodium chloride concentration in the similar magnitude, it is difficult to assay the changes of the washout peaks. In general, with the increase in sodium chloride concentration, the peak height decreased. However, the total area under the time-resolved signal was increased (concentration / mmol dm^{-3} , counts; water, 28139624; 1.0, 28269960; 2.0, 32414099; 5.0, 36799145). It seems that sodium ion at very low concentration can increase electron number density and promote indium ionization in the central channel of plasma. It leads to the enhancement of indium mass spectrometric signals.

The time-resolved signals of mercury show that the increase in NaCl concentration leads to mercury signal intensity decrease. Comparing mercury signals obtained from 1.0 mmol dm^{-3} HCl and NaCl solutions, the signal intensities are 15033 and 15130 cps respectively. There is not significant difference. Due to the concentration of chloric ion is more critical, any change in the concentration of chloric ion may lead to a significant

variation in the shape of the time-resolved signal of mercury. It can be found that the plot of mercury obtained from 1.0 mol dm^{-3} sodium chloride solution shows a washout peak. However, it does not emerge in the plot obtained from 1.0 mol dm^{-3} hydrochloric acid solution. Mercury plots obtained from 2.0 and 5.0 mol dm^{-3} sodium chloride solutions show no significant differences in the signal intensities. The reasons are still unknown. It is likely attributed to the critical mercury signal response and/or the influence from sodium ions. In fact, the shapes of these two plots are different. It is difficult to be distinguished from the black-white figure. For the plot obtained from 2.0 mol dm^{-3} NaCl solution, the signal increases gradually. During the nebulization of leaching solution, a trace amount of mercury was eluted from the system. It shows that mercury memory happens. Comparing with this, the plot obtained from 5.0 mol dm^{-3} NaCl solution is more horizontal. The sampling-washout plot is more clean-cut. Therefore, the memory of mercury in the sampling system is less suspectable.

Based upon the discussions above, the presence of chloric ion in mercury standard solution will suppress mercury signal and reduce mercury memory. It reproduced the chemical suppression on mercury compound atomization by shifting the complex formation equilibrium. However, this equilibrium position is more close to the right side and favors to the formation of mercury complexes, even at very low concentration.

The comparison of the complexing capabilities among the halogen ligands of chloric, bromic and iodic ions gives the further evidences to support the complex formation effects on mercury compounds dissociation in the central channel of plasma. Potassium chloride, potassium bromide and potassium iodide were chosen to verify the influence of complexing capability on mercury compound dissociation. To make sure the influence is only from the halogen ions, mercury standard solution was prepared by blending certain amount of halogen potassium solution. Acid and indium internal standard were not used.

When potassium chloride was added into mercury standard solution, the shape of the time-resolved signal of mercury changed more significantly. After starting the nebulization of mercury standard in pure water solution, the signal increased slowly. The washout peak is so huge. It shows that most of the mercury was adsorbed in the sampling system. With the increase in the concentration of potassium chloride, mercury memory was gradually inhibited. It shows that the mercury signal level was raised up and the washout peak was reduced drastically. The higher the concentration of chloric

ion, the more clean-cut the shape of the sampling-washout plot. When chloric ion concentration is higher than 50 mmol dm^{-3} , memory is almost eliminated.

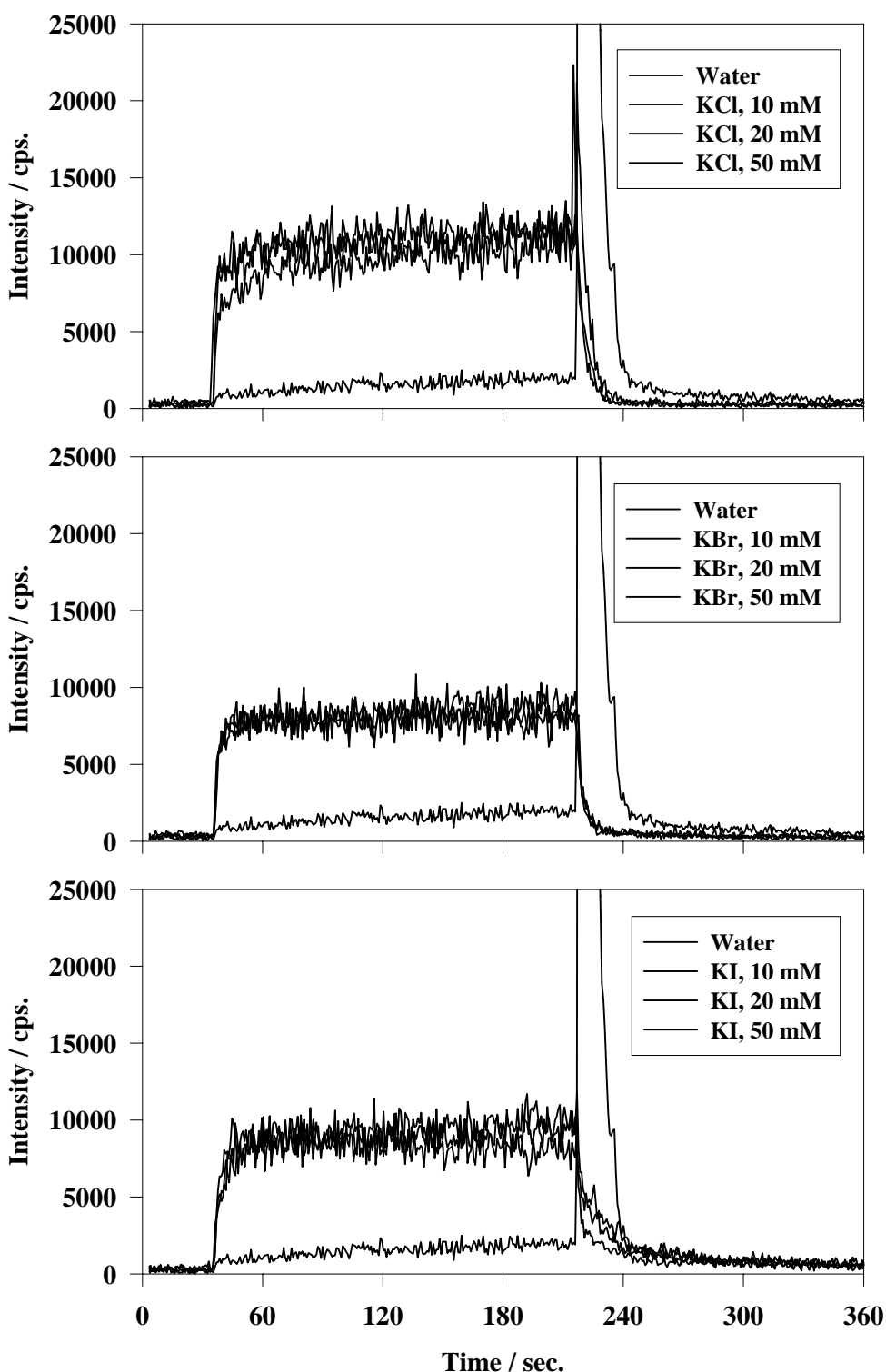


Fig. 4.3.3: Potassium haloids influences on the time-resolved signal of mercury. The concentration of mercury is $20 \text{ } \mu\text{g dm}^{-3}$. The solutions are without nitric acid.

It has been proved that the mercury memory is correlated to the signal suppression. Therefore, in certain meanings, chloric ion inhibition on mercury memory indicates the chemical suppression on mercury compound dissociation in the central channel of plasma.

When potassium bromide was added into mercury standard solution, there was not too much significant change in the time-resolved signal of mercury standard in the KBr solutions. Although the signal slightly increased when starting the nebulization of mercury standard in 10 mmol dm^{-3} KBr solution, there is no detectable mercury memory in the sampling system. Therefore, when the concentration of potassium bromide is higher than 10 mmol dm^{-3} , the memory of mercury seems to be completely eliminated. This may be due to the higher complexing power of bromic ion than chloric ion (see Table 4.3.1). It should be noticed that the invariable signal obtained from potassium bromide matrix is significantly lower than from potassium chloride matrix. Obviously, this fact is related to the higher complexing capability of bromic ion than chloric ion. Up to now, the complex formation equilibrium influence on mercury compounds dissociation in the central channel of plasma has been well proved. It is the shift of the complex formation equilibrium that leads to the change in the standard reduction potential of mercury. The more stable the complex, the higher its resistance to reductive decomposition (equal to the thermal dissociation in the central channel of plasma). In this instance, Br^- forms complexes that are thermodynamically more stable than those formed by Cl^- . As a result, the dissociation efficiency of mercury bromide complexes in the central channel of plasma will be inhibited more severely than chloride complexes. The observed result is that mercury mass spectrometric signal obtained from KBr solution is suppressed more severe than the signal obtained from KCl solutions.

A surprising result was obtained when potassium iodide was introduced into mercury standard solution. Comparing the time-resolved signal of mercury, the intensities obtained from potassium iodide solutions are slightly higher than the intensities obtained from potassium bromide solutions. This non-significant change implies that the difference in the stability of iodide complexes and bromide complexes in the central channel of plasma is not so significant, because both iodide and bromide complexes are so stable. The surprising result is that the washout plots obtained by rinsing out mercury in KI solution are not so clean-cut as the plots obtained from KBr solution. It rises a question: mercury in potassium iodide solution exists as complexes or

in other forms? It should be pointed out that when KI concentration in mercury solution was 50 mmol dm^{-3} , the time-resolved signal of mercury deviated from the horizon and went down slowly. The washout peak is also more clean-cut. Provided that mercury exists as complexes, assaying from the stable constants, all the three potassium iodide solutions should show the same washout peaks as observed with potassium bromide solution. However, there is no proof to support this argument. It is likely, at high iodide ion concentration, mercury was first reduced to Hg(I), and then precipitated. This precipitate is difficult to be washed out by the leaching solution. Therefore, in the case of 50 mmol dm^{-3} KI solution, the plot shows no mercury eluted from the sampling system. Unfortunately, there is not a direct proof to conform this assumption.

4.3.3 Halogen complex formation equilibrium in concentrated aqueous solution

The effects of hydrochloric acid and sodium chloride on the mass spectrometric signal of mercury have been investigated from very low concentration to the high concentration. With the freshly prepared standard solutions, mercury signal intensities are rather stable in the HCl solutions from 0.1 to 0.5 mol dm^{-3} . It reproduced the published result [6]. In the same concentration NaCl solutions, mercury signals are decreased significantly. At very low concentrations, mercury signal in HCl solutions changed not so vigorous. However, in NaCl solutions, the signal rose up at 0.01 mol dm^{-3} , and then continually decreased (see Fig. 4.3.4-*fresh*). The same measurement was repeated 24 hours later. Within the whole NaCl concentration examined, the effects were similar to the fresh prepared solutions (see Fig. 4.3.4-*over night*). In HCl solutions, mercury signal intensities changed significantly. The signals did not change when HCl concentration higher than 0.2 mol dm^{-3} . However, at the concentrations lower than 0.2 mol dm^{-3} , some of the signals increased obviously. Surprisingly, in 0.01 mol dm^{-3} HCl solution, mercury signal intensity shows a drastic increase. Comparing these two figures, it is easy to find that mercury signal in the aged 0.01 mol dm^{-3} HCl solution and in the fresh/aged 0.01 mol dm^{-3} NaCl solutions has the highest intensity. It implies that a thermodynamically stable species of mercury may exist in the 0.01 mol dm^{-3} chloric ion solutions. Mercury(II) chloride is a covalent compound that even in aqueous solution is present mainly as un-ionized covalent molecules [105]. The complex of mercury chloride mainly exists in the two ligands form for the special stable constants. Therefore, in such solutions, mercury exists as covalent molecule or as complexes are still unknown.

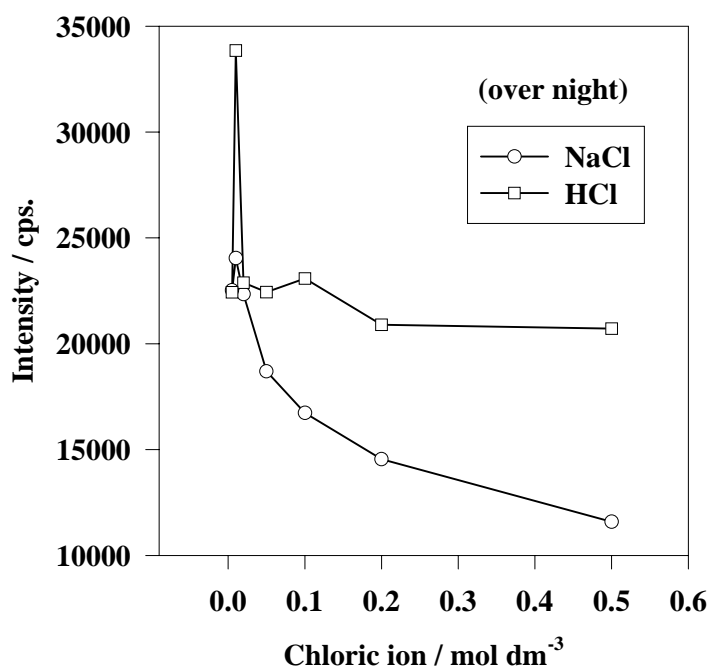
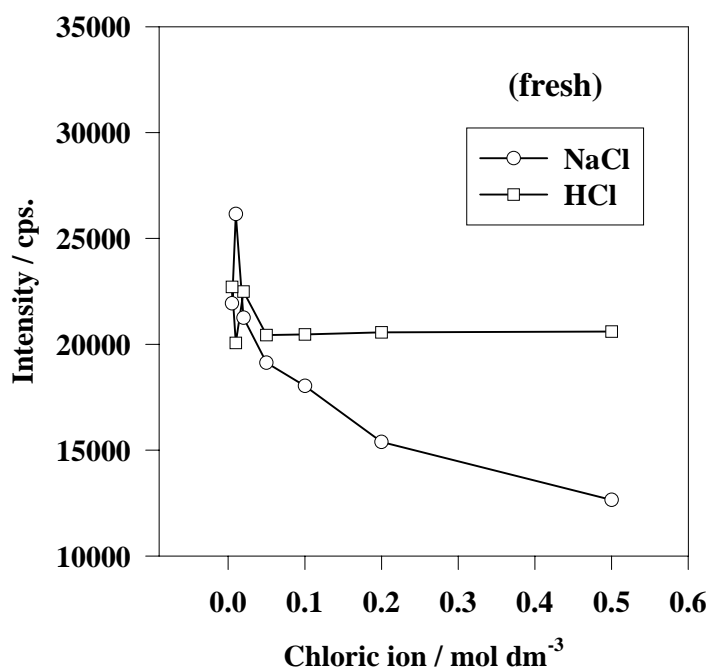


Fig. 4.3.4: The steady state signals of mercury and the influences from chloric ion concentration. The concentration of mercury is $20 \mu\text{g dm}^{-3}$. The solutions were without nitric acid. Mercury were measured with freshly prepared standard solutions and repeated with the same solutions 24 hours later.

Mercury signal intensity decreases significantly with the increase in sodium chloride concentration. No difference between the freshly prepared standard solutions and the overnight aged standard solutions could be observed. This indicates that the signal suppression is related to the sodium ion influences on the ionization equilibrium in the central channel of plasma. It has been discussed in Section 2 that the desolvating droplets and the vaporizing particles may lead to a drastically temperature drop around the droplets and the particles. As a result, the atomization and ionization equilibria nearby those particles are inhibited. Therefore, mercury signal depression is expected.

4.3.4 Halogen complex formation equilibrium in nitric acid solution in the ICP

Provided that mercury halide complex formation reaction exists in the central channel of plasma, in theory, this equilibrium is not so sensitive to the change of acidity in mercury standard solution. This properties is quite different from the equilibrium between mercury (II) ion and ammonia because there is no hydronium involved in the reaction for mercury halide complex formation. The apparent stability of mercury ammonia complexes is changed by the acid concentration in solution for the varied overall stable constant of the complex formation equilibrium. However, the apparent stable constants of mercury halide complexes do not change with the varied acid concentration in the standard solution. Therefore, in certain concentration of halogen acid solutions, it can be predicted that nitric acid has not a significant influence on the mass spectrometric signal of mercury. In these cases, the complexing abilities of halide ion mainly govern the mercury signal response in the central channel of plasma. To confirm this prediction, mercury standards were prepared in 0.2 and 0.5 mol dm⁻³ halide acid solutions with the varying nitric acid concentrations. With the freshly prepared 0.2 mol dm⁻³ hydrochloric acid solutions, mercury signal intensity decreased when nitric acid presented in the standard solution (see Fig. 4.3.5a). However, the decrease extent is independent on the nitric acid concentration. This indicates that mercury chloride complex in such solutions is not stable enough, or the standard reduction potential of the complex is not low enough, to resist the oxidizing power of nitric acid in the central channel of plasma. With the freshly prepared 0.2 mol dm⁻³ hydrobromic acid solutions, mercury signal intensities are more stable than the signal from 0.2 mol dm⁻³ hydrochloric acid solutions. This is due to the higher stability and lower standard reduction potential of bromide complex than chloride complex.

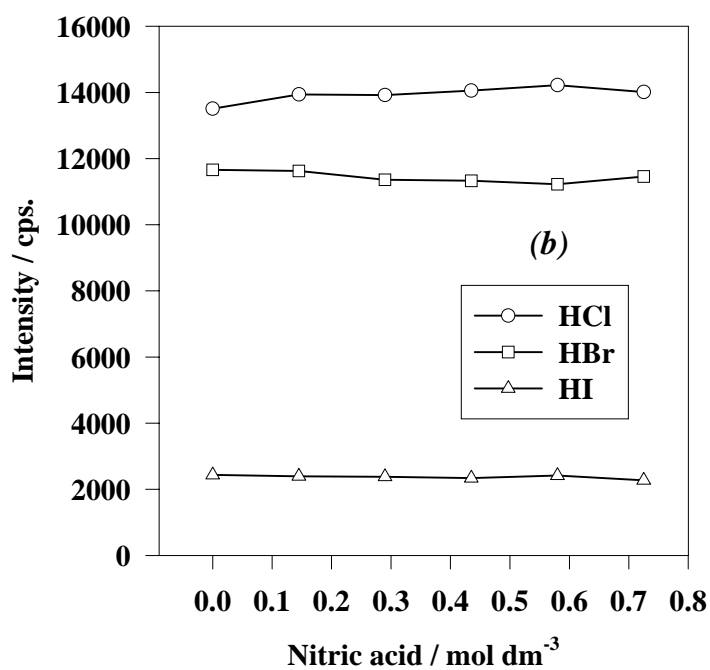
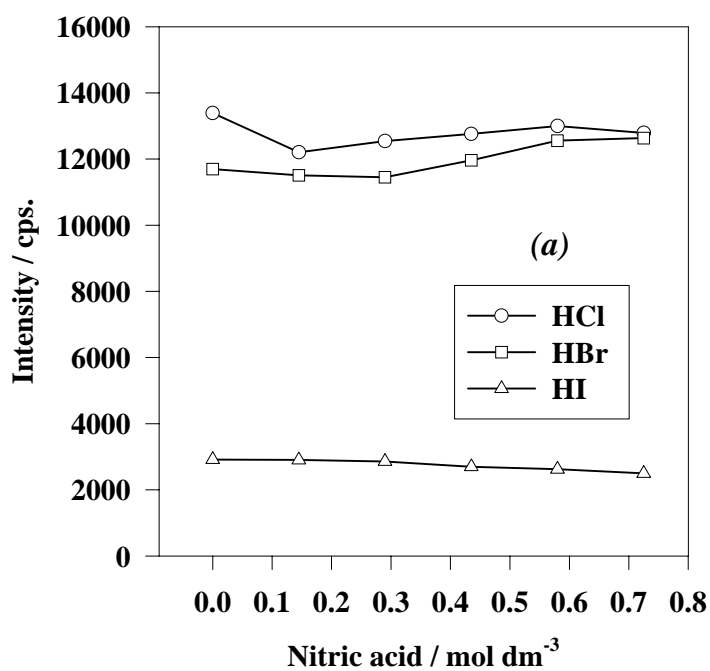


Fig. 4.3.5: Nitric acid influence on the steady state signal of mercury in 0.2 mol dm⁻³ halogen acid solutions. Mercury concentration is 20 µg dm⁻³ without internal standard. (a) freshly prepared mercury standard solutions; (b) overnight stood mercury standard solutions.

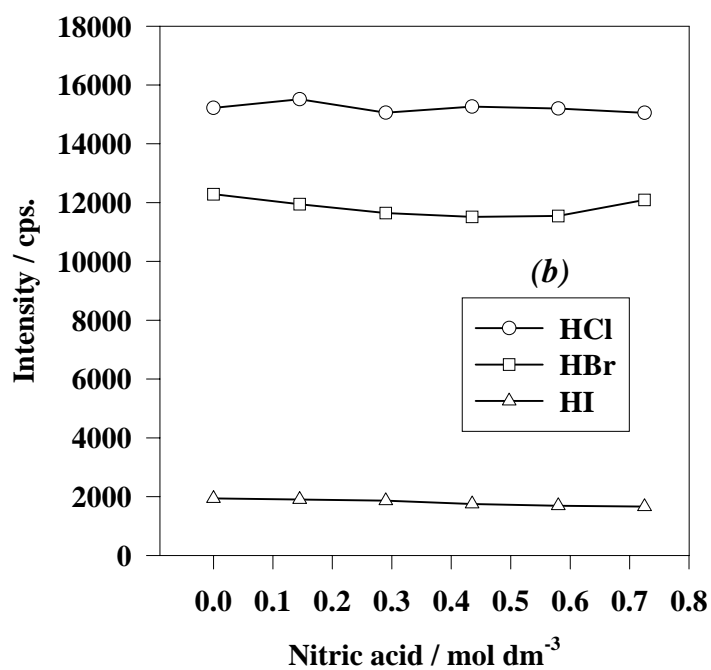
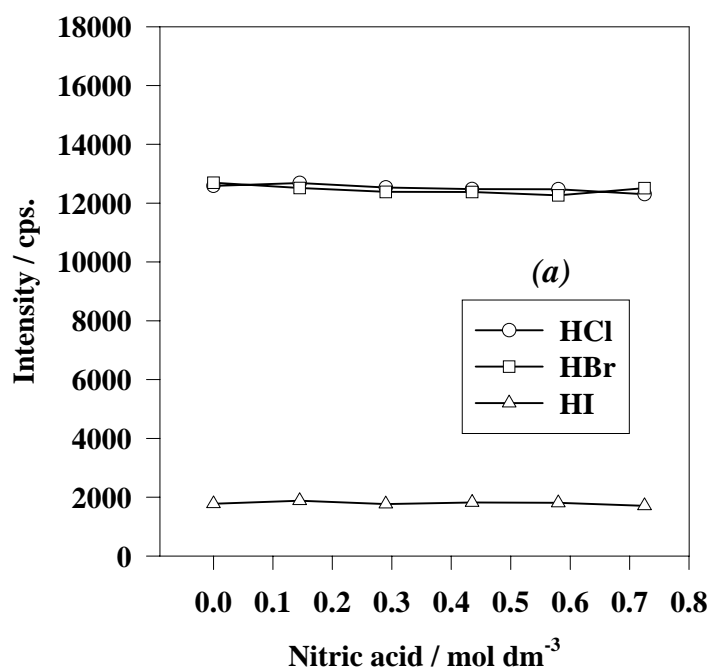


Fig. 4.3.6: Nitric acid influence on the steady state signal of mercury in 0.5 mol dm⁻³ halogen acid solutions. Mercury concentration is 20 µg dm⁻³ without internal standard. (a) freshly prepared mercury standard solutions; (b) overnight stood mercury standard solutions.

After stood for exact 24 hours, the mercury signal intensity of those mercury standard solutions increased significantly in 0.2 mol dm^{-3} HCl solutions (see Fig. 4.3.5b). The signal intensity is independent on the nitric acid concentration. This phenomenon suggests that the mercury mass spectrometric signals come out of a more stable thermodynamic mercury species in the standard solution. This has been briefly discussed before in this Section. It is likely that this species is mercury chloride, the covalent molecule. If though, the production of mercury signal in chloride ion matrix becomes more complicate. In the case of 0.2 mol dm^{-3} HBr solutions, there is a little change in the dependence of mercury intensity and nitric acid concentration. However, mercury signals from the aged solutions are rather stable with the increase in nitric acid concentration. That is the species discrimination among the mercury bromide compounds is not so significant.

There is an exception. With the 0.2 mol dm^{-3} HI solutions, no matter what the freshly prepared or overnight stood standard solutions, mercury mass spectrometric signals are extremely lower than the signals obtained with mercury standard in the same concentration of HCl or HBr matrix. During the experiment, it was found that the addition of nitric acid led to the standard solution became brown. The color became deep with the increase in nitric acid concentration. Clearly, the iodide ions have been oxidized by nitric acid because HI is a very strong reductive. At ambient temperature, mercury (II) ion reactions in HI solution are complicate. It becomes even more complicate when the temperature factor is involved in the chemical reaction system. The observed signal suppression is probably related to many reasons. The first is that mercury (II) might be reduced to mercury (I) and precipitate in the solutions. That led to the mercury entering into plasma decreased. The second one is that the mercury iodide complex is too stable to be thermally dissociated. That leads to the species discrimination. The third one is that the first thermal ionization potential of iodine (10.45126 eV) is very close to the one of mercury (10.43750 eV) [106]. When a large amount of iodide ion exists in the mercury standard solution, the iodide will be inevitably brought into the central channel of plasma by the nebulization. As a result, comparing with mercury, huge amount of iodide will be atomized and ionized in the central channel of plasma. Iodide ionization in the sampling zone of plasma will then exhaust almost all of the energetic plasma species, of which the energy levels are around the first thermal ionization potential of iodine. Thus, the possibility of ionization for mercury atom will be significantly reduced. Finally, it leads to a severe inhibition on

mercury signal intensity. If though, it can be expected that nitric acid have no significant influence on mercury spectrometric signal intensity in the concentrated iodide ion solutions. This is in a good agreement with the experimental results (see Fig. 4.3.5).

With the freshly prepared 0.5 mol dm^{-3} halide acid solutions, mercury signal intensities are very stable (see Fig. 4.3.6a). It could be found that the signal intensities obtained from HCl and HBr solutions are almost the same at any nitric acid concentrations in the experimental ranges. After the solutions were stood for 24 hours, comparing with the freshly prepared solutions, the mercury signal intensities from the aged 0.5 mol dm^{-3} HBr solutions did not change (see Fig. 4.3.6b). However, the mercury signal intensities from the aged 0.5 mol dm^{-3} HCl solutions increased more vigorous than the one from the aged 0.2 mol dm^{-3} HCl solutions. This suggests that the unknown mercury chloride species have higher sampling efficiency than the species in the freshly prepared hydrochloric acid solutions. It is likely related to the formation of a more volatile species.

With the freshly prepared and the aged 0.5 mol dm^{-3} iodide acid solutions, iodide ion inhibition on mercury signal intensity was observed again. In general, mercury signal intensities obtained from the freshly prepared and/or the aged 0.5 mol dm^{-3} iodide acid solutions are lower than the intensities obtained from the freshly prepared and/or the aged 0.2 mol dm^{-3} iodide acid solutions. It seems related to the ionization inhibition by quenching certain energetic species in the sampling zone of plasma with the dense iodine cloud.

4.3.5 Mercury determination with halide acid as modifier

In the last section, it has been proved that mercury in halide acid solution is free from the influence as changing the nitric acid concentration in mercury standard solution. Although nitric acid leads to severe suppression on mercury signal intensity, the addition of halide acids makes it possible to determine mercury in the varying nitric acid concentration solutions with high accuracy. In this meaning, halide acid acts as *chemical modifier* to minimize or eliminate the nitric acid influences on the mercury mass spectrometric signal. As far as the author is aware, this description is the first such attempt.

To put this idea into practice, the biological reference material Chinese Human Hair GBW-09101 was chosen as a target sample. The first advantage is for its well done sample digestion method in this laboratory. The second one is that there is a published

work of this laboratory can be directly used as references. In that paper, the conclusion is that the accurate results for mercury determination with ICP-MS can be obtained with standard addition method, acid matrix matching method and mathematical correction method after the external calibration. The simply external calibration will lead to significant low results [6].

After the sample (~200 mg) was mineralized with 2.5 HNO₃ + 0.5 H₂O₂, the digest was moved into 50 cm³ volumetric flask. The flask was filled with pure water to the mark. Then, four aliquots of the exactly 10 cm³ sample solution was moved into four pieces of PE test tubes. They were added with 0.2 cm³ HCl, 0.5 cm³ HCl, 0.2 cm³ HBr, and 0.5 cm³ HBr, respectively. Mercury external calibrating solutions were prepared in 0.29 mol dm⁻³ nitric acid matrix. They were handled as the sample solutions. The solutions were stood 24 hours after the halide acid modifier was added. Then the samples were measured using ICP-MS. The external calibration method, with halide acid as chemical modifier, was employed to determine the total mercury in the Chinese Human Hair reference material. The measured results of mercury under different modification conditions and the certified value were listed in Table 6-2.

Table 4.3.2. Mercury in Chinese Human Hair GBW 09101 reference material.

	<i>Modified</i>	<i>Modified</i>	<i>Modified</i>	<i>Modified</i>	<i>Without</i>	
<i>Modifying</i>	<i>with</i>	<i>with</i>	<i>with</i>	<i>with</i>	<i>modifier in</i>	<i>Certified</i>
<i>conditions</i>	<i>0.2 M HCl</i>	<i>0.5 M HCl</i>	<i>0.2 M HBr</i>	<i>0.2 M HBr</i>	<i>solution*</i>	<i>value</i>
in µg g ⁻¹	2.26±0.08	2.21±0.11	2.13±0.06	2.06±0.07	1.61±0.05	2.16±0.21

*Data from reference [6].

If the external standard calibration method was directly used for mercury determination, the result is significantly lower than the certified value (see Table.4.3.2). After modified the solutions with halide acids, all the results are in good agreements with the certified value. The advantages of chemical modification on mercury in the sample solution are obvious. The first benefit is that, even though the analyst has not the knowledge about the acid matrix in detail, an accurate result is available. The second advantage is more prominent for the simplified sample preparation and the enhanced capability for the bulk sample analysis. In a word, external standard calibration method can be used to get the results as qualified as using a standard addition method.

4.4 Redox equilibria between nitric acid and precious metals in ICP and the influences on the mass spectrometric signals

Platinum group elements and gold (PGEs + Au) exist in nature at very low levels. The use of catalytic converters for automobiles leads to a conspicuous anthropogenic emission of some PGEs along the roadsides. It has drawn a lot of attentions of the analysts [107-108]. However, normal analytical methods, even inductively coupled plasma optical emission spectrometry (ICP-OES), do not entirely meet the requirements on determining PGEs + Au in geological and environmental samples. The development of inductively coupled plasma mass spectrometry (ICP-MS) has offered a high sensitive detection technique for most elements. However, for PGEs + Au, the high sensitivity does not always bring about the practical detection limits as low as expected. Inaccuracy and imprecision are the fatal drawbacks, which always obstruct the determination of PGEs + Au in the complicate matrixes or at the low concentrations.

Uncertain signals and low recoveries are frequently encountered when measuring PGEs + Au using ICP-MS with pneumatic nebulization techniques. The memory effects always deteriorate the practical detection limits [109-110]. Barefoot [111] summarized that nickel sulfide fire assay (NiS-FA) followed by *aqua regia* (AR) leaching of samples did not yield accurate results for precious metals. The recoveries were too low. However, instrumental neutron activation analysis [112] shows little loss of PGEs + Au in the NiS-FA collectors. Vlasankova et al. [113] achieved quantitative recoveries for Pd, Pt and Au in pure solution with high repeatability. Whereas, the determination of those metals in reference material *NIES No. 8* showed large differences between individual measurements. The presence of NO_3^- was believed to diminish the recovery of those metals and the use of AR should be avoided. Using NiS-FA collection and tellurium coprecipitation method, Jackson et al. [99] claimed that gold was less efficiently recovered and with a high relative standard deviation, which indicates a larger and more variable loss than other PGEs. It may relate to the unmatched matrix between the standards and the AR dissolved samples. Their results for *SU-1a* also showed that Pt and Pd were over 10% less than the certified values. Contrarily, HCl has little influences on PGEs recovery. McDonald et al. [114] found that the residual AR and ethanol in sample solutions presented a problem. For PGEs + Au, good linear calibrations could be generated in both AR and HCl solutions. However, significant differences in the intensity of some isotopes were observed between these two matrices.

^{101}Ru , ^{103}Rh and ^{192}Os produced similar slopes but ^{106}Pd , ^{191}Ir , ^{195}Pt and ^{197}Au consistently produced lower values in the sulphide sample matrix.

Sun et al. [115] analyzed a group of geological reference materials. No HNO_3 was used for dissolving the NiS collectors. Li et al. [116] carried out PEGs speciation in geological samples without using HNO_3 . In both cases, the results agreed well with the certified values. After examined the PGEs + Au with various ICP-AES and ICP-MS systems, Kanicky et al. [117] reported that the matrix of HCl and Septonex has no significant interferences or deterioration of limits of detection. Reference [118] showed quantitative recovery of Au in HCl matrix. Whereas, in water or HNO_3 solutions, the signals of $10 \mu\text{g Au dm}^{-3}$ were almost undetectable.

The recoveries of PGEs + Au are fairly dependent on the digestion method [119]. With $\text{HNO}_3\text{-HCl-HF-HClO}_4$ digesting system, HNO_3 was completely repelled by fuming HClO_4 and the results met the certified values very well. With *aqua regia*-HF method, HNO_3 was still in the digest and caused a low recovery.

Non-spectral interference on PGEs signals could be effectively overcome by accurately matching the standard calibration solutions to the sample matrix [120-123] or by standard addition methods [124]. However, for Au, the remarkable poor reproducibility [122] and systematically low recovery [125] were still encountered. Isotope dilution (ID) technique does not require full elemental recovery. It could be used to compensate for low recoveries of Ru, Pd, Ir and Pt [126] and enable the accurate and precise measurement of Pt [127]. When the actual analysis measurements were initiated, the palladium signals changed in an uncharacteristically rapid fashion, perhaps due to selective (ad)absorption on the walls of the sample introduction system [127]. It seems, for the same reason, that the recovery of Au even depends on the concentration in samples [125].

The addition of $\text{Ni}(\text{NO}_3)_2$ can increase the efficiency of evaporation and transport for ETV-ICP-MS. However, the signals of Pd and Pt suffered severe suppressions from $\text{Ni}(\text{NO}_3)_2$ matrix by using pneumatic nebulization introduction [128]. Parent et al. [129] compared the thermospray nebulization (TN) with the pneumatic nebulization (PN) coupled with a FI-ICP-MS system for the determination of trace levels of platinum. TN was better than PN in the measuring precision and the agreement among three calibration methods. It seems that the wet aerosol and the desolvated particles behave different in the transport, evaporation, atomization, and ionization in the central channel of plasma.

The ion-exchange techniques are the strategies to separate or enrich PGEs + Au in the practical samples. Pu et al. [130], using 2-Mercaptobenzothiazole-bonded silica gel, effectively separated Au, Pt and Pd from matrix and quantitatively recovered them in HCl solutions for ICP-OES analysis. The results were in good agreement with the certified values. Rehkaeper and Halliday [131] used anion-exchange technique to separate the PGEs and other siderophile elements in the reference material *SU-1a*. The residual HNO₃ in digest might be retained on the column and enter into the eluate together with the PGEs. The highly discrepant results of Pt and Pd might relate to the matrix changes in HNO₃ concentration. After the anion-exchange, Jarvis et al. [132] decomposed thiourea in the eluate by HNO₃. The surplus HNO₃ could lead to the low results for PGEs + Au.

During cation exchange, the chlorocomplexes species of PGEs + Au and the HNO₃ in digest pass through the resin and are collected in the eluate. Mukai et al. [133] carried out a cation-exchange on-line FIA-ICP-MS. Quantitative recovery was achieved for hexachloroplatinic acid. However, after digested the reference material *SU-1a* with HNO₃-HF-HClO₄ and treated with AR, the recovery of platinum was found to be very poor (47% ± 20%). Ely et al. [123] used cation exchange pretreatment and ultrasonic nebulization ICP-MS to quantify PGEs + Au in geological samples. Nitric acid in the eluate severely inhibited the MS signals of PGEs + Au. The result of Au showed significant variability. Loss on the column was suspected. However, the results of standard addition method supported that the low recovery of Au was the signal loss, other than the analyte loss. Jarvis et al. [134] digested samples with AR-HF. The PGEs were quantitatively recovered. However, the recoveries of gold from the separated samples were low for all the materials. The authors believed that gold was lost during the ion exchange. The percentage loss of gold, although relatively reproducible, was not the same for different levels and / or materials, thus no simple mathematical correction is possible to compensate for the low recoveries. The emergence of the eluting plateau and the high reproducibility of the low recovery (~ 80%) among the different amounts of resin seem not related to the Au loss on column.

Apparently, in most cases, the irregular signal responses of PGEs + Au can be traced back to the use of HNO₃ during the sample preparation. Accurate results could be obtained only when the standard calibration solutions well matched the sample solutions, used standard addition or isotope dilution methods [135]. It indicates that the chemical properties of sample solution would be the main reason for the signal loss,

instead of the loss of precious metals during sample preparation. The matrix-induced chemical influences on ICP source spectrometric signal of mercury have been proven in the early studies [6-7]. In this work, we try to find out the inherent factors which lead to PGEs + Au behave different to other elements in HNO₃ matrix. It will further support the hypothesis of chemical interference in the central channel of plasma.

4.4.1 Procedures

The steady state signals were obtained by aspirating the working solutions in the descendant order of HNO₃ concentration. The aspiration procedure was a 60-second of diluted *aqua regia*, followed by a 60-second working solution uptake, then a 60-second × 3 integration. The time-resolved signals were obtained by a successive aspiration of pure water (180 s), working solution (180 s), 1% HNO₃ solution (40 s), and diluted *aqua regia* (140 s). The time-resolved signal collection started at the beginning of the working solution aspiration.

4.4.2 Gold memory and elimination

Gold memory in ICP-MS system is frequently encountered. The memorized gold bleeds irregularly, which deteriorates the accuracy and precision of the analytical methods. This makes it even impossible to measure Au at extremely low concentration.

To examine gold memory, the time-resolved signal of ¹⁹⁷Au was monitored in the sampling-rinsing circle (see Fig. 4.4.1). During the aspiration of a gold single standard solution, Au was partially retained in the system. The memorized gold could not be significantly washed out with 1% HNO₃ in 40 seconds. The following washout with diluted *aqua regia* resulted in a gold peak with a sharp leading edge and then the signal quickly went back to the background. It indicated that the memorized gold was effectively released from the sampling system. This phenomenon proved that the memorized Au was not retained in the spray chamber. Owing to the memorized gold compound can be washed off by diluted *aqua regia* instead of 1% HNO₃, ¹⁹⁷Au signals must come from the gold metal that deposits onto the inner surface of the tip of injector. Gold deposition fairly relates to the properties of aerosol. Wet aerosol, as normally introduced, can be partially evaporated when it passes by the injector. The droplet explosion in the injector inevitably spurts certain amount of analyte or fine droplets onto the inner wall. Due to the thermal conduction, thermal diffusion, thermal radiation

(photothermal effects) from the plasma, the deposited analyte suffers from thermolysis (atomization) and then accumulates as metal. Contrarily, dried aerosol goes through the injector as a laminar flow. No gold memory was observed [129]. The thermolysis can be reduced or inhibited by the presence of HNO_3 in sample solution (see in this section).

The increase in the nitric acid concentrations not only inhibits gold memory in the sampling system, but also suppresses the mass spectrometric signal intensities of ^{197}Au . The dependence of gold mass spectrometric signal intensities on the nitric acid concentration was examined with the increasing HNO_3 concentration. The steady state signals of ^{197}Au were collected from gold single standard solutions in the range of 0-0.725 mol dm^{-3} HNO_3 . The signals are normalized to the intensity obtained from the standard solution in 0.725 mol dm^{-3} HNO_3 matrix. The exponential descending plot of gold relative signal intensities shows that nitric acid has a strong suppression effect on the gold ion generation in the central channel of plasma (see Fig. 4.4.2). Under the same experimental conditions, the similar suppression trend on mercury mass spectrometric signals had been observed [6]. In Section 4.1, this effect has been proven to be a chemical inhibition on the atomization efficiency in the sampling zone of plasma by the oxidizing power of nitric acid. The increase in nitric acid concentration shifts the red-ox equilibrium towards the product side. Thus the atomization of gold and mercury are inhibited.

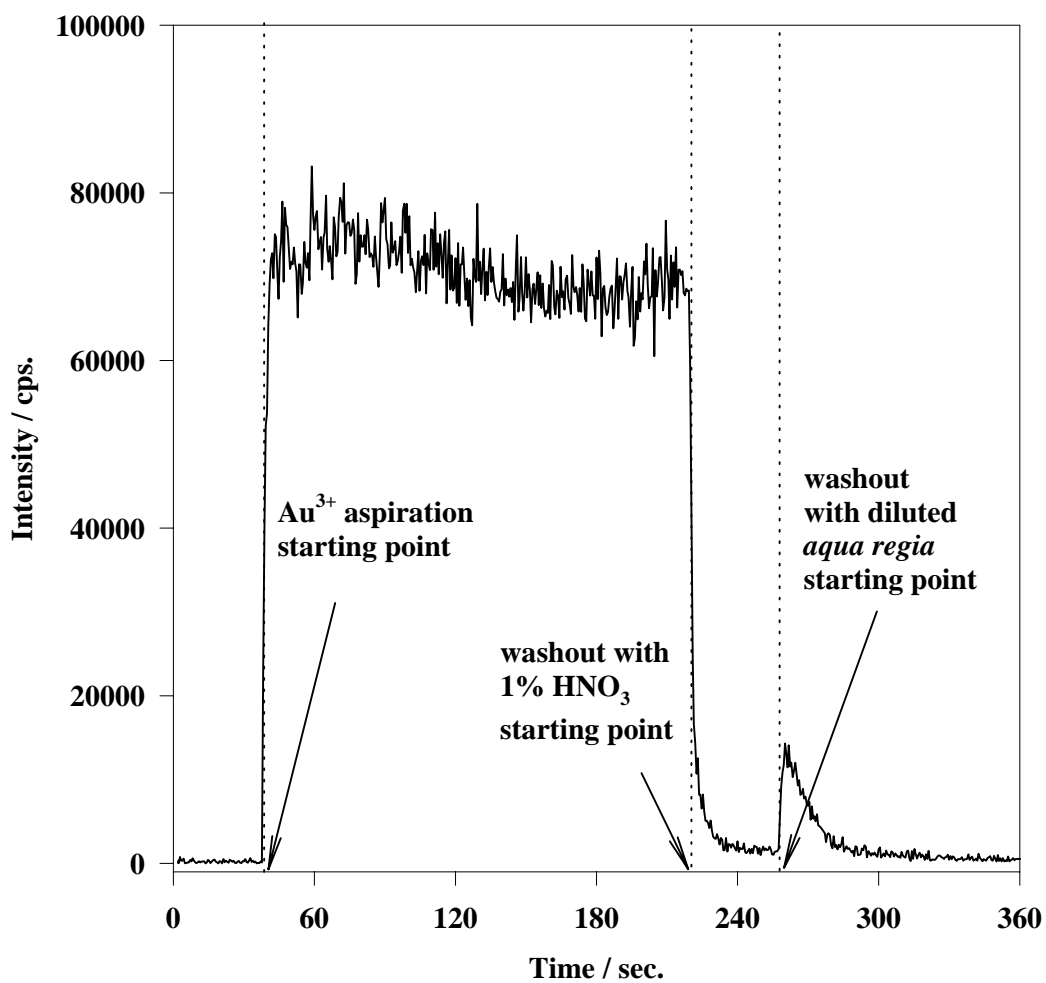


Fig. 4.4.1: The time-resolved signal of ^{197}Au in monitoring the aspiration and washout processes. The standard is 20 ng cm^{-3} Au in pure water solution. Rinsing solution 1, 1% HNO_3 solution; Rinsing solution 2, diluted *aqua regia* solution ($1 \text{ cm}^3 \text{ HNO}_3 + 3 \text{ cm}^3 \text{ HCl}$, diluted to 100 cm^3).

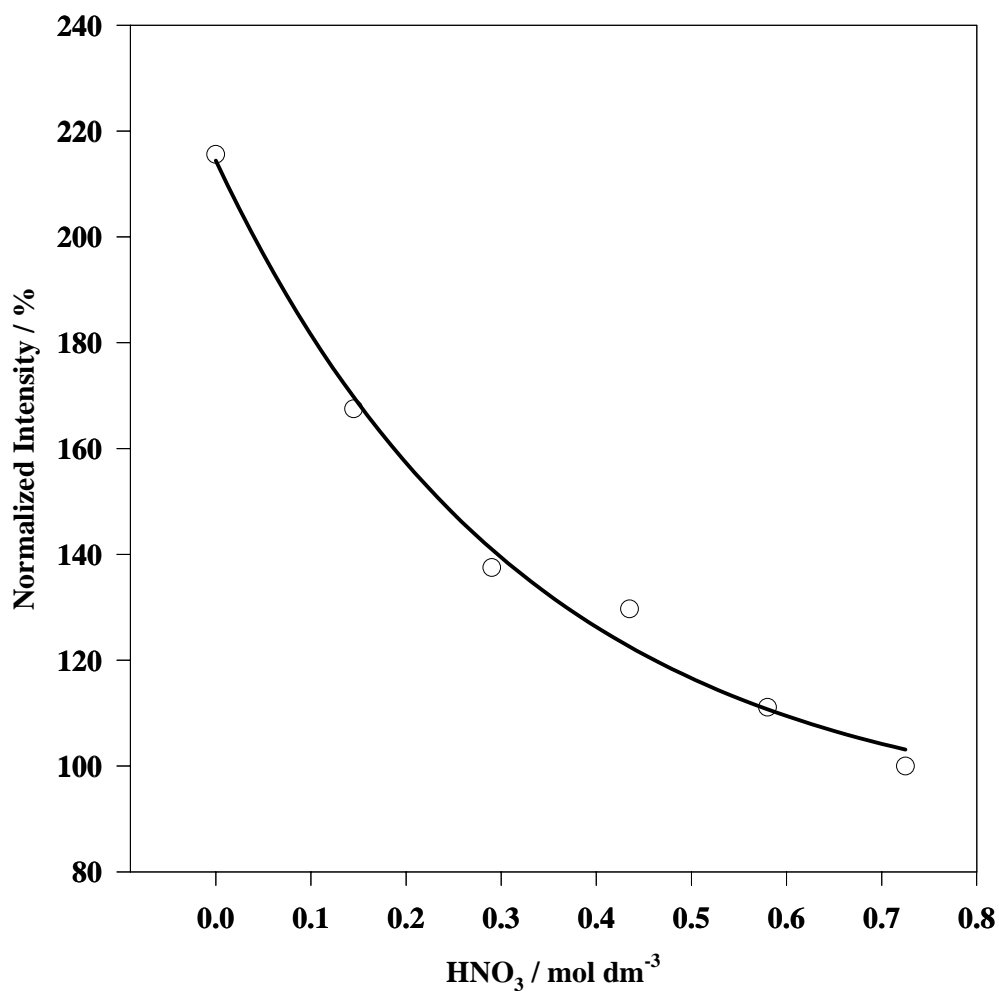


Fig. 4.4.2: The dependence of ¹⁹⁷Au mass spectrometric signals on the nitric acid concentrations. The gold single standards of 20 μg Au dm⁻³ in different nitric acid concentration solutions were used.

4.4.3 Time-resolved signal of platinum group elements and gold

Following the same procedure above, the time-resolved signals of PGEs + Au were monitored with the multi-standard solutions in different HNO₃ concentrations. The memory effects of precious metals were uncovered (see Fig. 4.4.3). It could be inhibited by increasing HNO₃ concentration in standard solutions for the enhanced oxidizing power. In the 0.725 mol dm⁻³ HNO₃ matrix, memory effect is almost negligible. Palladium and gold have the similar memory characteristics for their diagonal relationship in the element periodic table. The continually climbed ¹⁹³Ir signal meant that iridium in neutral solution suffered from the most serious memory. It could be easily rinsed out by the 1% HNO₃ solution. The climbing signal and the huge washout peak of iridium show its high thermolysis tendency. When the aerosol passes by the injector or enters the central channel of plasma, this properties resulted in a high dense of iridium atoms in the injector and in the sampling zone of plasma. Iridium atoms could capture and induce other precious elements to form an alloy or co-deposit as metals. It had been indirectly proven by the washout behaviors of Ir, Pt and Au. During standard solution aspiration, their signals rose up slowly. When washout started, almost all of the deposited Ir was instantly released by the 1% HNO₃ solution. With the fast release of Ir, other miscellaneous precious elements were brought together into the argon flow stream. Comparing with the time-resolved signals of ¹⁹⁷Au in Fig. 4.4.1 and Fig. 4.4.3 in the neutral solutions, it can be easily found that the deposited gold from Au single standard could not be washed out by a 1% HNO₃ solution. However, gold deposited from the multi-standard solution could be partially released by a 1% HNO₃ solution. The rear edge of the rinsing plot of gold was not so clear-cut as the one from Au single standard solution. The subsequent washout with the diluted *aqua regia* released a gold peak. After then, the signals went back to the baselines. After rinsing with HNO₃, there was still a small amount of iridium remained in the gold phase. Shown in the plot, it could be released together with gold by the diluted *aqua regia*. The alloy effects need further more direct evidences.

4.4.4 Standard reduction potentials and the nitric acid effects

The dependence of PGEs + Au mass spectrometric signal intensities on the nitric acid concentration was investigated in the range of 0-0.87 mol dm⁻³ HNO₃. For each element, the steady state signals were normalized to the intensity obtained from the standard solution in 0.87 mol dm⁻³ HNO₃ matrix.

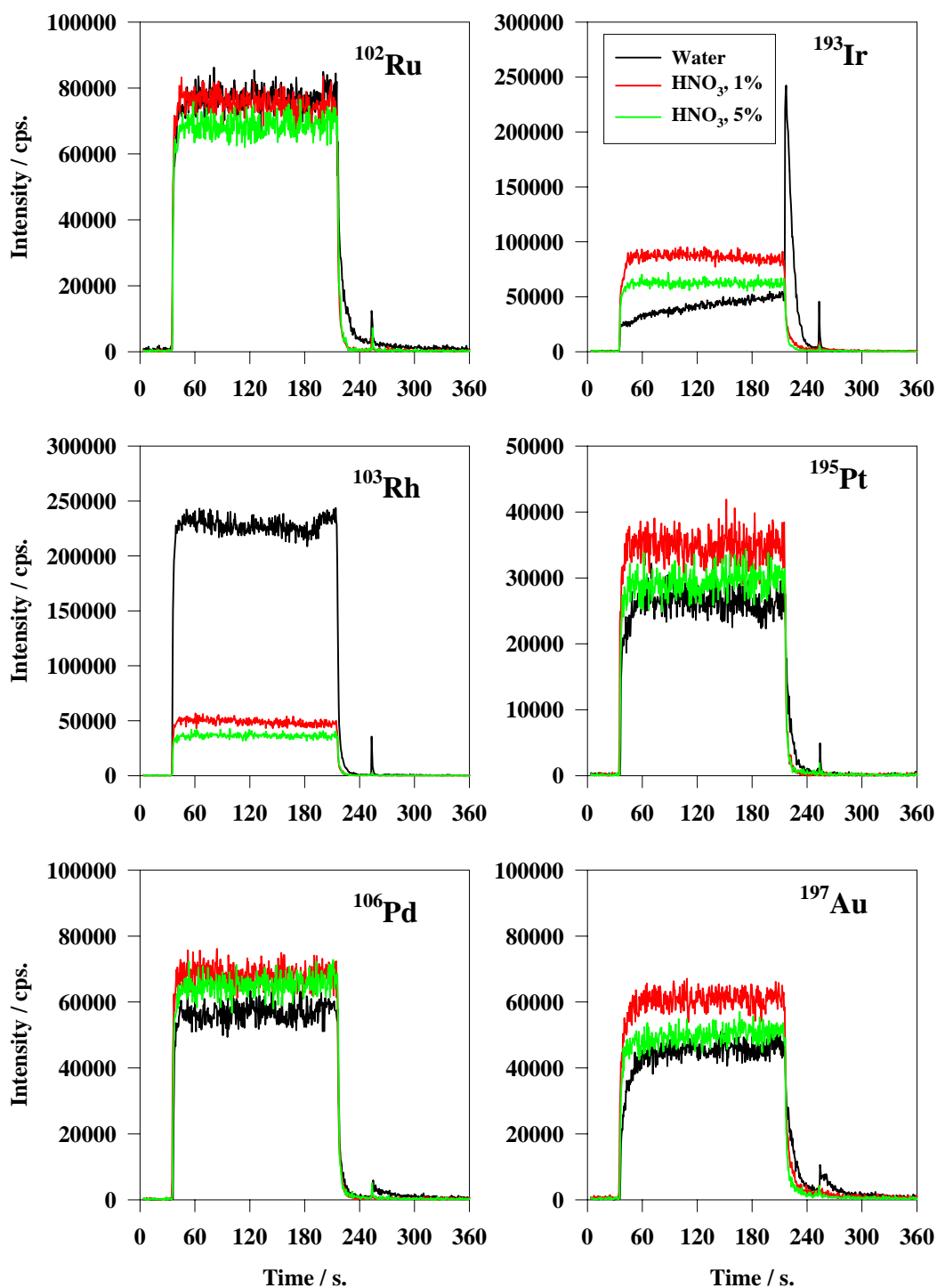


Fig. 4.4.3: Time-resolved signal of PGEs + Au for monitoring the aspiration and washout processes. The multi-standard solutions are 20 ng cm⁻³ (for each element) in water, 0.145 mol dm⁻³ HNO₃, and 0.725 mol dm⁻³ HNO₃. Rinsing solutions were the same as described in Fig. 4.4.1.

These six elements were apparently divided into two subgroups (see Fig. 4.4.4). For the light PGEs, including Ru, Rh, and Pd, the signals were little changed with the increasing HNO_3 concentration. For gold and the heavy PGEs, namely Ir and Pt, the signals were severely influenced by HNO_3 matrix. Although the ionization potentials are different between these two subgroups elements (see Table 4.4.1), it lacks direct evidences to prove that the increase of nitric acid concentration in such low levels can disturb the plasma thermal conditions and inhibit the ionization of PGEs + Au. The significant differences in the standard reduction potentials E° also exists between two subgroups of the precious elements (see also Table 4.4.1). The high E° values of PGEs + Au mean that those ions are easily to be reduced to element or atomized in the central channel of plasma. Unfortunately, under the normal plasma working conditions, these properties bring about a more variable atomization yield in the central channel of plasma. In this case, the atomization of precious metal compounds is possibly influenced by the chemical atmosphere in the central channel of the plasma, like it happens in the case of mercury. The low atomization efficiency directly leads to a low population of PGEs + Au ions in the plasma. Finally, the mass spectrometric signals of PGEs + Au are suppressed by the presence of nitric acid in the standard solutions. Since the MS signals of PGEs + Au not only rely on the nitric acid concentration, but also rely on the E° values, it is reasonable to hypothesize that nitric acid influences are related to the red-ox equilibrium in the central channel of plasma.

Provided that the nitric acid suppression on PGEs + Au mass spectrometric signals is attributed to the redox equilibrium between precious metals and nitric acid in the central channel of plasma, the inhibition on the atomization of PGEs + Au must happen before HNO_3 dissociation. In other words, it must happen before the droplet is completely desolvated. The existence of desolvating droplets in the central channel of plasma has been proven by theory simulations and by experimental results. Therefore, it is reasonable to say that the principles of chemical equilibrium in aqueous solution still work in the central channel of plasma. We can roughly estimate that the E° value of 0.75 V as the criteria for the ICP-MS system used in this work. If the E° value of a species is higher than 0.75 V, HNO_3 inhibition would happen. If the E° value of a species is lower than 0.75 V, HNO_3 inhibition is not so significant. In summary, it is the standard reduction potential of ions or species, that determines whether the atomization will be suppressed or not. In this experimental range, nitric acid in plasma could not

directly influence the ionization efficiency of PGEs + Au in the plasma. However, the increase in HNO₃ concentration could reduce the atomization efficiency of PGEs + Au in the central channel of plasma and lead to low ionization efficiencies. Therefore, the observed low signal response, to a great extent, is the result of the low atomization efficiency. The accompanying decrease in the thermolysis efficiency could also reduce the memory extent of precious elements.

Table 4.4.1 Some physiochemical properties of PGEs + Au.

Reduction reaction	Standard reduction potential (E°/V)*	Ionization potential (eV)**
$\text{Ru}^{2+} + 3\text{e} \rightleftharpoons \text{Ru}$	0.455	7.3605
$\text{Rh}^{3+} + 3\text{e} \rightleftharpoons \text{Rh}$	0.758	7.45890
$\text{Pd}^{2+} + 2\text{e} \rightleftharpoons \text{Pd}$	0.951	8.3369
$\text{Ir}^{3+} + 3\text{e} \rightleftharpoons \text{Ir}$	1.156	9.1
$\text{Pt}^{2+} + 2\text{e} \rightleftharpoons \text{Pt}$	1.18	9.0
$\text{Au}^{3+} + 3\text{e} \rightleftharpoons \text{Au}$	1.498	9.22567
$[\text{RhCl}_6]^{3-} + 3\text{e} \rightleftharpoons \text{Rh} + 6 \text{Cl}^-$	0.431	
$[\text{PdCl}_4]^{2-} + 2\text{e} \rightleftharpoons \text{Pd} + 4 \text{Cl}^-$	0.591	
$[\text{IrCl}_6]^{3-} + 3\text{e} \rightleftharpoons \text{Ir} + 6 \text{Cl}^-$	0.77	
$[\text{PtCl}_4]^{2-} + 2\text{e} \rightleftharpoons \text{Pt} + 4 \text{Cl}^-$	0.755	
$\text{AuCl}_4^- + 3\text{e} \rightleftharpoons \text{Au} + 4 \text{Cl}^-$	1.002	

*Reference [136].

**Reference [137].

A notable phenomenon is that nitric acid suppression on the mass spectrometric signals of gold depones on the concomitant iridium in the standard solutions. For gold single standard solutions, the increase in nitric acid concentration brought about an exponential descending plot of the isotope signal of ¹⁹⁷Au. Contrarily, under the same experimental conditions, a convex plot of ¹⁹⁷Au was obtained from the multi-standard solutions (see Fig. 4.4.2). This is due to the thermal dissociation iridium compounds was nonlinearly inhibited by increasing the nitric acid concentration. As a result, the inducing ability of iridium atoms to platinum and gold was inhibited nonlinearly with the increase of nitric acid concentration. Thus, the convex plots of the isotopes of ¹⁹³Ir, ¹⁹⁵Pt, and ¹⁹⁷Au were observed. It becomes another proof to support the Ir induced alloy effects.

After rinsing with the diluted *aqua regia* in between the measurements of two PGEs + Au standard solutions, the residual acidic aerosol and the released HCl molecules in spray chamber could form a HCl-rich atmosphere. When sample aerosol come into the spray chamber, HCl would be transferred into the droplets by collision, evaporation and absorption. It would change the precious metal ions into chlorocomplex ions. Before the droplet enters into the plasma, a considerable amount of the analyte is still confined in the liquid phase. It takes extremely short time to undergo desolvation, evaporation, atomization, and ionization in the central channel of plasma. Then the free ions in the sampling zone of the plasma are attracted into the mass spectrometer. For the low standard reduction potentials ($E^\circ < 0.75$ V), the atomization of Ru^{2+} , $[\text{RhCl}_6]^{3-}$, and $[\text{PdCl}_4]^{2-}$ is not influenced by HNO_3 . The signals were almost free from the change of HNO_3 concentration. As for $[\text{IrCl}_6]^{3-}$, $[\text{PtCl}_4]^{2-}$, and $[\text{AuCl}_4]^-$, the standard reduction potentials are higher than 0.75 V. It clearly shows that the signal inhibition strongly depends on the nitric acid concentration (see Fig. 4.4.4).

A 3-minute washout with pure water would expel HCl out of the sampling system. The steady signals in the HCl-rare atmosphere were obtained by taking the average of the corresponding time-resolved signals between 120-180 seconds (in Fig. 4.4.3). Those results were compared with the signals obtained in the HCl-rich atmosphere (see Fig. 4.4.5). It can be found, in the HCl-rare atmosphere, HNO_3 influences on the signals of Rh^{3+} , Pd^{2+} , Ir^{3+} , Pt^{2+} , and Au^{3+} are more pronounced. Except the neutral solution, the signal intensities of Pd, Ir, Pt, and Au obtained in the HCl-rare atmosphere are higher than those obtained in the HCl-rich atmosphere. This is due to the free ions have high standard reduction potentials. They are more easily atomized than the chlorocomplex ions of the low standard reduction potentials. For the same element, high E° value must lead to a high atomization yield and high signal response. There are exceptions for Ru and Rh. The E° value of ruthenium, both ions and the chlorocomplex ions, are lower than 0.75 V. The interference from HNO_3 are not so significant. The signal variation is in the experimental error tolerance. Contrarily, between the HCl-rare and HCl-rich atmosphere, nearly five-fold difference in rhodium signals is not negligible. The E° value of $[\text{RhCl}_6]^{3-}$ is 0.431 V. In the HCl-rich atmosphere, no influences arose from HNO_3 . However, the E° value of Rh^{3+} aqua complexes is 0.758 V. Therefore, in the HCl-rare atmosphere, the atomization of rhodium is seriously inhibited by nitric acid even at a low concentration.

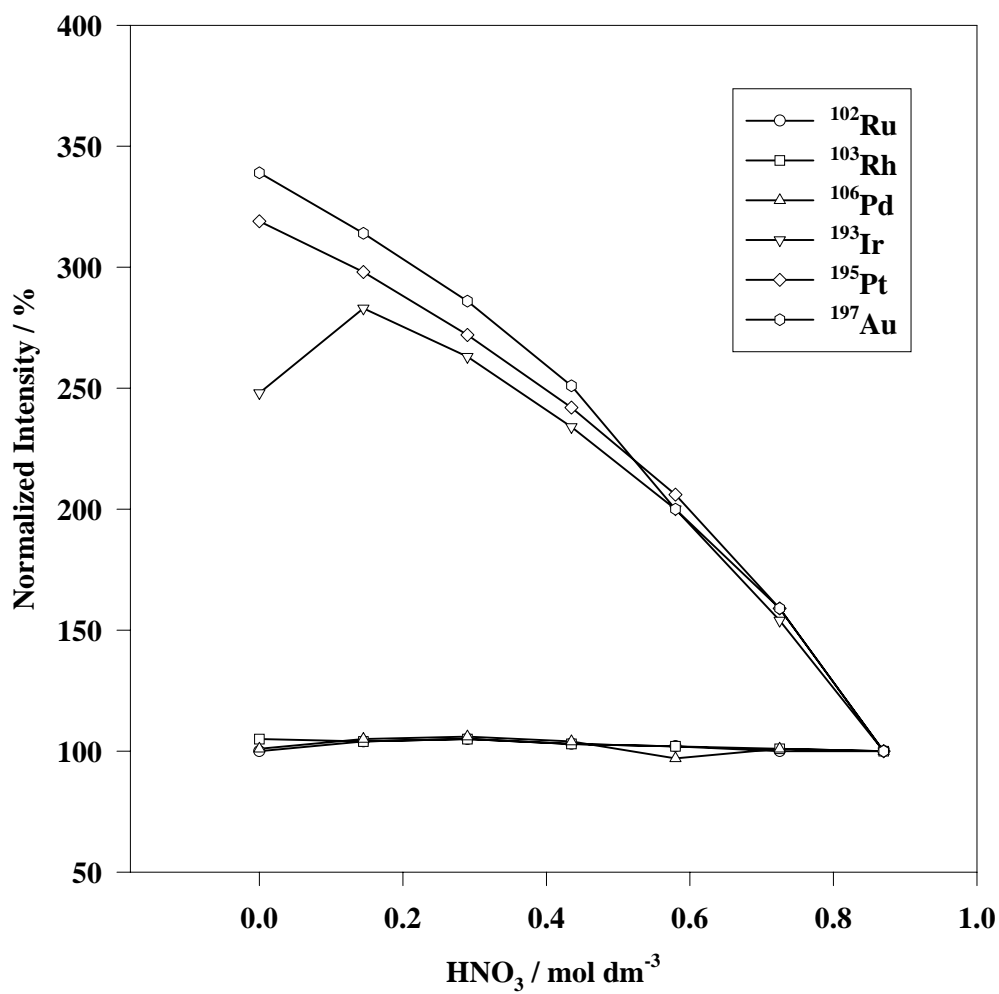


Fig. 4.4.4: Dependence of the normalized PGEs + Au signals on the concentration of nitric acid. The multi-standard solutions were the same as described in Fig. 4.4.3.

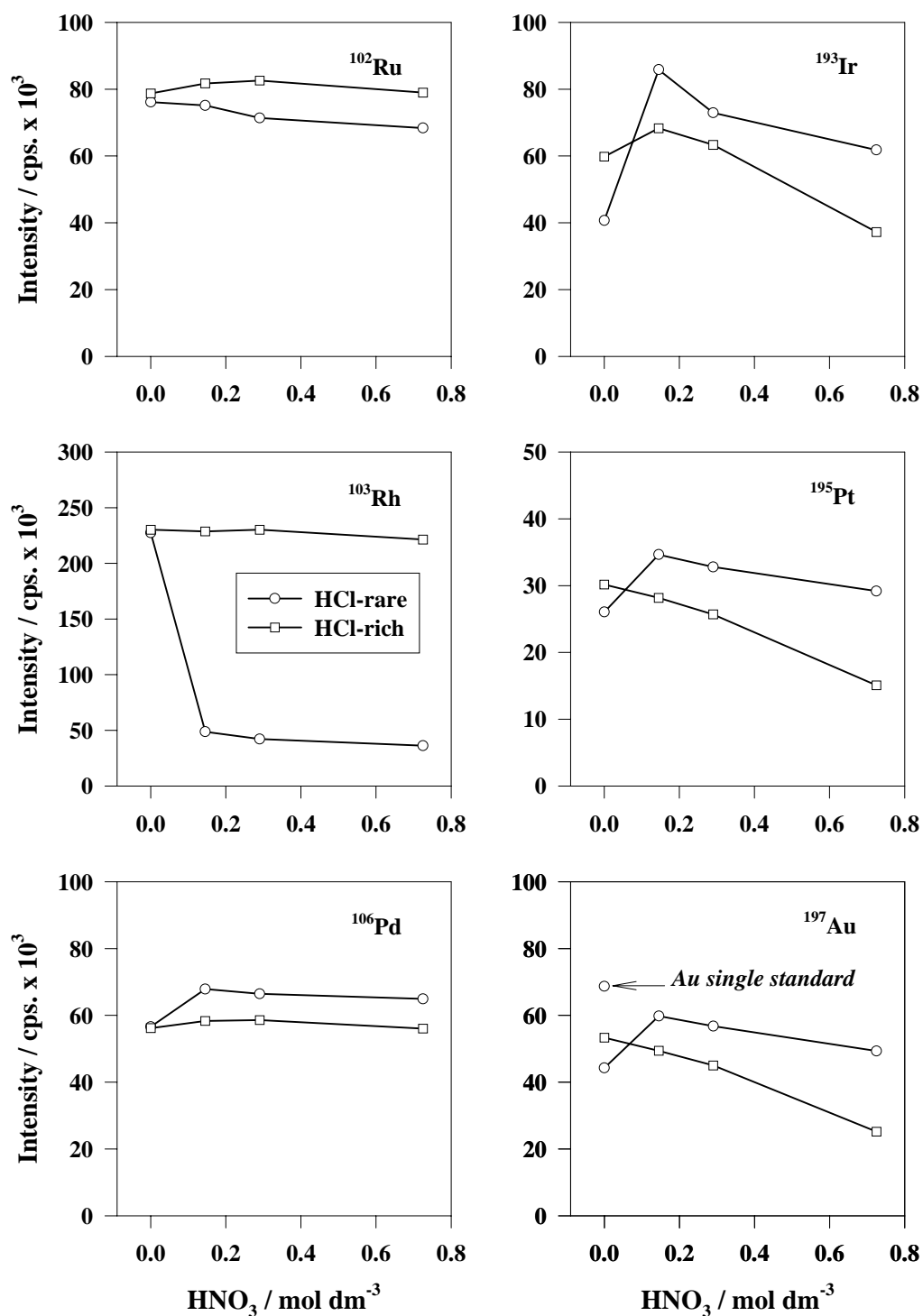


Fig. 4.4.5: Comparison of the dependence of PGEs + Au integration signals on nitric acid concentration in the HCl rich and rare atmosphere. The multi-standard solutions were the same as described in Fig. 4.4.3.

In the HCl-rare atmosphere, the neutral PGEs + Au standard solution should have had the highest signal response. However, the alloy effects intend to reduce the atomization yields and inhibit PGEs + Au mass spectrometric signals. The abundantly dissociated iridium atoms in plasma would capture and induce Pd, Pt, and Au to form an alloy or some metal molecules. The formation of alloy is also possible when the dried particles or the clusters of atoms were simultaneously dissociated in the same place. This will lead to a low atomization yield for PGEs + Au. As results, the signals were suppressed. For the single standard solution, the steady signal intensity of gold was 68700 cps. For the multi-standard solution, the steady signal intensity of gold was reduced to 44300 cps (see Fig. 4.4.5). The E° value of Ru and Rh are much lower than the heavy PGEs + Au. The differences in the E° value would lead to a sequential atomization in plasma. The temporal difference in the atomization process determines the alloy effect would be restricted by the spatial obstacle. That means the individual atomization does not happen at the same time and at the same site in plasma. When heavy PGEs + Au are atomized, Ru and Rh are still in the compound forms. Therefore, the alloy effects on Ru and Rh are not as severe as Pd, Pt, and Au.

More recently, Montaser [24] reported that the aerosol is often altered by passing it through a spray chamber or a desolvation device prior to introduction into the plasma. The nebulizer-spray chamber arrangement suffers from shortcomings such as analyte loss, memory effects, interferences, and inferior precision, which are mainly attributed to the spray chamber. This comments strongly support the deduction about the chemical atmosphere change in spray chamber can alter the chemical components in the droplets and then influence the mass spectrometric signals. It had been experimentally proven in Section 4.5 using a donut spray chamber hyphenated to the high power microwave induced plasma optical emission spectrometer.

In addition, the agreement among the nitric acid effects on Pt, Ir, and Au makes it possible to take any one as an internal standard to compensate the signal change for the other two elements in the measurement [138].

4.4.5 Summary

Memory and irregular signal response always obstruct the accurate determination of PGEs + Au with inductively coupled plasma mass spectrometry. It becomes more serious at ultra-trace level. The variable signals mainly aroused from the chemical

interference on the atomization efficiency. They not only depend on nitric acid concentration, but also on the standard reduction potential (E°) of precious metal species in solution. In concordance with the elemental periodic law, it clearly divides the precious elements into two subgroups. The signals of gold and heavy PGEs are severely inhibited by nitric acid. Contrarily, light PGEs are not so sensitive to the change of HNO_3 concentration. The nitric acid inhibition on the thermolysis of PGEs + Au could reduce the memory in the sampling system. The nitric acid inhibition on the dissociation of PGEs + Au in the central channel of plasma could reduce the atomization yields and suppress the mass spectrometric signals. The chemical matrix influences in inductively coupled plasma depend on the plasma thermal conditions and the heat exchange efficiency. For the analyte in a droplet, if the heating processes of desolvation, vaporization, and atomization overlap too much in the central channel of plasma, the more variable signals are expected. This case is often encountered when introduce the wet aerosol of precious elements or some other high standard reduction potential elements. For the neutral solution, iridium compound atomization yields an abundance of iridium atoms in plasma central channel. They are possible to capture and induce other precious metals to form alloy or combine as metallic molecule, which also suppresses the mass spectrometric signals of PGEs and gold by inhibiting the atomization yields. For the determination of PGEs + Au, an accurate matrix matching among the standards and the sample solutions is necessary for the external calibration method. The internal calibration is not as reliable as the applications for the general elements. The standard addition or isotope dilution techniques are more useful to improve the accuracy and precision for the measurement of the high standard reduction potential element with ICP-MS methods.

4.5 High power microwave induced plasma optical emission spectrometry

As discussed in the former sections, the chemical equilibrium interference on the spectrometric signal intensity of some high reduction potential elements is attributed to the competition between the plasma thermal conditions and the chemical potentialities that keep the metals in the original species in sample solution. This is related to the robustness of the plasma. In other words, it is the robustness of the plasma that governs the shift of the chemical equilibrium and changes the spectrometric signal intensity. The robustness of inductively coupled plasma indicates the capabilities of plasma to ingest aerosol and to protect the disturbance from the foreign factors. It not only depends on the forward power of rf generator, but also relies on the rf frequency of ICP. Generally, the higher the rf frequency, the lower the excitation temperature, and the less robust the plasma [100]. As expected, it has been observed that the chemical interference with the 40.68 MHz ICP is more severe than with the 27.12 MHz ICP (see section 4.1). The inductively coupled plasma sequential spectrometer ICP 2070, used in this work, is sustained by a rf generator of 40.68 MHz. When nebulizing pure water, the excitation temperature in the observation zone (14 mm ALC and along the axial direction) was measured as 4750 K by means of an Ar atomic eight-line set [140]. It is lower than the literature values of the 27 MHz inductively coupled plasma [141]. Normally, the microwave induced plasma has the lowest excitation temperature among these three kinds of plasma (for the high power MIP system used in this work is 3940 K, see below in this section). Provided that the robustness of plasma is simply related to the excitation conditions, the most severe signal intensity suppression will be observed with the microwave induced plasma, because it has the lowest excitation temperature.

According to the discussions in Section 2.2.6, the robust plasma is generally achieved with higher forward power, lower carrying gas flow, and lower liquid uptake rate. It is normally evaluated by the intensity ratio of Mg II to Mg I. Therefore, the concept of the robustness seems like an experimental description more than a theoretical explanation. What are the inherent factors that influence the plasma thermal conditions, especially the robustness of plasma? And what are the true effects of the robustness of plasma? It is difficult to get more direct proofs to identify the main factors with ICP only. The high power microwave induced plasma is generated in another mechanism. It is significantly different from the inductively coupled plasma. By means of which, it is possible to answer those questions.

4.5.1 The make-up of the spectrometer and the system optimization

The high power microwave induced plasma optical emission spectrometer used for this study has been well established in this laboratory. Figure 4.5.1 shows the schematic of the MIP-OES system used in this work. The optimized working conditions had been described in Chapter 3. More detail descriptions about the spectrometer and the electronics of the generator system are far from this work.

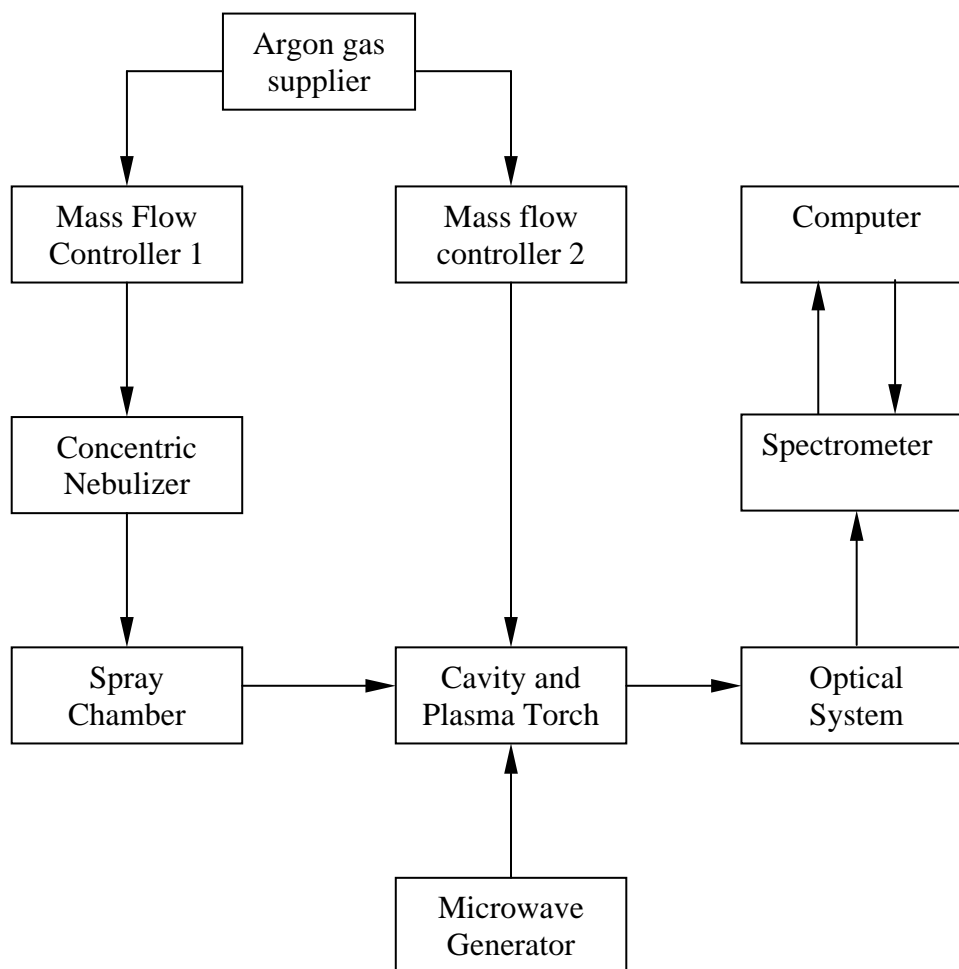


Fig. 4.5.1: The schematic of the high power MIP-OES system.

To make the comparable experiments with the 40.68 MHz ICP-OES, the same donut-shaped spray chamber and a quite similar concentric nebulizer were equipped for the high power MIP system. Comparing with the original pneumatic nebulization system, it improved the sampling efficiency and the signal stability. In addition, the donut-shaped spray chamber offers the possibility to observe the change of the inner pressure in the sampling system with the difference in the hydraulic columns. In the

original design, the hydraulic columns are used as a water seal to force the aerosol into plasma and to buffer off the pressure impulse in the sampling system [19]. However, in this study, the new function of the hydraulic columns has been developed as a pressure meter, by which it can indicate the pressure change in the spray chamber and indirectly indicate the change in the gas temperature of the plasma. The other modification on this MIP-OES system is the novel design of the torch. The first change was made by enlarging the diameter of the base of the torch body, the part out of the resonant cavity. The purposes are to reduce the resistance when the argon gas flow passes by the gap between the injector and the torch body, and to keep the kinetic energy of the coolant gas flow. The second modification is the addition of a cyclone guide in between the injector and the base of the torch body (the large diameter part). The cross-section area of the channel of the cyclone guide is slightly larger than the cross-section area of the gap between the injector and the tube of the torch body in the resonant cavity. As a result, after the argon gas flow left the cyclone guide, it forms a high speed and homogenous tornado between the gap of the two tubes. It was observed that the flame turned along the cyclone direction and formed an asymmetric plasma. The modifications on the torch design brought about the high cooling efficiency and more stable plasma. It prolongs the lifetime of the torch from 20 hours to at least 70 hours if the sample solutions contain only acids or water.

It should be mentioned that the main purpose for this study is to uncover the mechanism of the chemical interference on the spectrometric signals other than a practical application for mercury determination. Therefore, to get the highest and the most stable mercury signal intensity is out of the aim of this study. Contrarily, the principle to optimize the high power MIP-OES system was made to enhance the possible chemical interference that has been observed when ICP-OES system was employed to carry on a mercury determination. The optimized operating conditions for the high power microwave induced plasma optical emission spectrometer has been described in the experimental part.

4.5.2 Nitric acid interference on the time-resolved signal of mercury

Based upon the discussions in the former sections, the redox equilibrium between mercury and nitric acid in the central channel of ICP was shifted by the plasma thermal conditions and the nitric acid concentration in mercury solution. As a result, mercury signal intensity is suppressed with the increase in the nitric acid concentration. The

plasma thermal conditions have broad meanings. It not only includes the working parameters and the varied physical temperatures of plasma, but also includes the robustness of plasma. Any change in the plasma thermal conditions may affect the thermal processes that happen in the central channel of plasma, such as desolvation, vaporization, atomization, ionization, and excitation. Although there is not a direct comparison of the robustness among the plasmas with different frequency, the comparison of the plasma excitation temperatures among the different plasmas is available. Under the same operating conditions, the excitation temperature of ICP normally follows the sequence: 27 MHz ICP > 40 MHz ICP. With the normal operating conditions, microwave induced plasma has the lowest excitation temperature. Although it has been proved that the increase in nitric acid concentration did not influence the excitation process in inductively coupled plasma [7, 47], it does not mean that the same conclusion is still true for the high power MIP because the excitation temperature is low.

The first attempt to find out nitric acid influence on mercury signal intensity was made by monitoring the time-resolved signals of mercury with the high power MIP-OES system. The monitoring process was exact the same as carried out in the case of ICP-OES with the ICP-2070 system. Although the efforts have been made to enlarge the chemical interference, except the memory effect, mercury signal intensity did not change with the increase in the nitric acid concentration (see Fig. 4.5.2). The memory only happened when the nitric acid concentration was lower than $0.001 \text{ mol dm}^{-3}$. The gradually and slowly increased mercury signal could be observed when mercury standard in the non-acidified solution was nebulized. That is because mercury was accumulated in the sampling system and it gradually reached the absorption equilibrium. The memorized mercury can be washout by the diluted *aqua regia* solution. The weak memory effect did not influence mercury signal intensities when nebulizing mercury standard in the diluted nitric acid solutions.

When nitric acid in mercury standard solution is higher than 0.5 mol dm^{-3} , mercury memory are completely eliminated. However, it was also observed that mercury signals increased gradually. The ascending gradient of mercury signal intensity is proportional to the change in nitric acid concentration. It took several minutes to reach the steady state signals. This phenomenon is attributed to the so-called transient effect described by Stewart and Olesik [78]. It is related to the aerosol evaporation process in the spray chamber.

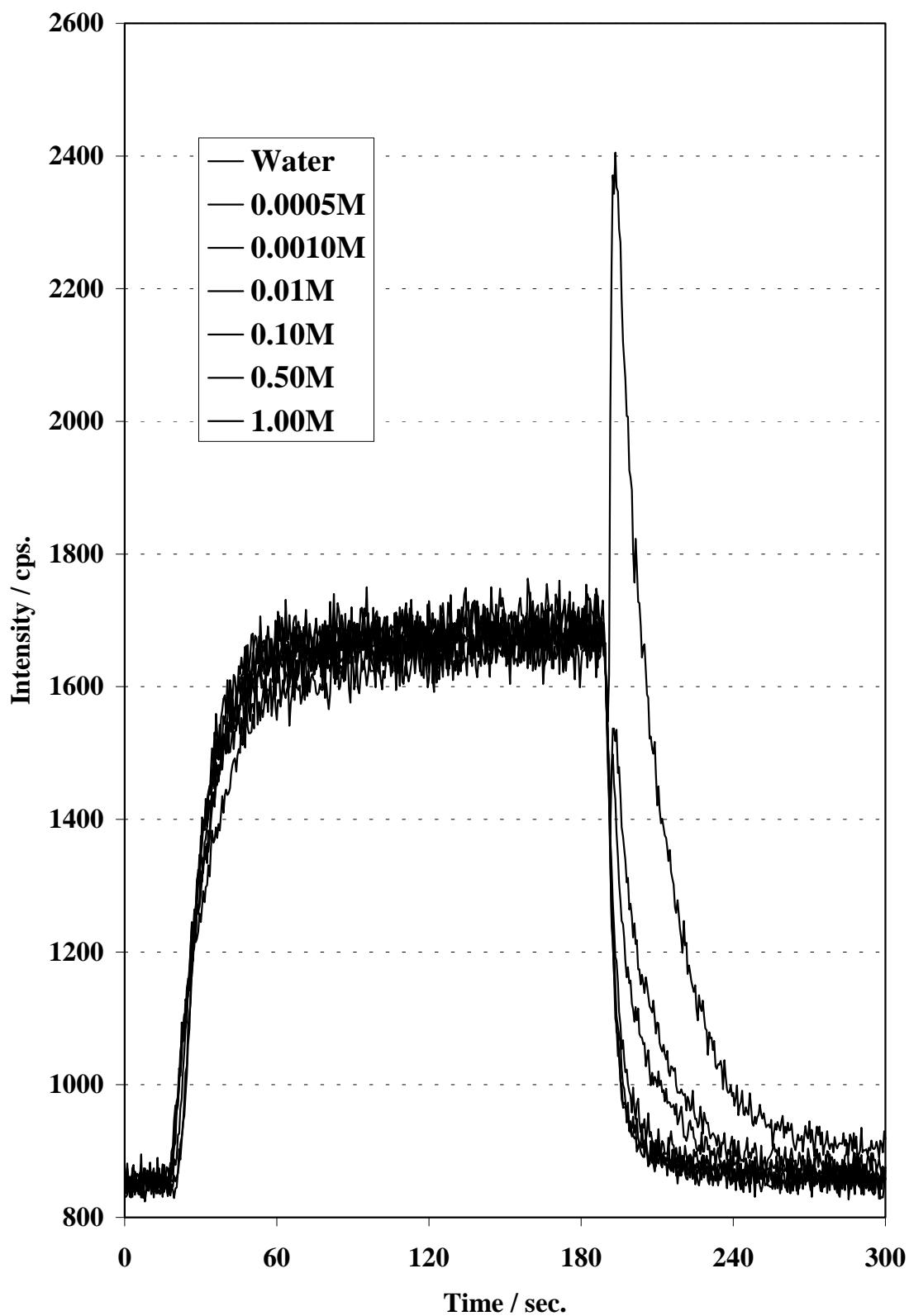


Fig. 4.5.2: Time-resolved signals for mercury standard in different nitric acid solutions.

4.5.3 Nitric acid interference on the steady signal of mercury

A continuous steady state signal collection was carried out with the mercury standard solutions in the ascending nitric acid concentrations (see Fig. 4.5.3). Every measurement took 6 seconds. During changing mercury standard solutions to the next nitric acid concentration, pure water was aspirated to wash out the residue mercury standard in the sampling system. The signal intensities were also measured as the background signal. It is easily found, when nitric acid concentration is lower than 0.1 mol dm^{-3} , nitric acid effect on mercury signal intensity is not so significant. The increasing signal intensity obtained from water standard shows mercury has been retained in the sampling system. When mercury standard in $0.001 \text{ mol dm}^{-3}$ nitric acid solution was nebulized, the memorized mercury was partially washed out. It made the signal intensity slightly higher than it should be. When nitric acid in mercury standard solution was higher than 0.5 mol dm^{-3} , the transient effect on the mercury signal intensity was observed. It became severe with the increase in the nitric acid concentration. After measuring the mercury standard solution in 3.0 mol dm^{-3} nitric acid, mercury standard in $0.005 \text{ mol dm}^{-3}$ nitric acid solution was measured again. The signals obtained from this standard solution were significantly higher than the original intensities. This is due to the transient effect from high concentration nitric acid to the relatively low concentration nitric acid, by which the sample aerosol evaporation in the spray chamber was accelerated. As a result, the energy consumed for droplet desolvation in the central channel of plasma was reduced. It makes the plasma more robust and produces stronger mercury signal intensity.

The experimental results presented a question, why the redox equilibrium between mercury and nitric acid has not a significant influence on the mercury signal intensity. Comparing with the excitation temperatures, the microwave induced plasma is lower than the inductively coupled plasma. If the robustness of plasma can be generally characterized by the excitation capabilities, mercury signal suppression by nitric acid should have been observed. However, it is difficult to find out any clue from the experimental results to prove this assumption. The possible interpretation is that the mechanism to generate the high power microwave induced plasma is completely different from the inductively coupled plasma. Provided that the high power microwave radiation can tolerate the introduction of aerosol and sustain a stable plasma, in the resonant cavity, the electromagnetic radiation of the microwave can lead to the aerosol completely desolvated in the central channel of plasma. Due to the liquid phase has

already disappeared before the analyte entered into the observation zone, the redox equilibrium that takes place in the aqua solution was no longer existed. Of cause, it is impossible to observe the shift of the status of chemical equilibrium. In contrary to the MIP, sample aerosol desolvation in the central channel of inductively coupled plasma is not as efficient as it in the microwave induce plasma. In the central channel of ICP, part of the analytes and nitric acid still exist in the liquid phase. As a result, the redox equilibrium comes into effect and suppresses mercury signal intensity.

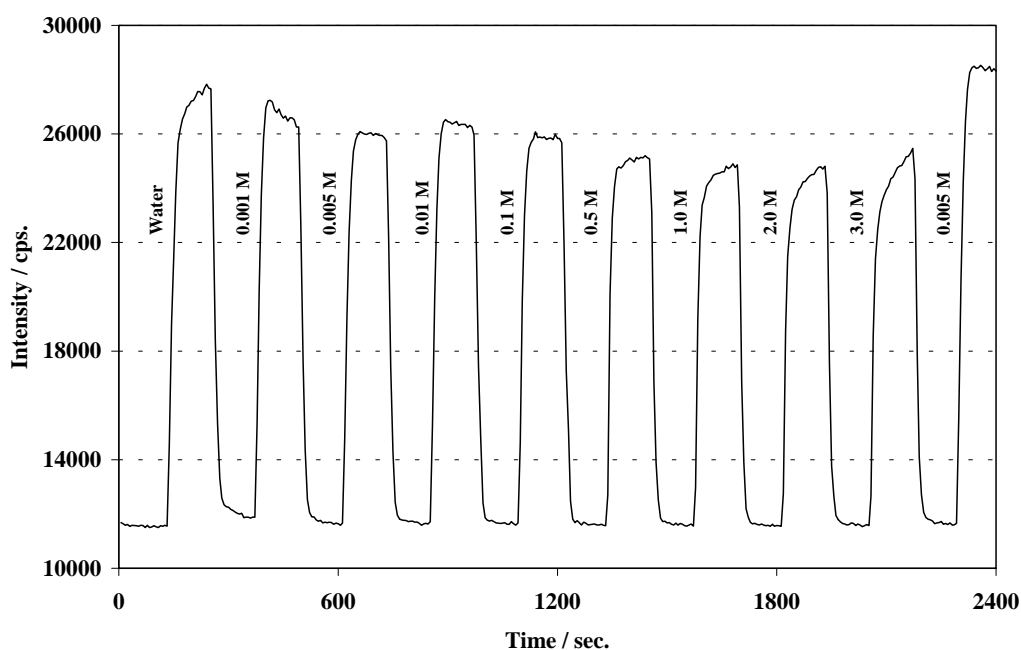


Fig. 4.5.3: Nitric acid effects on the steady state signals of mercury. Mercury standard solution contained 5.0 mg dm^{-3} of Hg in varied nitric acid concentration.

4.5.4 The transient effect of nitric acid on the time-resolved signal of mercury

The transient effect has been briefly discussed in the last section. It happened when mercury standard in high concentration of nitric acid solution was introduced into a water balanced spray chamber. The extent of transient effect is related to the relative extent of water evaporation from the spray chamber walls and from aerosol droplets, which is controlled by the relative nitric acid concentrations between the two phases.

The time-resolved signals of mercury show that the extent of the transient effect is dependent on the nitric acid concentration (see Fig. 4.5.4a). The higher the nitric acid concentration, the severer the transient effects. Due to the transient acid effect arises from the difference in the relative rate of water evaporation from the spray chamber walls and from the droplet, it is possible to eliminate the transient effect by saturating the spray chamber with the same nitric acid blank solution [78]. It was observed, when the spray chamber was balanced with the blank nitric acid solution in the same concentration as it is in mercury standard solution, the transient acid effect on the time-resolved signals of mercury disappeared (see Fig. 4.5.4b). Nitric acid has no longer the transient effects on the features of the time-resolved signals of mercury. That is because the difference in the evaporation rate is uniformed. As a result, water transport between the liquid on the spray chamber walls and the aerosol droplet is eliminated.

The similar transient effect was obtained with hydrochloric acid (see Fig. 4.5.5a and Fig. 4.5.5b). However, the extent of the transient effect of hydrochloric acid is more severe than the one of nitric acid.

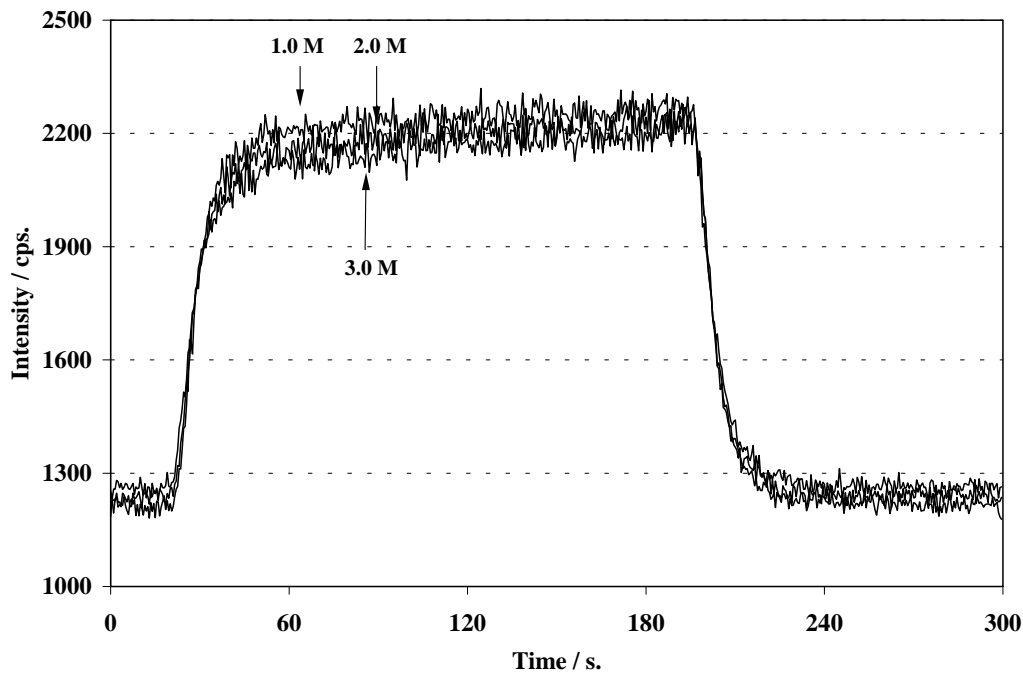


Fig. 4.5.4a: Transient effect of nitric acid on the time-resolved signal of mercury. The aspirating sequence was water blank-mercury in nitric acid-water blank. Mercury standard is $5.0 \text{ mg dm}^{-3} \text{ Hg}$.

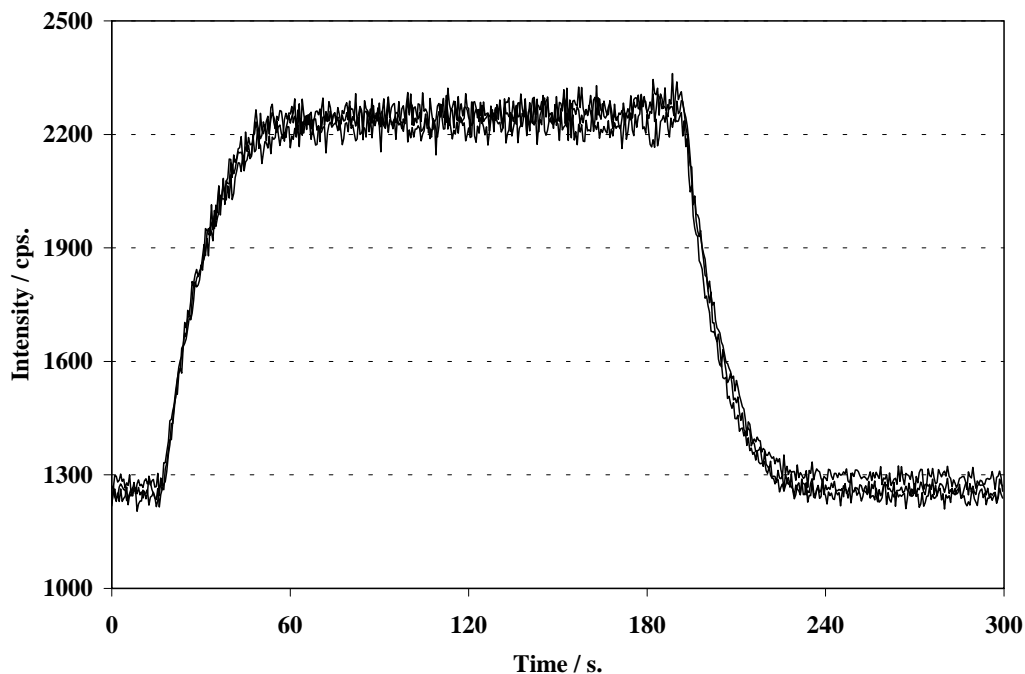


Fig. 4.5.4b: Transient effect of nitric acid on the time-resolved signal of mercury. The aspirating sequence was acid blank-mercury in nitric acid-acid blank. Mercury standard is $5.0 \text{ mg dm}^{-3} \text{ Hg}$. For each plot, nitric acid concentration in blank and in standard is the same.

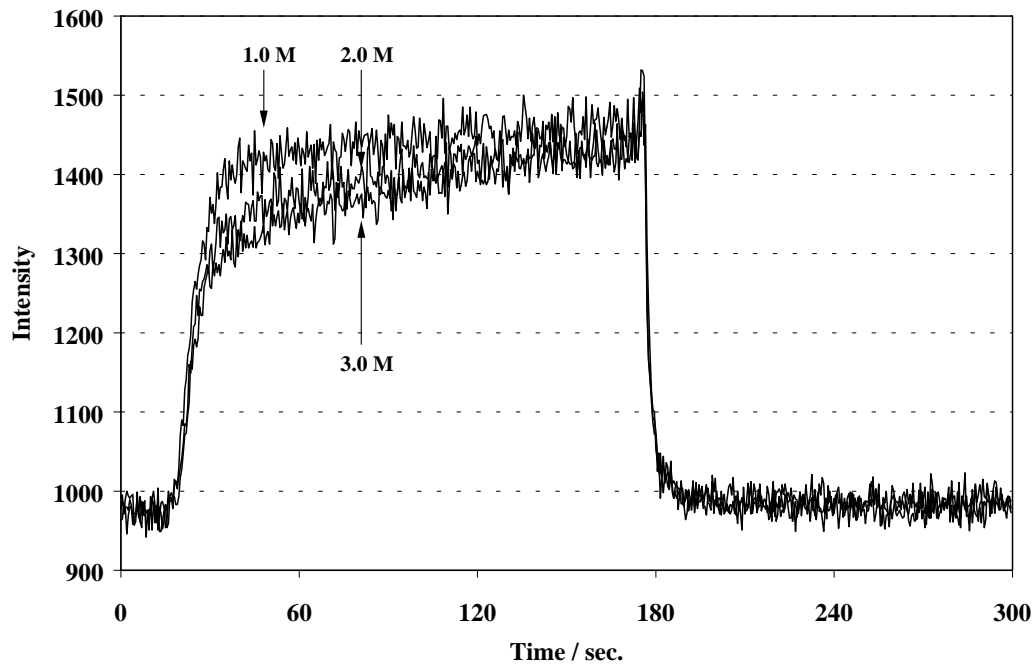


Fig. 4.5.5a: Transient effect of hydrochloric acid on the time-resolved signal of mercury. The aspirating sequence was water blank-mercury in HCl-water blank. Mercury standard is $5.0 \text{ mg dm}^{-3} \text{ Hg}$.

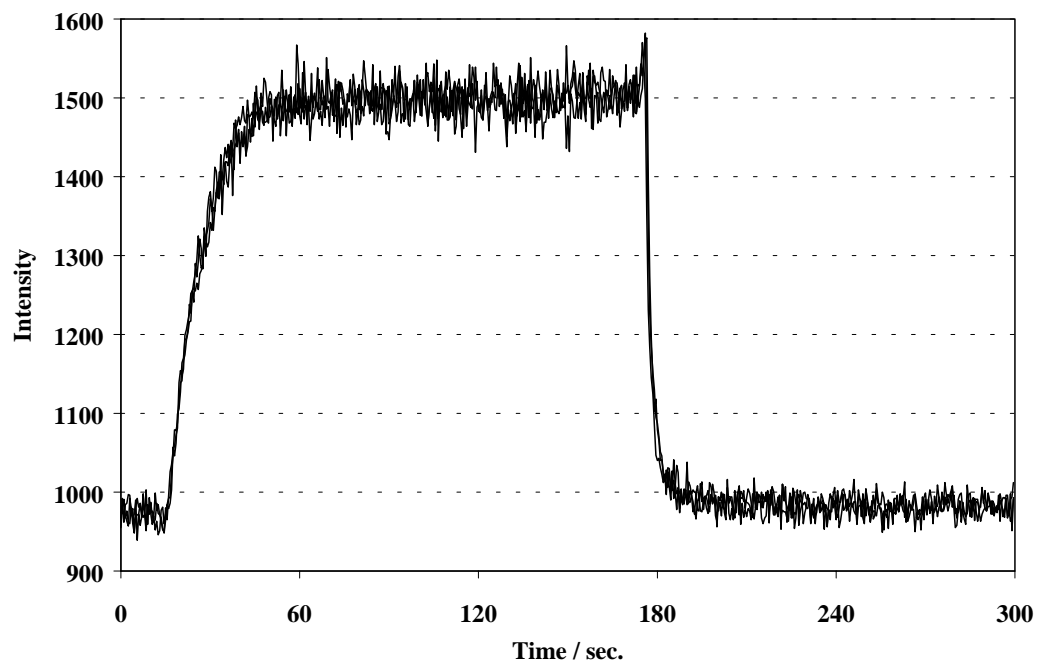


Fig. 4.5.5b: Transient effect of hydrochloric acid on the time-resolved signal of mercury. The aspirating sequence was acid blank-mercury in HCl-acid blank. Mercury standard is $5.0 \text{ mg dm}^{-3} \text{ Hg}$. For each plot, HCl concentration in blank and in mercury standard is the same.

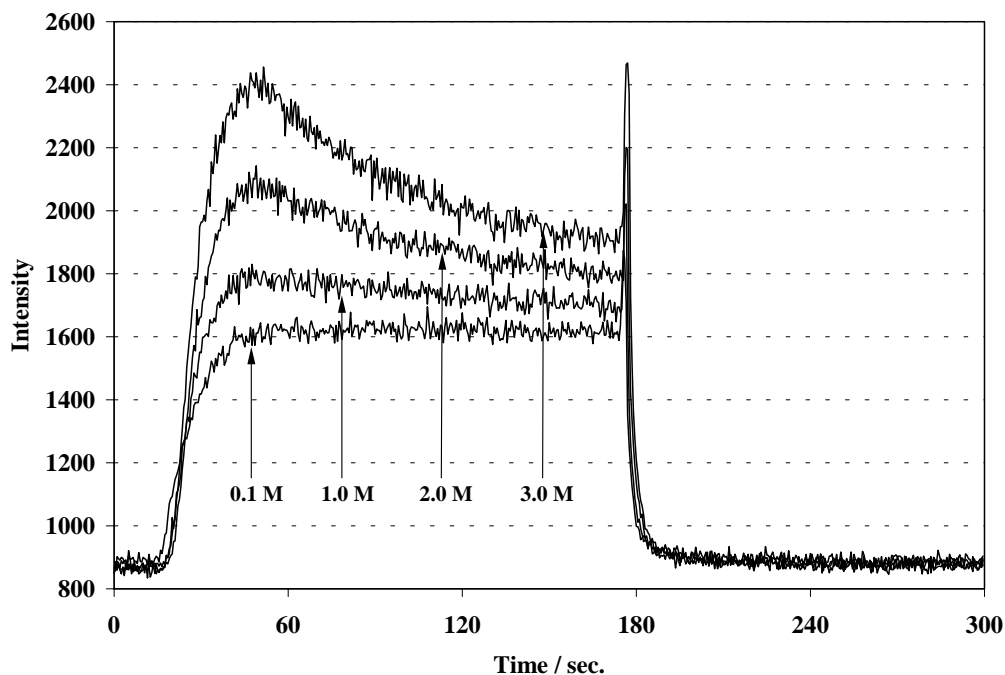


Fig. 4.5.6: Transient effect of hydrochloric acid on the time-resolved signal of mercury. The aspirating sequence is hydrochloric acid blank-mercury standard in water-hydrochloric acid blank. Mercury standard is $5.0 \text{ mg dm}^{-3} \text{ Hg}$. The spray chamber was balanced with 0.1, 1.0, 2.0, and 3.0 mol dm^{-3} hydrochloric acid blank solution, respectively.

When the spray chamber was balanced with the blank hydrochloric acid solution at high concentration and followed by the nebulization of mercury in pure water solution, the transient effect of hydrochloric acid was also observed (see Fig. 4.5.6). It is easily found that the transient effect became more severe with the increase in hydrochloric acid concentration. Comparing with the transient effect observed when introducing mercury standard in hydrochloric acid solution into the water-balanced spray chamber, in the reversed direction, the introduction of non-acidified mercury solution into the hydrochloric acid-balanced spray chamber showed even more severe transient effect of hydrochloric acid. As it was observed, the higher the hydrochloric acid concentration, the higher the time-resolved signals of mercury. Meanwhile, the time needed to achieve an invariable steady state signal is longer than the time needed in the procedure of water-mercury standard in HCl-water.

The different scales in the transient effect are due to that mercury signal comes out of the aerosol. When the spray chamber is balanced with water, the introduction of acidified mercury standard solution will slow down water evaporation rate from the

aerosol in the spray chamber or the water vapor that is released from the spray chamber walls will condense on the droplet. Therefore, aerosol evaporation in the central channel of plasma will consume more energy and lead to the low mercury signal intensity. Contrarily to the acidified mercury standard solution, the water evaporation rate from the aerosol that is generated from mercury water solution will be speeded up by the presence of hydrochloric acid film at high concentration. That is because the water vapor generated from the aerosol will soon condense onto the hydrochloric acid film that covered on the inner wall of the spray chamber. In general, the volume of the hydrochloric acid film is larger than the total volume of aerosol. It is not significantly affected by the change of acid concentration. Therefore, the condensation of water vapor is far from the equilibrium state. Water evaporation from aerosol can be realized to a great extent and the condensation of water vapor lasts long time in the spray chamber (see Fig. 4.5.6). As a result, the mean diameter of the droplets is greatly reduced and the desolvation of aerosol in the central channel of plasma will consume less energy. Hence the desolvation of aerosol brings about less disturbance on the plasma thermal conditions and produce high mercury signal intensity. With the nebulization of water, hydrochloric acid films in the spray chamber are gradually diluted by capturing the big droplets of non-acidified mercury solution. As a result, the difference in water evaporation rate between the hydrochloric acid film and the droplet is gradually reduced. Hence, mercury signal intensity gradually decreased and closed to the signal intensity as it should be. The evaporation equilibrium between the droplets and the hydrochloric acid film takes longer time than the equilibrium between non-acidified droplets and the nitric acid film. Obviously, in the limited experimental period, mercury signal intensity could not reach the normal signal level (see Fig. 4.5.6).

4.5.5 Transient effect on aerosol properties and the laser light scattering measurement

The laser light scattering technique was employed to monitor the aerosol changes during the aspiration alternated from high concentration nitric acid to water, and then changed back to the same nitric acid solutions (see Fig. 4.5.7). The concentration of nitric acid changed in the range of 0–3.0 mol dm⁻³. Although the He-Ne laser used in this experiment could not give the characteristics about the droplet diameter of the aerosol, it released some information about the transient effect of nitric acid. It was observed, when the aspiration changed from nitric acid solution to pure water, the

intensities of the scattering laser light show the continually descending extent during the first two minutes of the nebulization. It relates to the change in the diameter and refraction of the droplet of aerosol. The scattering intensity of water aerosol is dependent on the nitric acid concentration that was employed to balance the spray chamber. The higher the nitric acid concentration, the weaker the scattering intensity. However, the difference among the three transient plots is not so significant. When the aspiration changed from water to the nitric acid solution, the transient effect became more significant than the one from nitric acid solution to water. It took about one minute to reach the invariable signal intensity. Therefore, the transient effect of nitric acid acts in a short time.

The transient effect of hydrochloric acid was also examined with the laser light scattering method. After the spray chamber was balanced with hydrochloric acid solution, the nebulization of water led to the laser scattering intensity from water aerosol decreased gradually (see Fig. 4.5.8). Comparing with nitric acid, the extent of the transient effect of hydrochloric acid strongly depends on the acid concentration. Apart from the extent of the transient acid effect, the time needed to achieve the invariable scattering signal intensity is prolonged by increasing the concentration of hydrochloric acid, with which the spray chamber was balanced. It seems impossible to obtain the invariable scattering signal intensity in the limited experimental period after the spray chamber was balanced by 2.0 and 3.0 mol dm⁻³ hydrochloric acid solutions. This phenomenon consists with the results shown in Fig. 4.5.6. After the spray chamber was balanced with HCl solution, the nebulization of the non-acidified mercury standard solution brought about higher mercury signal intensity than the normal signal level. Then, mercury signal intensity gradually decreased as the difference between the hydrochloric acid and the droplets of non-acidified mercury standard solution was diminished.

In the reversed direction, after the spray chamber was balanced with water, the nebulization of hydrochloric acid solution led to the laser scattering intensity increased (see Fig. 4.5.9). With the introduction of hydrochloric acid solution, the water film on the spray chamber wall was gradually replaced by the big droplets of acid solution. The difference of the evaporation rate between the liquid film and the droplets was reduced. The laser scattering intensity quickly reached the steady signal level as it should be. The time, in this case, is much shorter than it is needed to reach the equilibrium from acid solution balanced spray chamber to water standard solution.

Hydrochloric acid is a volatile acid. Like the aerosol of water, the molecule of HCl may also transfer between the droplets and the liquid film on the inner wall of the spray chamber. In addition, the inertia of individual droplet is different. That leads to that the speed of each droplet is also different. As a result, there is the possibility that the droplets of water collide with the droplets of hydrochloric acid. Hence, the chemical properties of the combined aerosol will be changed. However, this kind of collision may happen only at the very beginning when the aspiration alternates between water and acid. The acidified aerosol can be soon replaced by the new aerosol of water, or *vice versa*. The remained transient effect is due to the difference in water evaporation between droplets and the liquid film on the inner wall of spray chamber. When the spray chamber was conditioned with diluted *aqua regia* solution (see Section 4.4.4), it has been observed that the modified aerosol in the spray chamber behaved quite different. As the chloric ions got into the droplets, the reduction potential of the platinum group elements were changed into the reduction potential of the chlorocomplex of the platinum group elements. Therefore, the redox equilibrium of PGEs + Au in the central channel of plasma were changed. That is the so-called the influence of chemical atmosphere in the spray chamber (see Section 4.4.4).

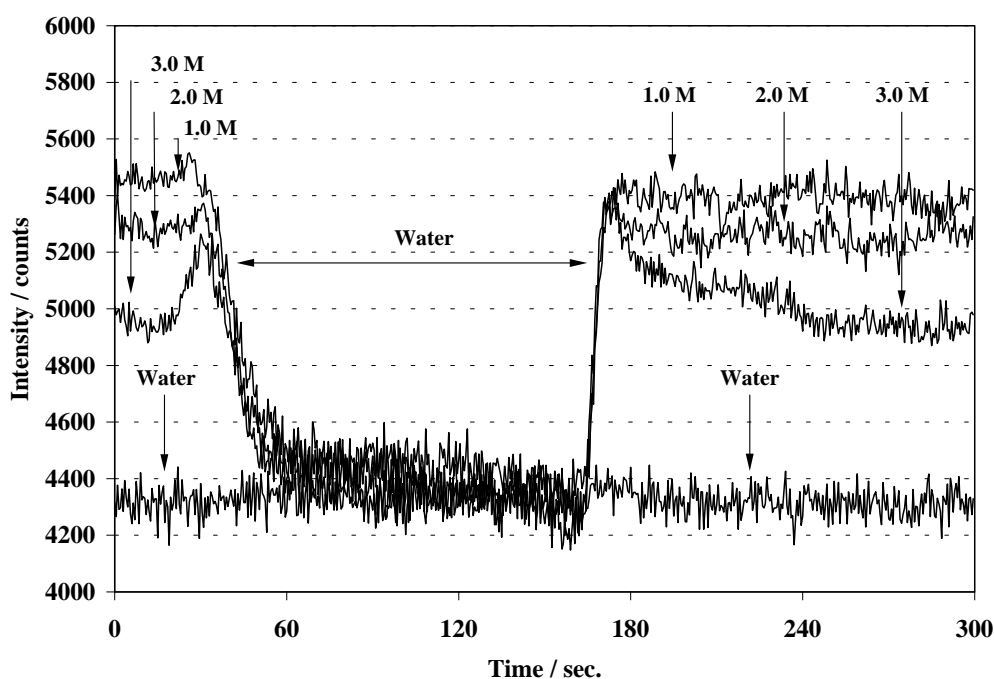


Fig. 4.5.7: The scattering intensity of 632.8 nm He-Ne laser during nitric acid-water-nitric acid aspiration process. The scattering light was observed axially.

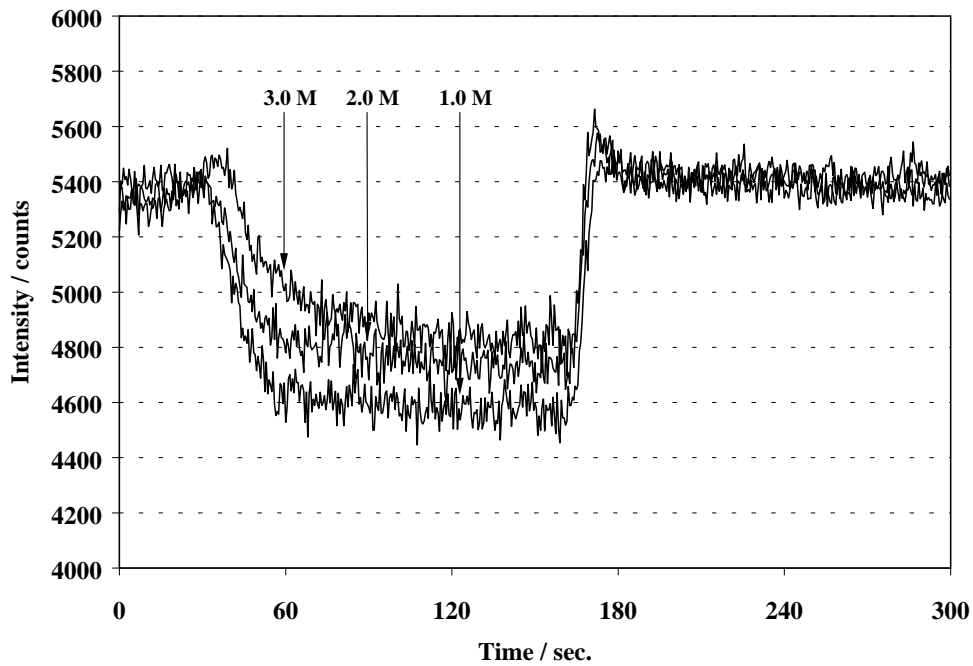


Fig. 4.5.8: The scattering intensity of 632.8 nm He-Ne laser during the aspiration of hydrochloric acid-water-hydrochloric acid. The scattering light was observed axially.

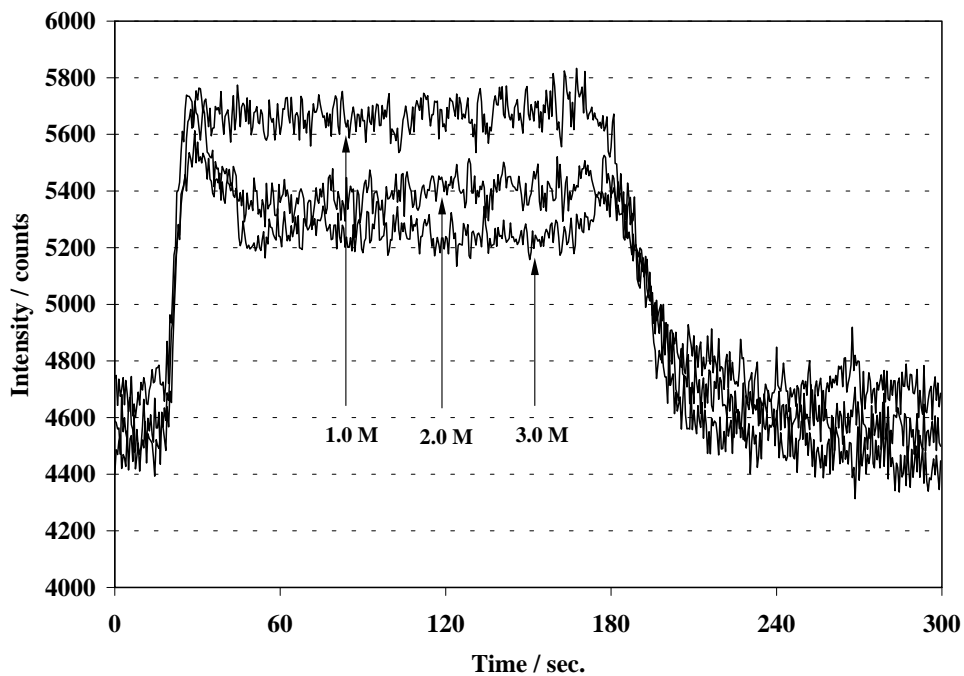


Fig. 4.5.9: The scattering intensity of 632.8 nm He-Ne laser during the water-hydrochloric acid-water aspiration. The scattering light was observed axially.

4.5.6 Sodium chloride interference on mercury signal intensity

For the high power microwave induced plasma optical emission spectrometry, the study on the matrix interference was also focused on the easily ionizable elements (EIEs) that exist in sample solutions. The easily ionizable element suppression on ICP mass spectrometric signal intensity of mercury is frequently reported for the inhibition on the thermal ionization [83-86]. However, for MIPs, matrix interference from EIEs leads to a significant signal enhancement in analyte response. Such interferences have been found to depend considerably on the sample introduction methods and the plasma conditions [140, 142].

Hydrochloric acid interference on the mercury signal intensity of MIP-OES was examined at low acid concentration ($< 0.5 \text{ mol dm}^{-3}$). The steady signal intensity of mercury was continually collected with the integration time of 6 minutes per point. There was no significant interference on mercury signal intensity as the presence of hydrochloric acid in mercury standards (see Fig. 4.5.10a). As expected, the shapes of mercury signals from water and 0.5 mol dm^{-3} HCl solutions are not so regular for the memory effect and transient effect, respectively. The results consist with the phenomenon observed in the case of nitric acid solutions.

In comparing with hydrochloric acid, the same experiment was carried out with sodium chloride solutions. It was observed that sodium chloride interferences on mercury signal intensity in two directions. In the range of $0 - 0.020 \text{ mol dm}^{-3}$, the presence of NaCl in mercury standard solution leads to the increase in mercury atomic line intensity. When the concentrations of sodium chloride in mercury standard solutions were higher than 0.05 mol dm^{-3} , the matrix inhibition on the signal intensity of mercury atomic line started (see Fig.4.5.9b). Comparing with the data shown in Fig. 4.5.10a and Fig. 4.5.10b, it is easily to be found that mercury signal suppression is not related to the change of chloric ion concentration. It is the presence of sodium ions in mercury standard solution that determines mercury signal suppression. The signal increase at low NaCl concentration may be related to the completely ionization of NaCl, that leads to the increase in the electron number density and the electron temperature. Therefore, the excitation abilities in the central channel of plasma are enhanced. When sodium chloride concentration is high enough, the increase in the electron number density and the electron temperature are no longer the main reasons to control mercury signal intensity. The decrease in the atomization temperature leads to a low atomization yield. It becomes a more significant factor. That is going to be discussed below.

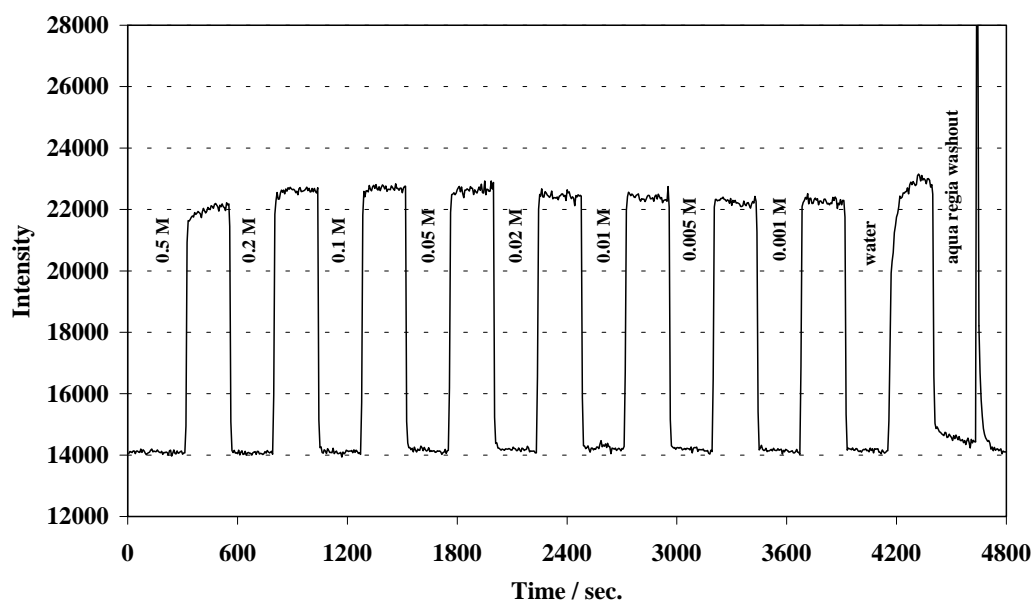


Fig. 4.5.10a: Hydrochloric acid interference on the steady state signals of mercury. Mercury standard is $5.0 \text{ mg dm}^{-3} \text{ Hg}$ in varied HCl concentration. The integration time for each steady signal is 6 seconds.

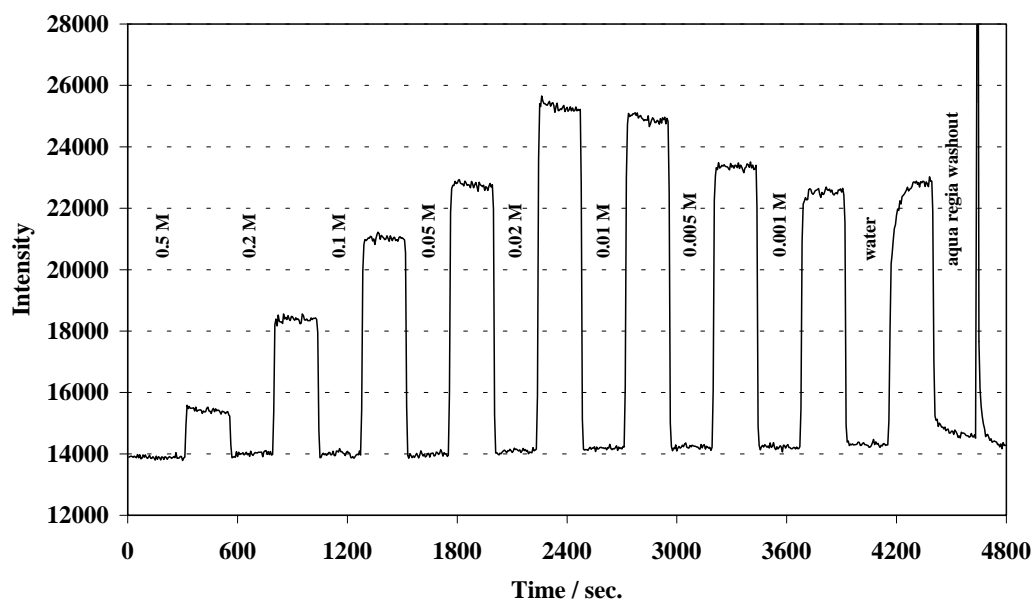


Fig. 4.5.10b: Sodium chloride interference on the steady state signals of mercury. Mercury standard contained 5.0 mg dm^{-3} of Hg in varied Sodium chloride concentration. The integration time for each steady signal is 6 seconds.

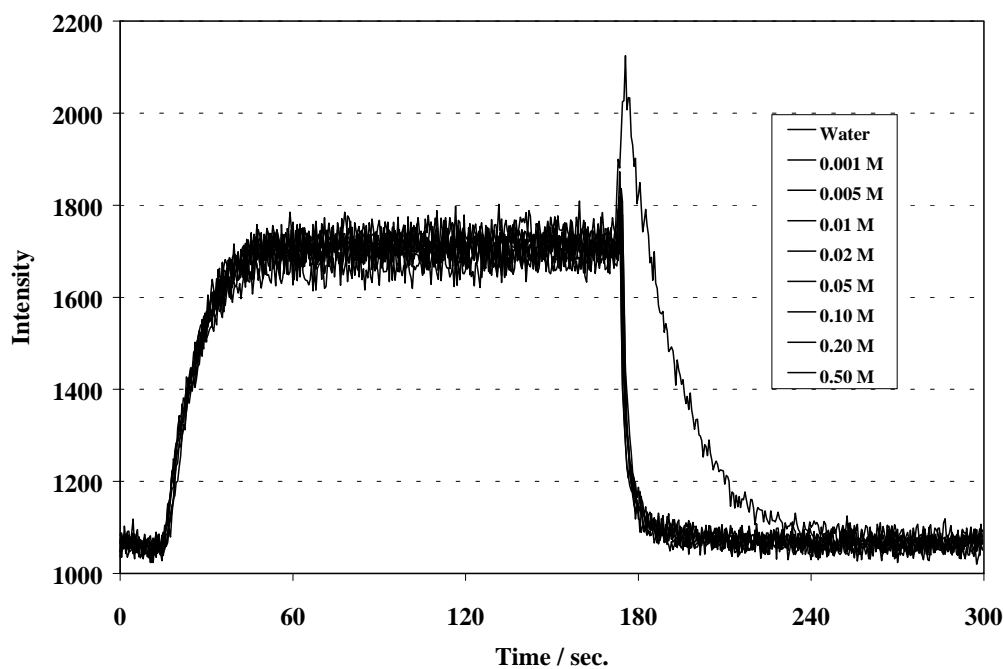


Fig. 4.5.11a: Time-resolved signals of mercury in different hydrochloric acid solutions. Mercury standard solution contains $5.0 \text{ mg dm}^{-3} \text{ Hg}$.

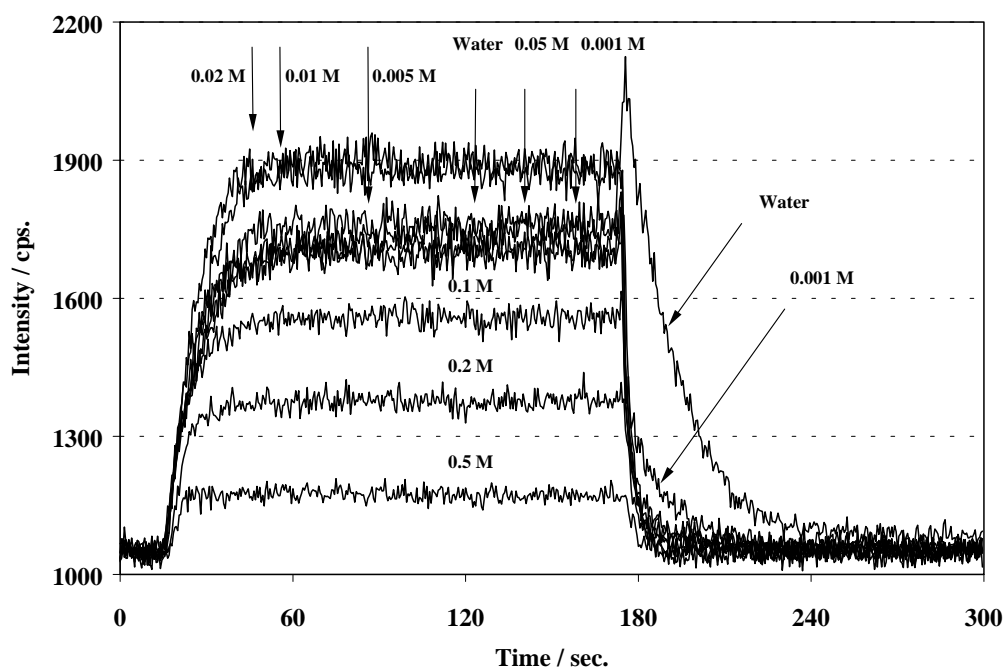


Fig. 4.5.11b: Time-resolved signals of mercury in different sodium chloride solutions. Mercury standard solution contains $5.0 \text{ mg dm}^{-3} \text{ Hg}$.

To confirm sodium chloride interferences on mercury steady signal intensity with the high power microwave induced plasma, the time-resolved signals of mercury were monitored as usual (see Fig. 4.5.11b). It proved that, at low NaCl concentration, mercury signal intensity was enhanced. However, at high NaCl concentration, mercury signal intensity was suppressed. These results consist with the observation on the sodium chloride effects on mercury steady signal intensity. The comparing experiment was carried out with hydrochloric acid solutions. It showed that, in the experimental range, hydrochloric acid has no significant interferences on the time-resolved signals of mercury (see Fig. 4.5.11a).

4.5.7 Sodium chloride interference on the excitation temperature of MIP

The presence of sodium chloride in mercury standard solution has been proved to enhance mercury signal intensity at low concentration and suppress mercury signal intensity at high concentration. The easily ionizable sodium atoms, which existed in the central channel of plasma, are likely to disturb the excitation conditions of the microwave induced plasma.

For a system in the local thermodynamic equilibrium, at temperature T , the population density of atomic or ionic level p follows a Boltzmann distribution. Starting from this assumption, the following equation is available to calculate the excitation temperature:

$$\ln\left(\frac{I_{pq}\lambda_{pq}}{g_p A_{pq}}\right) = \frac{-E_p}{kT} + \ln\left[\frac{nhc}{4\pi Z(T)}\right] \quad \text{eqn 4.5.1}$$

where λ_{pq} is the wavelength of transition $p \rightarrow q$; E_p is the excitation energy of the emitting level; g_p is the statistical weight of the emitting level; A_{pq} is the absolute transition probabilities; k is the Boltzmann constant; and the temperature governing this energy population is defined as the excitation temperature, T_{exc} . For a given plasma system, the last item is a constant.

Thus, T_{exc} is derived from the slope of the straight line ($-1/kT$) fitted to a plot of the left-hand side of the Equation 4.5.1 against E_p . In this work, an Ar atomic eight-line set was employed to measure the excitation temperature of the microwave induced plasma. The main purpose to use Ar I is to avoid the deviations arose from the thermometric species in the plasma. The necessary parameters of argon are well known and are shown in the Table 4.5.1.

Table 4.5.1 Ar I emission line data.

λ (nm)	E_p (cm ⁻¹)	g_p	$A_{pq} \times 10^{-7}$ (sec ⁻¹)
425.118	116660	3	0.0085
425.936	118871	1	0.360
426.629	117184	5	0.028
427.217	117151	3	0.071
430.010	116999	5	0.034
433.356	118469	5	0.049
433.535	118459	3	0.0333
434.545	118408	3	0.028

The microwave induced plasma is a cylindrically symmetrical plasma. Because the emission was observed radially and the emission beam from the central channel of plasma was focused onto one of the end of the light fiber, the light entering into the spectrometer are suitable to calculate the temperature of the central channel of the plasma. Abel inversion is not necessary.

According to this principle, the interferences of hydrochloric acid and sodium chloride on the excitation temperature of MIP were examined. When the concentration of hydrochloric acid ranged from 0 to 0.5 mol dm⁻³, as expected, there is no significant change in the excitation temperature of the plasma (see Fig. 4.5.12). The mean value of the excitation temperature is 3935 K. It is lower than 4750 K, the excitation temperature of the 40.68 MHz inductively coupled plasma that was used in this work. When the concentration of sodium chloride ranged from 0 to 0.5 mol dm⁻³, like in the case of hydrochloric acid, the excitation temperature of the microwave induced plasma was not sensitive to the change of the concentration of sodium chloride in solutions (see Fig. 4.5.12). The mean value of the excitation temperature is also 3935 K, although the standard deviation is slightly higher than the one in the case of hydrochloric acid. There is no significant difference between the introduction of hydrochloric acid and sodium chloride solutions. It is obvious that the excitation temperature of the high power microwave induced plasma could not be disturbed by introducing hydrochloric acid or sodium chloride solutions at the concentration lower than 0.5 mol dm⁻³. Therefore, mercury signal suppression, which is caused by the introduction of sodium chloride solution, does not relate to the excitation temperature of the plasma.

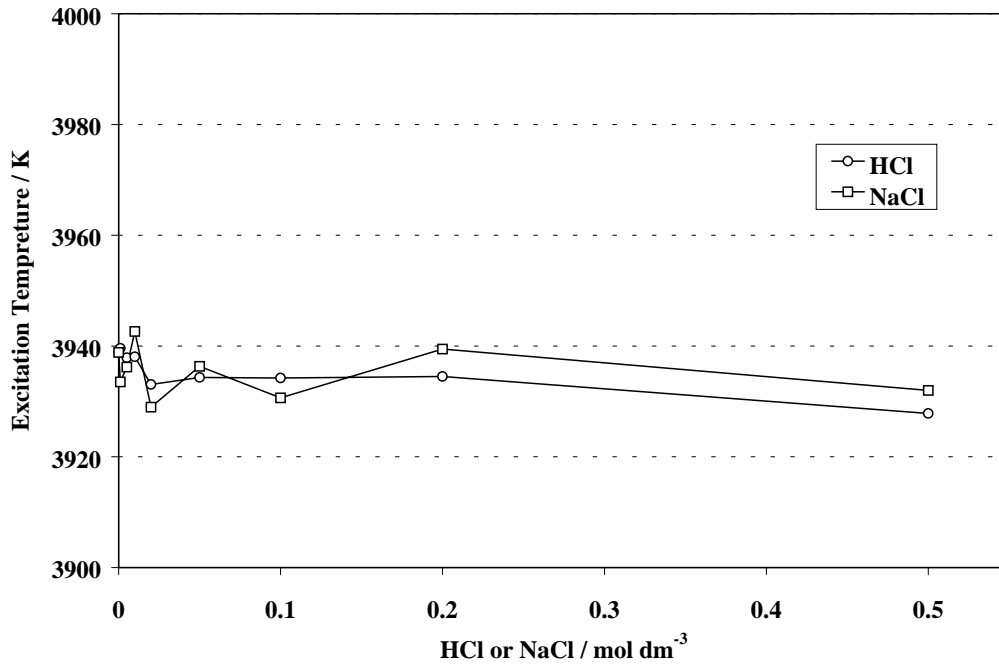


Fig. 4.5.12: The dependence of excitation temperature on the concentration of hydrochloric acid and sodium chloride.

4.5.8 Sodium chloride interference on the electron temperature and the electron number density of MIP

The theory and application of Stark broadening methods for the determination of electron number density in plasmas has been discussed elsewhere. Atomic hydrogen lines are frequently employed for these calculations because of the availability of extensive tabulations of Stark broadening parameters for the complete line profiles. In this work, the H_β line (486.133 nm) was selected for n_e calculations. The benefits were described in detail by Kalnicky et al. [81]. The calculation methods for T_e and n_e which had been described by Nowak et al. [143] were adopted.

When scanning the profiles of H_β line around 486.133 nm, it was found that the introduction of 0.5 mol dm⁻³ hydrochloric acid solution brought about the same profile as it was obtained from water. There is no significant difference in the peak heights (see Fig. 4.5.13). As a result, it is not necessary to think of the interference comes from hydrochloric acid at low concentration. However, the significant differences in the peak height were observed when introducing sodium chloride solutions into the plasma (see Fig. 4.5.13). Therefore, sodium chloride interference on the electron temperature and the electron number density must be studied.

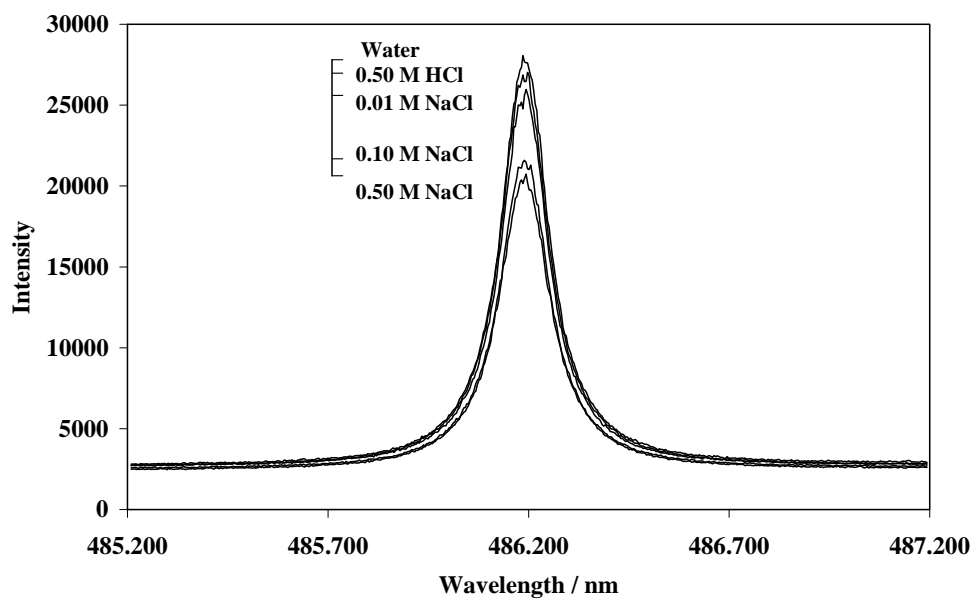


Fig. 4.5.13: The dependence of the emission intensity of H_{β} line (486.133 nm) on the concentration of hydrochloric acid and sodium chloride.

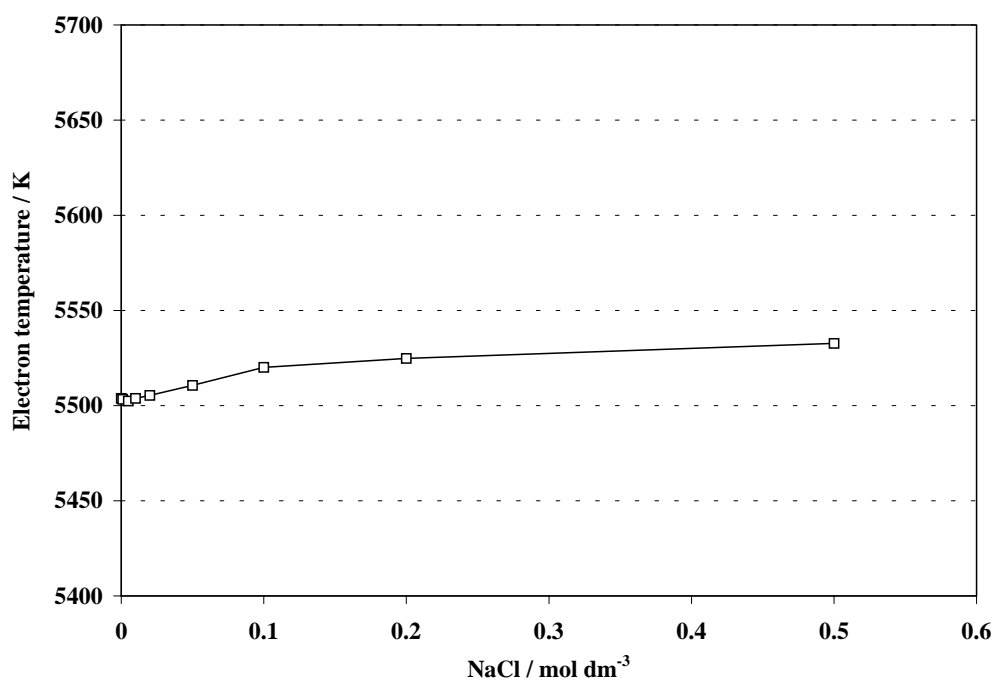


Fig. 4.5.14: The dependence of the electron temperature of the plasma on the concentration of sodium chloride in solution.

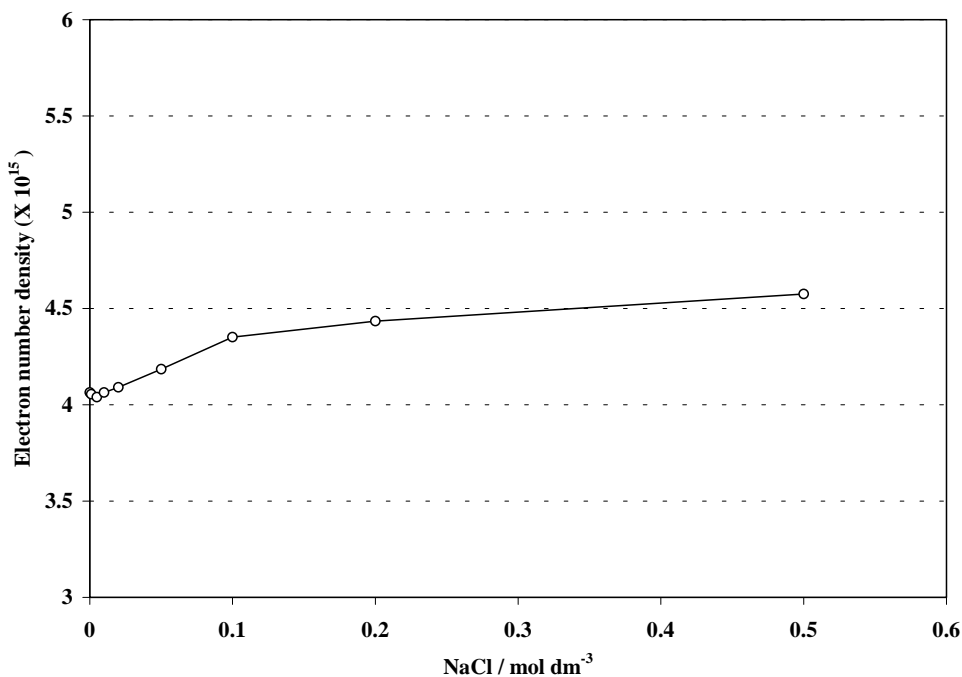


Fig. 4.5.15: The dependence of the electron number density in the plasma on the concentration of sodium chloride in solution.

Although the introduction of sodium chloride led to a significant change in the emission intensity of H_{β} line, the interference on the electron temperatures was not significant (see Fig. 4.5.14). In the range of 0-0.5 mol dm⁻³, the increase in the electron temperature was less than 1%. Obviously, the electron temperature changed too small to suppress mercury signal intensity by introducing sodium chloride into the plasma.

With the increase in the sodium chloride concentration, the electron number density in the plasma observation zone gradually increased (see Fig. 4.5.15). This is because that the ionization of sodium atoms releases abundance of electrons in the central channel of plasma. For mercury ionization equilibrium in the plasma, the increase in the electron number density favors to keep mercury as atoms.

In this experiment, signal suppression was observed at mercury atomic line (253.7 nm). In theory, slight increase in the excitation temperature and electron number density may enhance the excitation capability of the plasma and lead to mercury signal increase. It was confirmed when sodium chloride was introduced at low concentrations. However, the introduction of sodium chloride at high concentrations resulted in serious mercury signal suppression. No doubt, it suggested that mercury signal suppression arise from some other reasons, instead of the changes in the excitation temperature and the electron number density.

4.5.9 Sodium chloride interference on the rotational temperature of MIP

The emission intensities of the rotational lines emitted from a diatomic molecule are given by [144-145]:

$$\ln \left[\frac{I\lambda^4(K+1)}{((K+1)^2-1)} \right] = D - \frac{BhcK(K+1)}{kT} \quad \text{eqn.4.5.2}$$

where I is the intensity of the line, K is the rotational quantum number, D is a constant, and B is the rotational constant of the upper vibrational level. A plot of this function yields two parallel straight lines from which the rotational temperature T_{rot} is calculated in a manner similar to that for T_{exc} . The rotational temperature very often is assumed to be of the same magnitude as the gas-kinetic temperature because of the low energies involved in the rotational processes and the rapid exchange between rotational and kinetic energy of the molecule [146].

For measuring the rotational temperature, the emission signal intensity from OH rotation was scanned between 306.9-307.8 nm. The introduction of hydrochloric acid into the central channel of plasma has no significant influences on the emission signal intensity of OH rotation (see Fig. 4.5.16a).

The same experiments were carried out to monitor sodium chloride interferences on the emission signal intensity of OH rotation. The emission signal was scanned between 306.9-307.8 nm. It is obviously that the emission signal intensity drastically decreases with the increase of the concentration of sodium chloride (see Fig. 4.5.16b). Although the signal intensity decreased so much, there is no significant change in the rotational temperatures in the plasma (see Fig. 4.5.17).

The introduction of hydrochloric acid into the microwave induced plasma has no significant interference on mercury emission signal intensity. Contrarily, the presence of sodium chloride in the sample solution will inevitably bring about the severe influences on the mercury emission signal intensity. A comparison was made to prove that the different mercury signal response is irrelevant to the rotational temperature. It was found that the introduction of neither hydrochloric acid nor sodium chloride into the central channel of plasma could influence the rotational temperature of OH molecules (see Fig. 4.5.17). When the concentration of hydrochloric acid or sodium chloride changed within the experimental range, the rotational temperature of the plasma fluctuated in the tolerances. The mean rotational temperature is 2407 K for hydrochloric acid solutions and 2411 K for sodium chloride solutions.

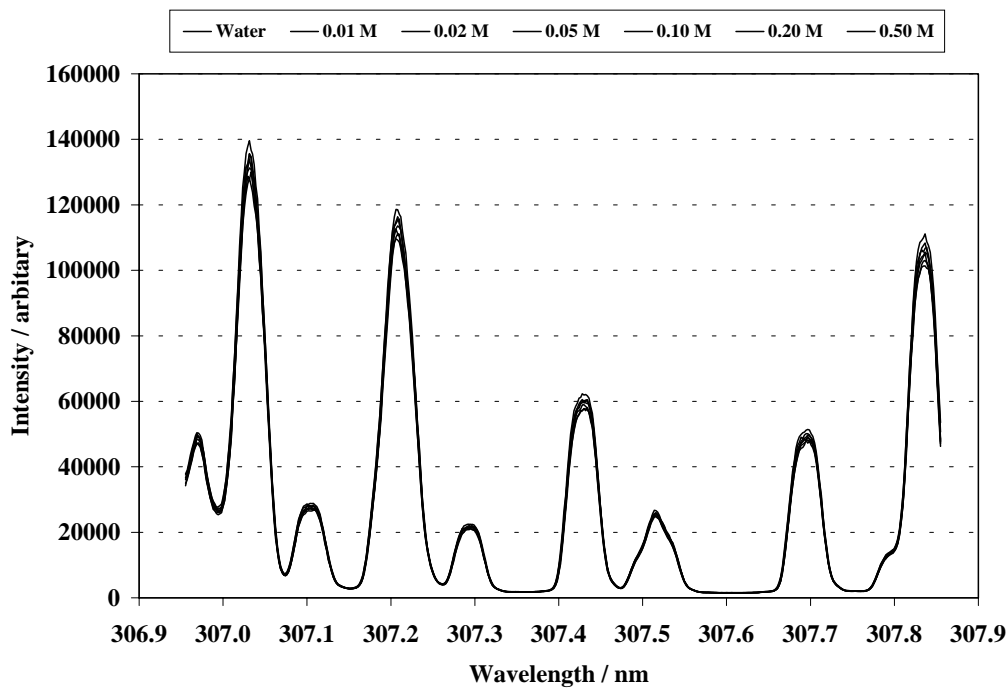


Fig. 4.5.16a: Hydrochloric acid influence on the emission signal intensity of OH rotation between 306.9-307.8 nm.

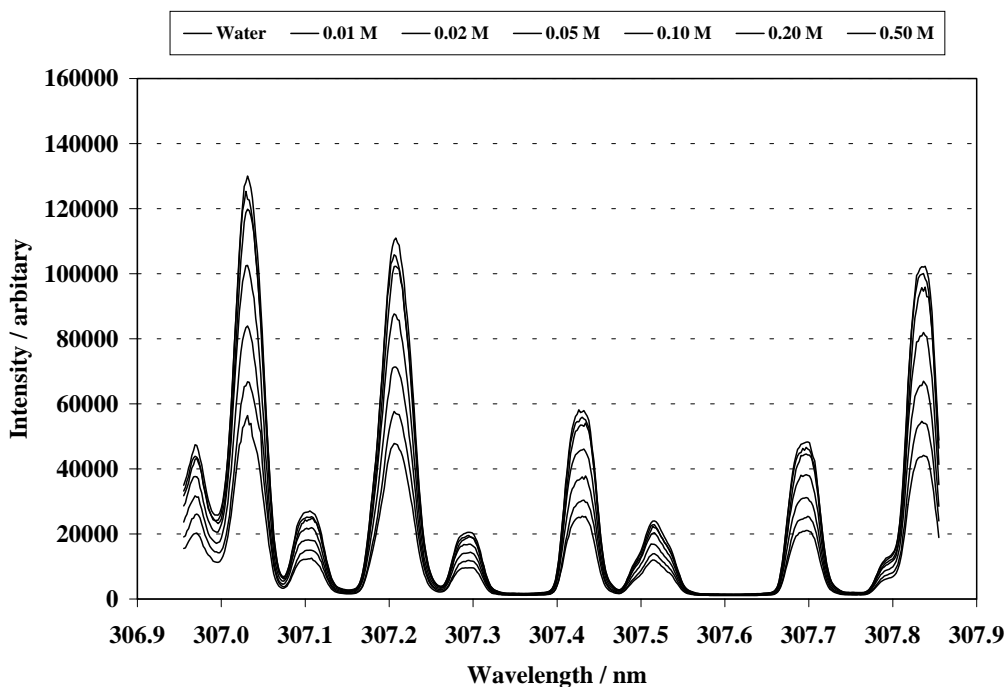


Fig. 4.5.16b: Sodium chloride influence on the emission signal intensity of OH rotation between 306.9-307.8 nm.

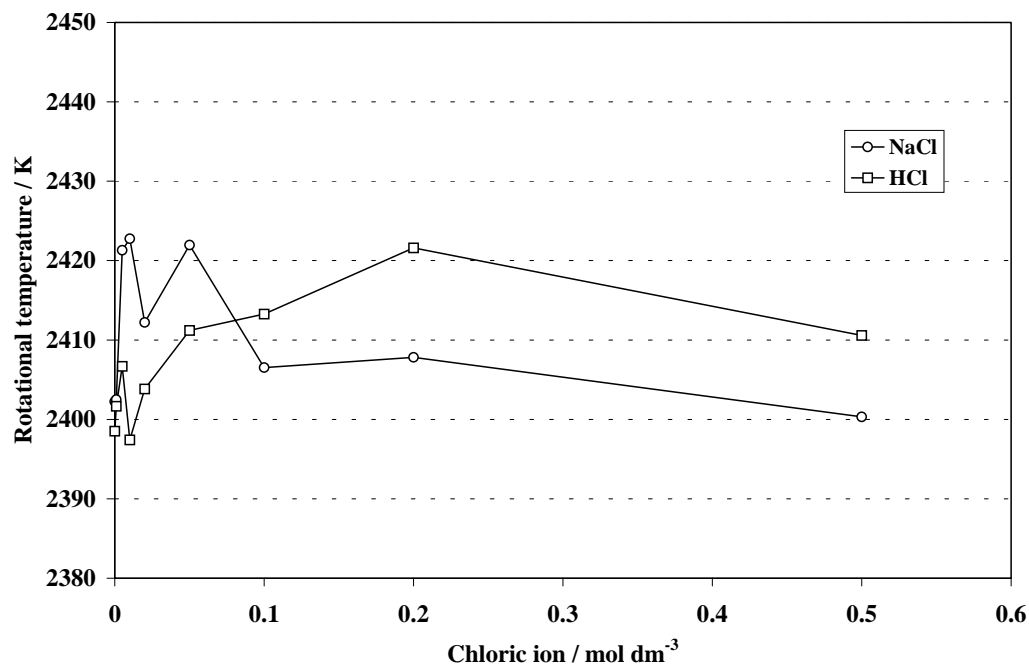


Fig. 4.5.17: The dependence of the rotational temperature of plasma on the concentration of hydrochloric acid and sodium chloride.

It has been proved that mercury signal suppression by sodium chloride is irrelevant to the excitation temperature, the electron temperature, the electron number density, and the rotational temperature in the central channel of the microwave induced plasma. These are the most important parameters to determine the excitation capabilities of plasma. Normally, for the inductively coupled plasma, the rotational temperature is close to the gas kinetic temperature. The gas kinetic temperature plays more important roles in the thermal exchange between the analytes and the plasma. However, in the case of MIP, the rotation of the diatomic molecule is controlled by the frequency of the electromagnetic field. Therefore, the rotational temperature of OH band is more constant. It could not indicate the thermal exchange in the plasma. Whereas, in many cases, the gas kinetic temperature governs the desolvation, evaporation, and atomization of the analytes in the plasma. The measurement of the gas kinetic temperature is quite difficult. Fortunately, the donut-shaped spray chamber offers the possibility to observe the change of the inner pressure in spray chamber. It relates to the change in the gas kinetic temperature. When the plasma is not fed with the wet aerosol, there is not energy to be consumed in the plasma. The gas kinetic temperature of the plasma is the highest one. It produces the highest flow resistance. Therefore, it forms the highest hydraulic column (see Fig. 4.5.18). When sodium chloride solution is introduced at low

concentration, the plasma is cooled down and the hydraulic column is shortened. When sodium chloride solution is introduced at high concentration, the plasma temperature is further cooled down. The flow resistance is further reduced and the hydraulic column is even shortened. The cooling down of the plasma gas kinetic temperature are related to the thermal capacity of salt solution and the heat consumed for the thermal atomization and ionization of sodium chloride. Therefore, the microwave energy to be used for mercury atomization is reduced. That may be one of the main reasons for mercury signal suppression.

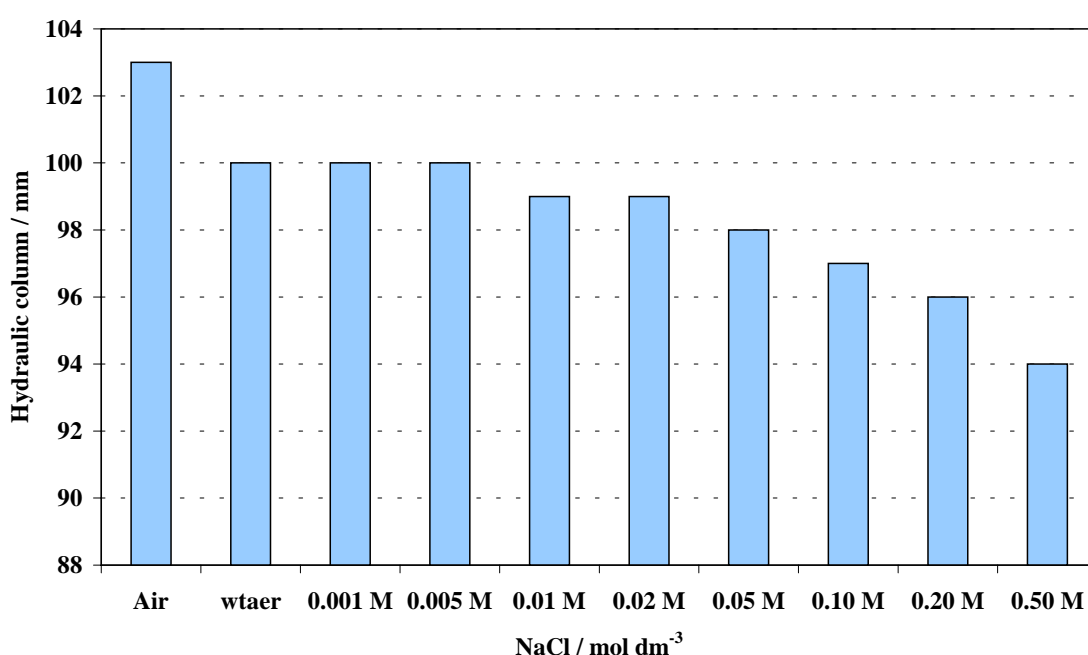


Fig. 4.5.18: The interference of Sodium chloride on the inner pressure in the donut-shaped spray chamber.

At the present, it is the right time to answer why nitric acid has no interference on the mercury signal intensity of high power MIP-OES. When the wet aerosol enters into the resonant cavity, it is completely desolvated in the powerful electromagnetic field. The liquid phase disappears from the plasma observation zone. As a result, the chemical equilibrium does not exist. Based upon the discussions, the robustness of the plasma, to a great extent, is determined by the capability to ingest the wet aerosol, to perform aerosol desolvation and atomization. To realize the unified atomization is the best way to solve the chemical matrix interferences on the plasma source spectrometry.

4.5.10 Cold vapor generation for mercury determination

Comparing with ICP-OES, the development of the high power microwave induced plasma optical emission spectrometer (MIP-OES) shows some advantages. It includes the compact instrument design, inexpensive investment, and reduced gas consumption. For the high power MIP-OES used in this work, the high stability of the overall system and the ability to ingest wet aerosol are the additional advantages. However, it is still unsuitable to be directly used to measure mercury in biological samples. The shortcomings are the low detectability (limits of detection: 30-50 mg dm⁻³) and the unforeseen interferences from the matrix, which relates to the suppression on mercury atomization by the easily ionizable elements (see Section 4.5.9).

To solve this problem, the cold vapor generation method was adopted to introduce mercury into the plasma. By means of this, mercury atomization was finished in the spray chamber. As the excitation conditions of microwave induced plasma (excitation temperature, electron temperature, electron number density, etc.) are irrelevant to the matrix in sample solution, the emission intensity of mercury atomic line is free from the matrix interferences. The sensitivity of the CV-MIP-OES is high enough to measure mercury in the reference material of dogfish muscle tissue (DORM-2). Standard addition method was employed to eliminate the unforeseen interference.

After the sample (~300 mg) was digested with 3.0 cm³ HNO₃ + 1.0 cm³ H₂O₂ in the microwave oven, the digest was moved into 50 cm³ volumetric flask. The flask was filled with pure water to the mark. Then, four aliquots of the exactly 10 cm³ sample solution was moved into four PE test tubes, respectively. For the standard addition calibration, the sample solutions were added 50, 100, and 150 mm⁻³ mercury standard solution, respectively. Mercury standard solution contained 5.0 mg dm⁻³ Hg. The reductant solution was prepared by dissolving 0.1 g sodium borohydride into 0.1% NaOH solution. The sample solution and the reductant solution were aspirated by the peristaltic pump. Two solutions merged and reacted in a Teflon-made mini-T-piece. Then the mixture was nebulized with a concentric nebulizer. The purpose to use a nebulizer is to enlarge the liquid surface area and to accelerate the escape speed of mercury vapor from the mixture. Meanwhile, it is more important to reduce the amount of matrix entering into plasma. Therefore, a nebulizer with low efficiency is desired. The nebulizer used in this work has quite low nebulizing efficiency. During the nebulization, there is no visible aerosol could be observed by naked eye. As a result, the amount of sodium matrix that was introduced into plasma was significantly reduced.

The emission intensity of sodium atoms in the flame tail was equal to the emission intensity by nebulizing a 0.1 mol dm^{-3} NaCl solution with the normal nebulizer. The gas-liquid separation was realized in the donut-shaped spray chamber.

In all cases, the excellent linearity was achieved for the standard addition calibration ($r^2 = 1.000$). The measured value of mercury in the certified reference material DORM-2 is $4.69 \pm 0.04 \text{ mg kg}^{-1}$ ($n = 5$). It is in a good agreement with the certified value of $4.64 \pm 0.26 \text{ mg kg}^{-1}$.

5 Conclusions

In this thesis, special efforts have been made to uncover the matrix interferences on the signal intensity of plasma source spectrometry. For the inductively coupled plasma spectrometry, signal suppression by mineral acids had been recognized for a long time. It is always explained as the physical interferences on the sampling processes, plasma conditions, and aerosol properties. However, in many cases, signal suppression relates to the elements to be measured. That indicates the signal suppression may arise from the chemical properties of element in the central channel of plasma. To prove this hypothesis, a group of elements with high standard reduction potentials were chosen as probes to observe the chemical reactions in the central channel of plasma. It included mercury, gold, and platinum group elements.

By means of mercury, the red-ox reaction, complex formation reactions, and acid-base neutralization reactions had been proven to exist in the central channel of plasma. Firstly, it has been found that mercury signal suppression depends on the plasma characteristics and nitric acid concentration in solution. The frequency of the rf generator strongly affects mercury signal intensity. As observed, signal suppression in 40.68 MHz ICP is more severe than it in 27.12 MHz one. It relates to the difference in the gas-kinetic temperature T_g for the skin effect of plasma. The increase in HNO_3 concentration could not change the intensity ratios of ionic to atomic lines of mercury. In addition, the aerosol of nitric acid could not affect the ionic line intensity of mercury cold vapor. Those suggested that the presence of HNO_3 in droplet do not disturb mercury ionization equilibrium in the central channel of plasma. Therefore, mercury signal suppression relates to mercury compounds atomization. It has been proven that the atomization yield was determined by nitric acid concentration, as the competition result between the oxidizing power of HNO_3 and the heat obtained from plasma. Once atomized, mercury atoms will instantly reach the ionization equilibrium. As results, mercury emission intensities of atomic and ionic lines are suppressed in the same extent. Therefore, it shows a great possibility that the red-ox equilibrium between mercury and nitric acid exists in the central channel of plasma.

Secondly, mercury complex formation equilibrium at ambient temperature has been proven to exert in the heated droplets in plasma. It was found that NH_4NO_3 could inhibit mercury atomization and lead to low emission signal. The equilibrium state is governed

by the chemo-shift and the thermo-shift. The chemo-shift relates to the complex formation by ammonium nitrate and the complex dissociation by nitric acid. At low nitric acid concentration, the equilibrium state is easily shifted by changing the concentration of NH_4NO_3 and HNO_3 . At high nitric acid concentration, the oxidizing power of HNO_3 becomes the main factor to inhibit mercury atomization. The thermo-shift relates to the heat obtained from plasma. With the increase of boiling point, the heat exchange between droplet and plasma is enhanced. It shifts the equilibrium state to the complex dissociation direction and reduces the red-ox inhibition of HNO_3 . As observed, at high nitric acid concentration, all the mercury signals increase with the increasing NH_4NO_3 concentration. The concept of complex formation equilibrium in plasma is useful to elucidate matrix influences, species discrimination, and mercury memory in practical samples. It also offers the possibility to eliminate the matrix influences and memory effects by the chemical modification on sample solution to get a precise and accurate method for mercury determination. This argument was further confirmed by the complex formation reactions between halogens and mercury in the central channel of plasma. Halogen ions, such as chloric and bromic ions, are able to form more stable complexes. The formation of mercury halogen complexes lowers the reduction potentials because the ability of the complex to accept an electron is reduced. The complex formation equilibrium between mercury and halogen is not sensitive to the changes in acidity. Therefore, the formation of halogen complexes is able to keep mercury free from nitric acid interferences and unify mercury atomization in the central channel of plasma. This properties has been successfully applied to modify the sample solution and to measure mercury using external standard calibration method.

Similar to mercury, the memory phenomenon and irregular signal response were also observed when determine PGEs + Au using inductively coupled plasma mass spectrometry. The uncertain signal mainly arises from the chemical interference on the atomization efficiency. It not only depends on nitric acid concentration, but also on the standard reduction potential (E°) of precious metal species in solution. In agreement with the elemental periodic law, the precious elements were divided into two subgroups. The signals of gold and heavy PGEs are severely effected by nitric acid. Contrarily, light PGEs are not so sensitive to the change of HNO_3 concentration. The nitric acid inhibition on the thermolysis of PGEs + Au could reduce the memory in the sampling system. Nitric acid inhibition on the dissociation of PGEs + Au in the central channel of

plasma could reduce the atomization yields and suppress the mass spectrometric signals. The chemical matrix influences in the central channel of plasma depend on the plasma thermal conditions and the heat exchange efficiency. For the analyte in a droplet, if the heating processes of desolvation, vaporization, and atomization overlap too much in the observation zone of plasma, more variable signals are expected. This case is often encountered when introduce the wet aerosol of precious elements or some other high standard reduction potential elements. For the non-acidified standard solution, iridium compound atomization yields an abundance of iridium atoms in plasma central channel. They are possible to capture and induce other precious metals to form alloy or combine as metallic molecule, that also suppresses the mass spectrometric signals of PGEs + Au by reducing the atomization yields. For the determination of PGEs + Au, an accurate matrix matching among the standards and the sample solutions is necessary for the external standard calibration method. Internal standard calibration is not as reliable as the applications for the general elements. Standard addition or isotope dilution methods are more useful to improve the accuracy and precision for the measurement of the high standard reduction potential elements with ICP-MS methods.

Chemical interference on the spectrometric signals is due to the competition between plasma thermal conditions and the chemical potentialities that keep the analytes in the original species. This is governed by the robustness of the plasma, the capabilities of plasma to ingest aerosol and to protect foreign disturbance. The robustness of plasma is not equal to the excitation conditions. It has been observed that nitric acid has no significant interferences on mercury signal intensity of MIP-OES, although the excitation temperature of microwave induced plasma is lower than inductively coupled plasma.

High-power microwave induced plasma is generated in another mechanism. When wet aerosol enters into the resonant cavity, it is completely desolvated in the powerful electromagnetic field. Liquid phase instantly disappears from the plasma observation zone. No doubt, the chemical equilibrium does not exist. Therefore, to a great extent, the robustness of plasma is determined by the capability to ingest wet aerosol, to carry out aerosol desolvation and atomization. In this meaning, the high-power MIP is more robust than ICP. It can keep mercury signal intensity free from the chemical interferences in plasma. Finally, the best way to overcome the chemical matrix interferences on the plasma source spectrometry is to realize the controllable atomization.

References

- 1 **Reed T. B., 1961, *J. Appl. Phys.*, **32**, 821.**
- 2 **Reed T. B., 1961, *J. Appl. Phys.*, **32**, 2534.**
- 3 **Reed T. B., 1962, *Int. Sci. Technol.*, **6**, 42.**
- 4 **Greenfield S., Jones I. L. W., and Berry C. T., 1964, *Analyst*, **89**, 713.**
- 5 **Wendt R. H. and Fassel V. A., 1965, *Anal. Chem.*, **37**, 920.**
- 6 **Liu J., Goessler W., and Irgolic K. J., 2000, Mercury determination with ICP-MS: signal suppression by acids, *Fresenius J. Anal. Chem.*, **366**, 48-53.**
- 7 **Liu J., Goessler W., Irgolic K. J., Huang B. L., Xie Y. Z., Zhang Z. G., and Zhuang Z. X., 1997, Mercury signal suppression in inductively coupled plasma caused by acids, *Proceedings of the Seventh Beijing Conference and Exhibition on Instrumental Analysis*, Shanghai, China, C55.**
- 8 **Smith R. G., 1993, Determination of mercury in environmental samples by isotope dilution/ICPMS, *Anal. Chem.*, **65**, 2485-2488.**
- 9 **Liu J., Goessler W., Irgolic K. J., and Telgheder U., 2000, Chemical interference on the mass spectrometric signals of precious elements, *The proceedings of the Fifth Symposium of Mass Spectrometric Techniques of Trace Element Analysis*, 19-21, Sept., Juelich, Germany.**
- 10 **Gustavsson A. G. T., 1992, in: Montaser A. and Golightly D. W. (Eds) *Inductively Coupled Plasma in Analytical Atomic Spectrometry (2ed)*, VCH Publishers, New York, p.681.**
- 11 **Berndt H. and Schaldach B., 1989, Improvement of power of detection in ICP-OES by a new way of sample introduction (Hydraulic High-Pressure Nebulization), *Fresenius Z. Anal. Chem.*, **335**, 367-369.**
- 12 **Weber G. and Berndt H., 1990, Effective on-line coupling of HPLC and flame-AAS by means of hydraulic high-pressure nebulization, *Chromatographia* **29**, 254-258.**
- 13 **Fassel V. A. and Dickinson, G. W., 1968, Continuous ultrasonic nebulization and spectrographic analysis of molten metals, *Anal. Chem.*, **40**, 247-249.**
- 14 **Fassel V. A. and Bear B. R., 1986, Ultrasonic nebulization of liquid samples for analytical inductively coupled plasma-atomic emission spectroscopy: An update, *Spectrochim. Acta*, **41B**, 1089-1113.**
- 15 **Koropchak J. A. and Winn D. H., 1987, Thermospray sample introduction for atomic spectrometry, *Trends Anal. Chem.*, **6**, 171-175.**

- 16 Meyer G. A., Roeck J. S., and Vestal M. L., 1985**, Thermospray nebulizer for inductively coupled plasma spectrochemical analysis, *ICP Inf. Newsl.*, **10**, 955-963.
- 17 Scott R. H., Fassel V. A., Kniseley R. N., and Nixon D. E., 1974**, Inductively coupled plasma optical emission analytical spectrometry, a compact facility for trace analysis of solutions, *Anal. Chem.*, **46**, 75-80.
- 18 Wu M. and Hieftje G. M., 1992**, A new spray chamber for inductively coupled plasma spectrometry, *Appl. Spectrosc.*, **46**, 1912-1918.
- 19 Liu J., Huang B., and Zeng X., 1998**, Donut-shaped spray chamber for inductively coupled plasma spectrometry, *Spectrochim. Acta*, **53B**, 1469-1474.
- 20 Olesik J. W., 1996**, Fundamental research in ICP-OES and ICP-MS, *Anal. Chem. News & Features*, August 1, 469A-474A.
- 21 Olesik J. W., and Bates L., 1995**, Characterization of aerosols produced by pneumatic nebulizers for inductively coupled plasma sample introduction: effect of liquid and gas flow rates on volume based drop size distributions, *Spectrochim. Acta*, **50B**, 285-303.
- 22 Canals A., Hernandis V., and Browner R. F., 1990**, Evolution of drop size distributions for pneumatically generated aerosols in inductively coupled plasma-atomic emission spectrometry, *Spectrochim. Acta*, **45B**, 591-601.
- 23 Porstendörfer J., Gebhart J., and Röbig G., 1977**, Effect of Evaporation on the Size Distribution of Nebulized Aerosols, *J. Aerosol Sci.* **8**, 371-380.
- 24 Montaser A., 2000**, A millennial mood swing: solution introduction coloring the future in atomic mass spectrometry, *The proceedings of the Fifth Symposium of Mass Spectrometric Techniques of Trace Element Analysis*, 19-21, Sept., Juelich, Germany.
- 25 Mclean J. A., Zhang H., and Montaser A., 1998a**, A direct injection high efficiency nebulizer for inductively coupled plasma mass spectrometry, *Anal. Chem.*, **70**, 1012-1020.
- 26 Mclean J. A., Minnich M. G., Iacone L. A., Liu H., and Montaser A., 1998b**, "Nebulizer diagnostics: fundamental parameters, challenges, and techniques on the horizon", *J. Anal. At. Spectrom.*, **13**, 829-842.
- 27 Mclean J. A., Acon B. W., Montaser A., Singh J., Pritchard D. L., and Patierno S. R., 2000**, The determination of Cr in human lung fibroblast cells using a large bore-direct injection high efficiency nebulizer with inductively coupled plasma mass spectrometry, *Appl. Spectrosc.*, **54**, 659-663.

- 28 Becker J. S., Dietze H-J., Mclean J. A., and Montaser A., 1999a**, Ultratrace and isotope analysis of long-lived radionuclides by inductively coupled plasma quadrupole mass spectrometry using a direct injection high efficiency nebulizer, *Anal. Chem.*, **71**, 3077-3084.
- 29 Becker J. S., and Dietze H-J., 1999b**, Application of double-focusing sector field ICP mass spectrometry with shielded torch using different nebulizers for ultratrace and precise isotope analysis of long-lived radionuclides, *J. Anal. At. Spectrom.*, **14**, 1493-1500.
- 30 Majidi V., Qvarnström J., Tu Q., Frech W., and Thomassen Y., 1999**, Improving sensitivity for CE-ICP-MS using multicapillary parallel separation, *J. Anal. At. Spectrom.*, **14**, 1933-1935.
- 31 Acon B. W., Mclean J. A., and Montaser A., 2000**, A Large bore-direct injection high efficiency nebulizer for inductively coupled plasma spectrometry, *Anal. Chem.*, **72**, 1885-1893.
- 32 Minnich M. G., and Montaser A., 2000**, Direct injection high efficiency nebulization in inductively coupled plasma mass spectrometry under cool and normal plasma conditions, *Appl. Spectrosc.*, **54**, 1261-1269.
- 33 Canals A., Hernandis V., and Browner, R. F., 1990**, Experimental evaluation of the Nukiyama-Tanasawa equation for pneumatic nebulizers used in plasma atomic emission spectrometry, *J. Anal. At. Spectrom.*, **5**, 61-66.
- 34 Mugele R. A. and Evans H. D., 1951**, Droplet size distribution in sprays, *Ind. Eng. Chem.* **43**, 1317-1324.
- 35 Nukiyama S. and Tanasawa Y., 1939**, Experiments on the Atomization of Liquids in Air Stream, *Trans. Soc. Mech. Eng. Japan.* **5**, 68.
- 36 Olsen S. D. and Strasheim A., 1983**, Correlation of the analytical signal to the characterized nebulizer spray, *Spectrochim. Acta*, **38B**, 973-975.
- 37 Canals A., wagner J., Browner R. F., and Hernandis, V., 1988**, Empirical model for estimating drop size distributions of aerosols generated by inductively coupled plasma nebulizers, *Spectrochim. Acta*, **43B**, 1321-1335.
- 38 Dubuisson C., Poussel E., Mermet J-M., and Todoli J. L., 1998a**, Comparison of the effect of acetic acid with axially and radially viewed inductively coupled plasma atomic emission spectrometry: influence of the operating conditions, *J. Anal. At. Spectrom.*, **13**, 63-67.

- 39 Todoli J. L. and Mermet J. M., 1999**, Acid interferences in atomic spectrometry: analyte signal effects and subsequent reduction, *Spectrochim. Acta*, **54B**, 895-929.
- 40 Gowing C. J. B. and Potts P. J., 1991**, Evaluation of a rapid technique for the determination of precious metals in geological samples on a selective *Aqua Regia* leach, *Analyst*, **116**, 773-779.
- 41 Greenfield S., McGeachin H. McD., and Smith P. B., 1976**, Nebulization effects with acid solutions in I.C.P.spectrometry, *Anal. Chim. Acta*, **84**, 67-78.
- 42 Clifford R. H., Sohal P., Liu H., and Montaser A., 1992**, Diagnostic studies on desolvated aerosols from ultrasonic nebulizers, *Spectrochim. Acta*, **47B**, 1107-1122.
- 43 Farino J., Miller J. R., Smith D. D., and Browner R. F., 1987**, Influence of solution uptake rate on signals and interferences in inductively coupled plasma optical emission spectrometry, *Anal. Chem.*, **59**, 2303-2309.
- 44 Dahlquist R. L. and Knoll J. W., 1978**, Inductively coupled plasma-atomic emission spectrometry: analysis of biological materials and soils for major, trace and ultratrace elements, *Appl. Spectrosc.*, **32**, 1-30.
- 45 Shen X. E. and Chen Q. L., 1983**, Effect of a small amount of phosphoric acid in inductively coupled plasma atomic spectroscopy, *Spectrochim. Acta*, **38B**, 115-121.
- 46 Marichy M., Mermet M., and Mermet J. M., 1990**, Some effects of low acid concentrations in inductively coupled plasma atomic emission spectrometry, *Spectrochim. Acta*, **45B**, 1195-1201.
- 47 Fernandez A., Murillo, M., Carrion N., and mermet J. M., 1994**, Influence of operating conditions on the effects of acids in inductively coupled plasma atomic emission spectroscopy, *J. Anal. At. Spectrom.*, **9**, 217-221.
- 48 Maessen F. J. M. J., Balke J., and M De Boer J. L., 1982**, Preservation of accuracy and precision in the analytical practice of low power ICP-AES, *Spectrochim. Acta*, **37B**, 517-526.
- 49 Chudinov E. G., Ostroukhova I. I., and Varvanina G. V., 1989**, Acid effects in ICP-AES, *Fresenius J. Anal. Chem.*, **335**, 25-33.
- 50 Yoshimura E., Suzuki H., Yamazaki S., and Toda S., 1990**, Interference by mineral acids in inductively coupled plasma atomic emission spectrometry, *Analyst*, **115**, 167-171.
- 51 Greenfield S. and Montaser A., 1992**, in: Montaser A. and Golightly D. W. (Eds) *Inductively Coupled Plasma in Analytical Atomic Spectrometry (2ed)*, VCH Publishers, New York, p.224.

- 52 Canals A., Hernandis V., Todoli J. L., and Browner R. F., 1995**, Fundamental studies on pneumatic generation and transport in atomic spectrometry: effect of mineral acids on emission intensity in inductively coupled plasma atomic emission spectrometry, *Spectrochim. Acta*, **50B**, 305-321.
- 53 Sharp B. L., 1988**, Pneumatic nebulizers and spray chambers for inductively coupled plasma spectrometry, A review: Part I. Nebulizers, *J. Anal. At. Spectrom.*, **3**, 613-652.
- 54 Todoli J. L., Mermet J. M., Canals A., and Hernandis V., 1998**, Acid effects in inductively coupled plasma atomic emission spectrometry with different nebulizers operated at very low sample consumption rates, *J. Anal. At. Spectrom.*, **13**, 55-62.
- 55 Stewart I. I., and Olesik J. W., 1998**, The effect of nitric acid concentration and nebulizer gas flow rates on aerosol properties and transport rates in inductively coupled plasma sample introduction, *J. Anal. At. Spectrom.*, **13**, 1249-1256.
- 56 Maestre S., Mora J., Todoli J. L., and Canals A., 1999**, Evaluation of several commercially available spray chambers for use in inductively coupled plasma atomic emission spectrometry, *J. Anal. At. Spectrom.*, **14**, 61-67.
- 57 Carre M., Lebas K., Marichy M., mermet M., Poussel E., and Mermet J. M., 1995**, Influence of the sample introduction system on acid effects in inductively coupled plasma atomic emission spectrometry, *Spectrochim. Acta*, **50B**, 271-283.
- 58 Mora J., Hernandis V., and Canals A., 1991**, Influence of solvent physical properties on drop size distribution, transport and sensitivity in flame atomic absorption spectrometry with pneumatic nebulization, *J. Anal. At. Spectrom.*, **6**, 573-579.
- 59 Liu H., and Montaser A., 1994**, Phase-Doppler diagnostic studies of primary and tertiary aerosols produced by a high-efficiency nebulizer, *Anal. Chem.* **66**, 3233-3242.
- 60 Olesik J. W., Kinzer J. A., and Harkleroad B., 1994b**, Inductively coupled plasma optical emission spectrometry using nebulizers with widely different sample consumption rates, *Anal. Chem.* **66**, 2022-2030.
- 61 Nam, S., Lim J., and Montaser A., 1994**, High-efficiency nebulizer for argon inductively coupled plasma mass spectrometry, *J. Anal. At. Spectrom.*, **9**, 1357-1362.
- 62 Liu H., Montaser A., Dolan S. P., and Schwartz R. S., 1996**, Evaluation of a low sample consumption, high-efficiency nebulizer for elemental analysis of biological samples using inductively coupled plasma mass spectrometry, *J. Anal. At. Spectrom.*, **11**, 307-311.

- 63 Smith D. D., and Browner R. F., 1982**, Measurement of aerosol transport efficiency in atomic spectrometry, *Anal. Chem.*, **54**, 533-537.
- 64 Tarr M. A., Zhu G., and Browner R. F., 1992**, Transport effects with a dribble and jet ultrasonic nebulizers, *J. Anal. At. Spectrom.*, **7**, 813-817.
- 65 Maessen F. J. M. J., Seeverens P. J. H., and Kreuning G., 1984**, Analytical aspects of organic solvent load reduction in normal-power ICPs by aerosol thermalstating at low temperatures, *Spectrochim. Acta*, **39B**, 1171-1180.
- 66 Hettipathirana T. D., Wade A. P., and Blades M. W.,** Effects of organic acids in low power inductively coupled argon plasma-optical emission spectroscopy, *Spectrochim. Acta*, **45B**, 271-280.
- 67 Budic B., and Hudnik V., 1994**, Matrix effects of potassium chloride and phosphoric acid in argon inductively coupled plasma atomic emission spectrometry, *J. Anal. At. Spectrom.*, **9**, 53-57.
- 68 Goldwasser and Mermet J. M., 1986**, Contribution of the charge-transfer process to the excitation mechanisms in the inductively coupled plasma atomic emission spectroscopy, *Spectrochim. Acta*, **41B**, 725-739.
- 69 Dubuisson C., Poussel E., Todoli J. L., and Mermet J-M., 1998b**, Effect of sodium during the aerosol transport and filtering in inductively coupled plasma atomic emission spectrometry, *Spectrochim. Acta*, **53B**, 593-600.
- 70 Novotny I., Farinas J. C., Wan J., Poussel E., and Mermet J. M., 1996**, Effect of power and carrier gas flow on the tolerance of water loading in inductively coupled plasma atomic emission spectrometry, *Spectrochim. Acta*, **51B**, 1517-1526.
- 71 Stewart I. I., and Olesik J. W., 1998**, Steady state acid effects in ICP-MS, *J. Anal. At. Spectrom.*, **13**, 1313-1320.
- 72 Fister III J. C. and Olesik J. W., 1991**, vertical and radial emission profiles and ion-atom intensity ratios in inductively coupled plasma: the connection to vaporizing droplets, *Spectrochim. Acta*, **46B**, 869-883.
- 73 Hobbs S. E., and Olesik J. W., 1993**, The effect of desolvating droplets and vaporizing particles on ionization and excitation in Ar inductively coupled plasma, *Spectrochim. Acta*, **48B**, 817-833.
- 74 Olesik J. W., and Hobbs S., 1994a**, Monodisperse dried microparticulate injector: A new tool for studying fundamental processes in inductively coupled plasma, *Anal. Chem.* **66**, 3371-3378.

- 75 Cicerone M. T. and Farnsworth P. B., 1989**, A simple, non-invasive method for the measurement of gas flow velocities in the inductively coupled plasma, *Spectrochim. Acta*, **44B**, 897-907.
- 76 Olesik J. W., Smith L. J., and Williamsen E. J., 1989**, Signal fluctuations due to individual droplets in inductively coupled plasma atomic emission spectrometry, *Anal. Chem.*, **61**, 2002-2008.
- 77 Olesik J. W., and Fister J. C., 1991**, Incompletely desolvated droplets in argon inductively coupled plasmas: their number, original size and effect on emission intensities, *Spectrochim. Acta*, **46B**, 851-868.
- 78 Stewart I. I., and Olesik J. W., 1998**, Transient acid effects in inductively coupled plasma optical emission spectrometry and inductively coupled plasma mass spectrometry, *J. Anal. At. Spectrom.*, **13**, 843-854.
- 79 Brenner I. B., Mermet J. M., Segal I., and Long G. L., 1995a**, Effect of nitric and hydrochloric acids on rare earth element (REE) intensities in inductively coupled plasma emission spectrometry, *Spectrochim. Acta*, **50B**, 323-331.
- 80 Brenner I. B., Segal I., Mermet M., and Mermet J. M., 1995b**, Study of the depressive effect of nitric acids on the line intensities of rare earth elements in inductively coupled plasma atomic emission spectrometry, *Spectrochim. Acta*, **50B**, 333-340.
- 81 Kalnicky D. J., Fassel V. A., and Kniseley R. N., 1977**, Excitation temperatures and electron number densities experienced by analyte species in inductively coupled plasmas with and without the presence of an easily ionized element, *Appl. Spectrosc.*, **31**, 137-150.
- 82 Kornblum G. R. and de Galan L., 1977**, A study of the interference of the cesium and phosphate in the low-power inductively radio frequency argon plasma using spatially resolved emission and absorption measurements, *Spectrochim. Acta*, **32B**, 455-478.
- 83 Vandecasteele C., Vanhoe H., and Dams R., 1993**, Inductively coupled plasma mass spectrometry of biological samples, *J. Anal. At. Spectrom.*, **8**, 781-786.
- 84 Beauchemin D., Siu K. W. M., and Berman S. S., 1988**, Determination of organomercury in biological reference materials by inductively coupled plasma mass spectrometry using flow injection analysis, *Anal. Chem.*, **60**, 2587-2590.

- 85 Berman S. S., Siu K. W. M., Maxwell P. S., Beauchemin D., and Clancy V. P., 1989,** Marine biological reference materials for methylmercury: analytical methodologies used in certification, *Fresenius. Z. Anal. Chem.*, **333**, 641-644.
- 86 Shum S. C. K., Pang H-M., and Houk R. S., 1992,** Speciation of mercury and lead compounds by microbore column liquid chromatography-inductively coupled plasma mass spectrometry with direct injection nebulization, *Anal. Chem.*, **64**, 2444-2450.
- 87 Galley P. J., Glick M., and Hieftje G. M., 1993,** Easily ionizable element interferences in inductively coupled plasma atomic emission spectroscopy – I. Effect on radial analyte emission patterns, *Spectrochim. Acta*, **48B**, 769-788.
- 88 Hobbs S. E., and Olesik J. W., 1997,** The influence of incompletely desolvated droplets and vaporizing particles on chemical matrix effects in inductively coupled plasma spectrometry: time-gated optical emission and laser-induced fluorescence measurements, *Spectrochim. Acta*, **52B**, 353-367.
- 89 Romeo X., Poussel E., and Mermet J. M., 1997,** The effect of sodium on analyte ionic line intensities in inductively couple plasma atomic emission spectrometry: influence of the operating conditions, *Spectrochim. Acta*, **52B**, 495-502.
- 90 Lindberg S., Stokes P. M., Goldberg E., and Wren C., 1987,** In: Hutchinson T C, Meema KM (eds) Lead, Mercury, Cadmium and Arsenic in the Environment. Scope 31, John Wiley & Sons, Great Britain, p 17
- 91 Tao G., Willie S. N., Sturgeon R. E., 1999,** Determination of inorganic mercury in biological tissues by cold vapor atomic absorption spectrometry following tetramethylammonium hydroxide solubilization, *J. Anal. At. Spectrom.*, **14**, 1929-1931.
- 92 Campbell M. J., Vermeir G., Dams R., Quevauviller P., 1992,** Influence of chemical species on the determination of mercury in a biological matrix (cod muscle) using inductively coupled plasma mass spectrometry, *J. Anal. At. Spectrom.*, **7**, 617-621.
- 93 Craig P. J., Jenkins R. O., and Stojak G. H., 1999,** The analysis of inorganic and methyl mercury by derivatisation methods, opportunities and difficulties, *Chemosphere*. **39**, 1181-1197.
- 94 Quevauviller P., Imbert J. L., Olle M., 1993,** Evaluation of the use of microwave oven systems for the digestion of environmental samples, *Mikrochim. Acta*, **112**, 147-154.

- 95 Liaw M., Jiang S. J., Li Y. C., 1997**, Determination of mercury in fish samples by slurry sampling electrothermal vaporization inductively coupled plasma mass spectrometry, *Spectrochim. Acta*, **52B**, 779-785.
- 96 Woller A., Garraud H., Martin F., Donard O. F. X., and Fodor P., 1997**, Determination of total mercury in sediments by microwave assisted digestion flow injection inductively coupled plasma mass spectrometry, *J. Anal. At. Spectrom.*, **12**, 53-56.
- 97 Yoshinaga J., Morita M., 1997**, Determination of mercury in biological and environmental samples by inductively coupled plasma mass spectrometry with the isotope dilution technique, *J. Anal. At. Spectrom.*, **12**, 417-420.
- 98 Liu J., and Goessler W.,** working experiences on mercury determination in biological and environmental sample during 1995-1997, The institute for analytical chemistry, Karl-Franzens-University Graz, Graz, Austria.
- 99 Capelle B., Mermet J. M., and Robin J., 1982**, Influence of the generator frequency on the spectral characteristics of inductively coupled plasma, *Appl. Spectrosc.*, **36**, 102-106.
- 100 Huang M., Lehn S. A., Andrews E. J., and Hieftje G. M., 1997**, Comparison of electron concentrations, electron temperatures, gas kinetic temperatures, and excitation temperatures in argon ICPs operated at 27 and 40 MHz, *Spectrochim. Acta, Part B*, **52**, 1173-1193.
- 101 Knacke O., Kubaschewski O., and Hesselmann K. (eds), 1991**, Thermochemical Springer, Berlin, p 861, p 879
- 102 Tölgyessy J., (ed.), 1993**, Chemistry and Biology of Water, Air, and Soil-Environmental Aspects, Elsevier.
- 103 Moreton J. A. and Delves H. T., 1998**, Simple direct method for the determination of total mercury levels in blood and urine and nitric acid digests of fish by inductively coupled plasma mass spectrometry, *J. Anal. At. Spectrom.*, **13**, 659-665.
- 104 Liao H-C. and Jiang S-J., 1999**, EDTA as the modifier for the determination of Cd, Hg and Pb in fish by slurry sampling electrothermal vaporization inductively coupled plasma mass spectrometry, *J. Anal. At. Spectrom.*, **14**, 1583-1588.
- 105 Gillespie R. J., Humphreys D. A., Baird N. C., and Robinson E. A. (ed.), 1988**, Chemistry (2nd edition), Allyn and Bacon, Inc., p.980.
- 106 Weast R. C. (ed.), 1986-1987**, *CRC Handbook of Chemistry and Physics*, CRC Press, Boca Raton, FL, **67th edition**, pp 10-215.

- 107 Zereini F., Skerstupp B., Alt F., Helmers E., and Urban H., 1997**, Geological behaviour of platinum-group elements (PGEs) in particulate emissions by automobile exhaust catalysts: experimental results and environmental investigations, *The Science of the Total Environment*, **206**, 137-146.
- 108 Petrucci F., Bocca B., Alimonti A., and Caroli S., 2000**, Determination of Pd, Pt and Rh in airborne particulate and road dust by high-resolution ICP-MS: a preliminary investigation of the emission from automotive catalysts in the urban area of Rome, *J. Anal. At. Spectrom.*, **15**, 525-528.
- 109 Jackson S. E., Fryer B. J., Gosse W., Healey D. C., Longerich H. P., and Strong D. F., 1990**, Determination of the precious metals in geological materials by inductively coupled plasma-mass spectrometry (ICP-MS) with nickel sulphide fire-assay collection and tellurium coprecipitation, *Chemical Geology*, **83**, 119-132.
- 110 Begerow J., Turfeld M., and Dunemann L., 1997**, Determination of physiological palladium, platinum, iridium and gold in human blood using double focusing magnetic sector field inductively coupled plasma mass spectrometry, *J. Anal. At. Spectrom.*, **12**, 1095-1098.
- 111 Barefoot R. R., 1998**, Determination of the precious metals in geological materials by inductively coupled plasma mass spectrometry, *J. Anal. At. Spectrom.*, **13**, 1077-1084.
- 112 Asif M., Parry S. J., and Malik H., 1992**, Instrumental neutron activation analysis of a nickel sulfide fire assay button to determine the platinum group elements and gold, *Analyst*, **117**, 1351-1353.
- 113 Vlasankova R., Otruba V., Bendl J., Fisera M., and Kanicky V., 1999**, Preconcentration of platinum group metals on modified silicagel and their determination by inductively coupled plasma atomic emission spectrometry and inductively coupled plasma mass spectrometry in airborne particulates, *Talanta*, **48**, 839-846.
- 114 McDonald I., Harris J. W., and Vaughan D. J., 1996**, Determination of noble metals in sulphide inclusions from diamonds using inductively coupled plasma-mass spectrometry, *Analytica Chimica Acta*, **333**, 41-49.
- 115 Sun Y., Guan X., and Du A., 1998**, Determination of platinum group elements by inductively coupled plasma-mass spectrometry combined with nickel sulfide fire assay and tellurium coprecipitation, *Spectrochimica Acta Part B*, **53**, 1463-1467.

- 116 Li C., Chai C., Mao X., and Ouyang H., 1998**, Chemical speciation study of platinum group elements in geological samples by stepwise dissolution and inductively coupled plasma mass spectrometry, *Analytica Chimica Acta*, , **374**, 93-98.
- 117 Kanicky V., Otruba V., and Mermet J. M., 1999**, Comparison of some analytical performance characteristics in inductively coupled plasma spectrometry of platinum group metals and gold, *Talanta*, **48**, 859-866.
- 118 Sun Y. C., Mierzwa J., Lin C. F., Yeh T. I., and Yang M. H., 1997**, Selective precipitation separation and inductively coupled plasma mass spectrometric determination of trace metal impurities in high purity silver, *Analyst*, **122**, 437-440.
- 119 Totland M. M., Jarvis I., and Jarvis K. E., 1995**, Microwave digestion and alkali fusion procedures for the determination of the platinum-group elements and gold in geological materials by ICP-MS, *Chemical Geology*, **124**, 21-36.
- 120 Coedo A. G., Dorado M. T., Padilla I., and Alguacil F., 1997**, Preconcentration and matrix separation of precious metals in geological and related materials using metalfix-chelamine resin prior to inductively coupled plasma mass spectrometry, *Analytica Chimica Acta*, **340**, 31-40.
- 121 Krachler M., Alimonti A., Petrucci F., Irgolic K. J., Forastiere F., and Caroli S., 1998**, Analytical problem in the determination of platinum-group metals in urine by quadrupole and magnetic sector field inductively coupled plasma mass spectrometry, *Analytica Chimica Acta*, **363**, 1-10.
- 122 Oguri K., Shimoda G., and Tatsumi Y., 1999**, Quantitative determination of gold and the platinum-group elements in geological samples using improved NiS fire-assay and tellurium coprecipitation with inductively coupled plasma-mass spectrometry (ICP-MS), *Chemical Geology*, **157**, 189-197.
- 123 Ely J. C., Neal C. R., O'Neill J. A., and Jain J. C., 1999**, Quantifying the platinum group elements (PGEs) and gold in geological samples using cation exchange pretreatment and ultrasonic nebulization inductively coupled plasma-mass spectrometry (USN-ICP-MS), *Chemical Geology*, **157**, 219-234.
- 124 Borisov O. V., Coleman D. M., Oudsema K. A., and Carter III R. O., 1997**, Determination of platinum, palladium, rhodium and titanium in automotive catalytic converters using inductively coupled plasma mass spectrometry with liquid nebulization, *J. Anal. At. Spectrom.*, **12**, 239-246.

- 125 Juvonen R., Kallio E., and Lakomaa T., 1994**, Determination of precious metals in rocks by inductively coupled plasma mass spectrometry using nickel sulfide concentration, Comparison with other pre-treatment methods, *Analyst*, **119**, 617-621.
- 126 Enzweiler J., Potts P. J., and Jarvis K. E., 1995**, Determination of platinum, palladium, ruthenium and iridium in geological samples by isotope dilution inductively coupled plasma-mass spectrometry using a sodium peroxide fusion and tellurium coprecipitation, *Analyst*, **120**, 1391-1396.
- 127 Beary E. S. and Paulsen P. J., 1995**, Development of high-accuracy ICP mass spectrometric procedures for the quantification of Pt, Pd, Rh, and Pb in used auto catalysts, *Anal. Chem.*, **67**, 3193-3201.
- 128 Hall G. E. M. and Pelchat J. C., 1993**, Determination of palladium and platinum in fresh water by inductively coupled plasma mass spectrometry and activated charcoal preconcentration, *J. Anal. At. Spectrom.*, **8**, 1059-1065.
- 129 Parent M., Vanhoe H., Moens L., and Dams R., 1996**, Evaluation of a flow injection system combined with an inductively coupled plasma spectrometer with thermospray nebulization for the determination of trace levels of platinum, *Analytica Chimica Acta*, **320**, 1-10.
- 130 Pu Q., Su Z., Hu Z., Chang X., and Yang M., 1998**, 2-Mercaptobenzothiazole-bonded silica gel as selective adsorbent for preconcentration of gold, platinum and palladium prior to their simultaneous inductively coupled plasma optical emission spectrometric determination, *J. Anal. At. Spectrom.*, **13**, 249-253.
- 131 Rehkamper M. and Halliday A. N., 1997**, Determination and application of new ion-exchange techniques for the separation of the platinum group and other siderophile elements from geological samples, *Talanta*, **44**, 663-672.
- 132 Jarvis I., Totland M. M., and Jarvis K. E., 1997a**, An assessment of Dowex 1-X8-based anion-exchange procedures for the separation and determination of ruthenium, rhodium, palladium, iridium, platinum and gold in geological samples by inductively coupled plasma-mass spectrometry, *Analyst*, **122**, 19-26.
- 133 Mukai H., Ambe Y. and Morita M., 1990**, Flow injection inductively coupled plasma mass spectrometry for the determination of platinum in airborne particulate matter, *J. Anal. At. Spectrom.*, **5**, 75-80.
- 134 Jarvis I., Totland M. M., and Jarvis K. E., 1997b**, Determination of the platinum-group elements in geological materials by ICP-MS using microwave

digestion, alkali fusion and cation-exchange chromatography, *Chemical Geology*, **143**, 27-42.

135 Krystek P. and Heumann K. G., 1999, Development of accurate mass spectrometric routine and reference methods for the determination of trace amounts of iridium and rhodium in photographic emulsions, *J. Anal. At. Spectrom.*, **14**, 1443-1447.

136 Lide D. R., 1996-1997, *CRC Handbook of Chemistry and Physics, 77th Edition*, pp. 8-20.

137 Lide D. R., 1996-1997, *CRC Handbook of Chemistry and Physics, 77th Edition*, pp. 10-214.

138 Williams C. A., Abou-Shakra F. R., and Ward N. I., 1995, Investigation into the use of inductively coupled plasma mass spectrometry for the determination of gold in plant materials, *Analyst*, **120**, 341-346.

139 Zander A. T., and Hieftje G. M., 1981, Microwave-supported Discharges, *Appl. Spectrosc.* **35**, 357-371.

140 Liu J., Chen D.Y., Huang B.L., Wang X.R., Sun D.H., Zhuang Z.X., 1999, Effect of Acetonitrile on Ionization and Excitation in Inductively Coupled Plasma Measured by Optical Emission Spectrometry, *Chemical Journal of Chinese Universities*, **20(Supplement)**, 77.

141 Hasegawa T., Umemoto M, Haraguchi H., Hsieh C., and Montaser A., 1992, in: Montaser A. and Golightly D. W. (Eds) *Inductively Coupled Plasma in Analytical Atomic Spectrometry (2ed)*, VCH Publishers, New York, pp.408-412.

142 Selby M., 1984, Ph.D. Thesis, University of New South Wales.

143 Nowak S., van der Mullen J. A. M., and Schram D. C., 1988, Electron density and temperature determination in an ICP using a non-equilibrium concept, *Spectrochimica Acta Part B*, **43**, 1235-1245.

144 Thorne A. P., "Spectrophysics," Chapman & Hall, London, 1974.

145 Alder J. F. and Mermet J. M., 1973, A spectroscopic study of some radio frequency mixed gas plasma, *Spectrochimica Acta Part B*, **28**, 421-433.

146 Kornblum G. R. and de Galan L., 1977, Spatial distribution of the temperature and the number densities of electrons and atomic and ionic species in an inductively coupled RF argon plasma, *Spectrochim. Acta*, **32B**, 71-96.

APPENDIX

CURRICULUM VITAE

Name: Jian LIU
Qualification: M. Sc, Research Associate
Born: Nov. 4th, 1960, Changchun, P. R. China
Nationality: P. R. China
Sex: Male
Marital Status: Married, with one daughter

EDUCATION & CAREER

1978-1982 College student, Chemistry Department, Jilin University, Changchun, China.

1982-1984 Assistant, Dept. of Chinese Traditional Medicine, Changchun Chinese Traditional Medical College, Changchun, China.

1984-1987 Graduate student, Changchun Institute of Applied Chemistry, Chinese Academy of Sciences, Changchun, China.

09, 1987 was granted the Master of science degree. The title of the thesis is "A novel cyclone spray chamber for the simultaneous determination of hydride-forming and non-hydride-forming elements."

1987-1995 Research Associate, Institute of Hematology, Chinese Academy of Medical Sciences(CAMS and PUMC), Tianjin, China.

1995-1997 Visiting Scientist, Institute for Analytical Chemistry, Karl Franzens-University Graz, Graz, Austria.

1997-1998 Visiting Scientist (Research Associate), The Research Lab of State Education Committee(SEDC) on Analytical Chemistry for Material and Life Science, Xiamen, China.

1998-1999 Visiting Scientist, Institute for Analytical Chemistry, Karl Franzens-University Graz, Graz, Austria.

Since 1999 Ph. D. candidate, Duisburg University, Duisburg, Germany. The title of the thesis is "Chemical interferences on the atomization yield of high reduction potential elements – Signal suppression in the plasma source spectrometry."